UCLA
UCLA Electronic Theses and Dissertations

Title
The Aster Proteins: Key Mediators of Plasma Membrane to ER Cholesterol Transport

Permalink
https://escholarship.org/uc/item/3jb6265h

Author
Sandhu, Jaspreet Singh

Publication Date
2018

Peer reviewed|Thesis/dissertation

eScholarship.org Powered by the California Digital Library
University of California

UNIVERSITY OF CALIFORNIA

Los Angeles

The Aster Proteins:

Key Mediators of Plasma Membrane to ER Cholesterol Transport

A dissertation submitted in partial satisfaction of the

requirements for the degree Doctor of Philosophy

in Molecular Biology

by

Jaspreet Singh Sandhu

2018

© Copyright by

Jaspreet Singh Sandhu

2018

ABSTRACT OF THE DISSERTATION

The Aster Proteins:

Key Mediators of Plasma Membrane to ER Cholesterol Transport

by

Jaspreet Singh Sandhu

Doctor of Philosophy in Molecular Biology

University of California, Los Angeles, 2018

Professor Peter John Tontonoz, Chair

Individual cells maintain tight control over their cholesterol content and its intracellular distribution. Abnormal cholesterol accumulation is cytotoxic and promotes coronary artery disease. How cholesterol is synthesized and exchanged between cells was elucidated in the past century. However, cholesterol transport between intracellular membranes is poorly understood. Most cellular cholesterol is found at the plasma membrane (PM), yet the endoplasmic reticulum (ER) is key for cholesterol sensing, biosynthesis, and storage. The pathway between cholesterol deposition at the plasma membrane and its subsequent transport to the ER represents a major gap in our understanding. We sought to address this by using genome-wide screens to identify novel target genes of the cholesterol-responsive transcription factor LXR. We discovered *Gramd1b* as a previously uncharacterized LXR target gene. Through bioinformatic analyses we determined that *Gramd1b* has two paralogs, *Gramd1a* and *Gramd1c,* that together encode a family of GRAM domain containing proteins. Secondary structural analyses of this family revealed remarkable similarity to StAR-family proteins despite little primary sequence conservation. We

named the *Gramd1a-c* protein products as the Aster (Greek, *aster* for "star") proteins. Through binding experiments and x-ray crystallography we determine the Aster proteins contain a unique cholesterol-binding ASTER domain. Next, we used live cell super-resolution microscopy and determined that the Aster proteins are tethered to the ER by a single pass transmembrane domain. Remarkably, cholesterol loading of the plasma membrane results in the dynamic recruitment of Aster-A, -B, and –C to ER-PM contact sites. The N-terminal GRAM domain showed high affinity for phosphatidylserine in binding experiments and mediates cholesterol-dependent Aster recruitment to the PM. To determine the biological role of Aster proteins we knocked down Aster-A in cells and generated Aster-B knockout mice. Cells lacking Aster-A have slowed PM to ER cholesterol transport. Mice lacking Aster-B are deficient in adrenal cholesterol ester storage and steroidogenesis due to defective cholesterol transport from SR-BI to the ER. Our findings identify a nonvesicular pathway for plasma membrane to ER cholesterol transport that is critical in cellular uptake of HDL-derived cholesterol.

The dissertation of Jaspreet Singh Sandhu is approved.

Karen Reue

Tomas Ganz

Steven J Bensinger

Luisa M Iruela-Arispe

Peter John Tontonoz, Committee Chair

University of California, Los Angeles

2018

Dedication

To my parents, Mohinderjit and Jaspal Sandhu.

Your love, hard work, and resilience have made me the man I am today.

Table of Contents

List of Figures

Chapter 2:

Acknowledgements

I am deeply grateful to my mentor, Dr. Peter Tontonoz, for his unwavering support for my development as a scientist. He gave me the freedom to develop and pursue my hypotheses, but also the guidance to succeed. Most importantly, he believed in me. He is my role model of an extraordinary physician scientist. While I still have much to learn, the stimulating environment of the Tontonoz laboratory gave me the foundation to build my scientific career.

I thank my fellow Tontonoz lab members for their guidance. In particular, I would like to give a special thanks to the scholars who went well out of their way to contribute towards my development as a scientist: Cindy Hong, Tamer Sallam, Stephen Lee, Prashant Rajbhandari, and David Strugatsky.

I would like to thank the 'ASTER Team': Xu Xiao, Alessandra Ferrari, and Jose Luis Orozco. It has been a true pleasure to work with you and I am looking forward with delight towards the scientific discoveries the future will bring.

Chapter 2 is a manuscript that is in press:

Jaspreet Sandhu, Shiqian Li, Louise Fairall, Simon G. Pfisterer, Jennifer E. Gurnett, Xu Xiao, Thomas A. Weston, Dipti Vashi, Alessandra Ferrari, Jose L. Orozco, Celine L. Hartman, David Strugatsky, Stephen D. Lee, Cuiwen He, Cynthia Hong, Haibo Jiang, Laurent A. Bentolila, Alberto T. Gatta, Tim P. Levine, Annie Ferng, Richard Lee, David A. Ford, Stephen G. Young, Elina Ikonen, John W.R. Schwabe and Peter Tontonoz (*In Press*). Aster proteins facilitate nonvesicular plasma membrane to ER cholesterol transport in mammalian cells. Cell.

This work was supported by the UCLA Medical Scientist Training Program (NIH training grant GM08042) and also supported by NIH T32HL69766 and the Philip Whitcome Fellowship.

Last but not least, I would like to thank my parents and my girlfriend for all that they have done for me.

VITA

EDUCATION

2013 to 2018	Molecular Biology Interdepartmental Program at UCLA, Los Angeles, California
2011 to present	David Geffen School of Medicine at UCLA, Los Angeles, CA
2009 to 2011	UCLA College of Letters and Science, Los Angeles, CA B.S. Microbiology, Immunology, and Molecular Genetics
2007 to 2009	Moorpark College, Moorpark, CA

AWARDS

2017-2018	Award Recipient/Trainee Whitcome Fellowship
2015-2017	Award Recipient/Trainee Vascular Biology Training Grant
2010-2011	Beckman Scholar

PUBLICATIONS

1. Sandhu, J, Li, S., Fairall, L, Pfisterer, SG, Gurnett, JE, Xiao, X, Weston, TA, Vashi, D, Ferrari, A, Orozco, JL, Hartman, CL, Strugatsky, D, Lee, SD, He, C, Hong, C, Jiang, H, Bentolila, LA, Gatta, AT, Levine, TP, Ferng, A, Lee, R, Ford, DA, Young, SG, Ikonen, E, Schwabe, JWR, Tontonoz, P. Aster proteins facilitate nonvesicular plasma membrane to ER cholesterol transport in mammalian cells. Cell. *In Press*.

2. He C, Hu X, Weston TA, Jung RS, Sandhu J, Huang S, Heizer P, Kim J, Ellison R, Xu J, Kilburn M, Bensinger SJ, Riezman H, Tontonoz P, Fong LG, Jiang H, Young SG. Macrophages release plasma membrane-derived particles rich in accessible cholesterol. Proc Natl Acad Sci U S A. 2018 Aug 20. pii: 201810724. doi: 10.1073/pnas.1810724115. [Epub ahead of print] PubMed PMID: 30127022.

3. Sallam T, Jones M, Thomas BJ, Wu X, Gilliland T, Qian K, Eskin A, Casero D, Zhang Z, Sandhu J, Salisbury D, Rajbhandari P, Civelek M, Hong C, Ito A, Liu X, Daniel B, Lusis AJ,

Whitelegge J, Nagy L, Castrillo A, Smale S, Tontonoz P. Transcriptional regulation of macrophage cholesterol efflux and atherogenesis by a long noncoding RNA. Nat Med. 2018;24(3):304-12. Epub 2018/02/13. doi: 10.1038/nm.4479. PubMed PMID: 29431742; PMCID: PMC5839972.

4. Rajbhandari P, Thomas BJ, Feng AC, Hong C, Wang J, Vergnes L, Sallam T, Wang B, Sandhu J, Seldin MM, Lusis AJ, Fong LG, Katz M, Lee R, Young SG, Reue K, Smale ST, Tontonoz P. IL-10 Signaling Remodels Adipose Chromatin Architecture to Limit Thermogenesis and Energy Expenditure. Cell. 2018;172(1-2):218-33 e17. Epub 2017/12/19. doi: 10.1016/j.cell.2017.11.019. PubMed PMID: 29249357; PMCID: PMC5766418.

5. Sallam T, Sandhu J, Tontonoz P. Long Noncoding RNA Discovery in Cardiovascular Disease: Decoding Form to Function. Circ Res. 2018;122(1):155-66. Epub 2018/01/06. doi: 10.1161/CIRCRESAHA.117.311802. PubMed PMID: 29301847; PMCID: PMC5902384.

6. Zhang L, Rajbhandari P, Priest C, Sandhu J, Wu X, Temel R, Castrillo A, de Aguiar Vallim TQ, Sallam T, Tontonoz P. Inhibition of cholesterol biosynthesis through RNF145-dependent ubiquitination of SCAP. Elife. 2017;6. Epub 2017/10/27. doi: 10.7554/eLife.28766. PubMed PMID: 29068315; PMCID: PMC5656429.

7. Sallam T, Jones MC, Gilliland T, Zhang L, Wu X, Eskin A, Sandhu J, Casero D, Vallim TQ, Hong C, Katz M, Lee R, Whitelegge J, Tontonoz P. Feedback modulation of cholesterol metabolism by the lipid-responsive non-coding RNA LeXis. Nature. 2016;534(7605):124-8. Epub 2016/06/03. doi: 10.1038/nature17674. PubMed PMID: 27251289; PMCID: PMC4896091.

8. Kim D-H, Kim J, Kwon J-S, Sandhu J, Tontonoz P, Lee S-K, Lee S, Lee JW. Critical Roles of the Histone Methyltransferase MLL4/KMT2D in Murine Hepatic Steatosis Directed by ABL1 and PPARγ2. Cell reports. 2016;17(6):1671-82. doi: 10.1016/j.celrep.2016.10.023. PubMed PMID: 27806304.

9. Nguyen HT*, Sandhu J*, Langousis G, Hill KL. CMF22 is a broadly conserved axonemal protein and is required for propulsive motility in Trypanosoma brucei. Eukaryot Cell. 2013;12(9):1202-13. Epub 2013/07/16. doi: 10.1128/EC.00068-13. PubMed PMID: 23851336; PMCID: PMC3811564.

Chapter 1:

Introduction to Cholesterol Trafficking

Introduction to Cholesterol Trafficking

Preface

Cholesterol (Greek, *chol* for *bile*, and *stereos* for *solid*) was first isolated from gallstones by French doctor Francois Poulletier de la Salle in the eighteenth century (Goldstein and Brown, 2015b). The critical importance of cholesterol in disease came to light in the past century following the recognition that high cholesterol levels promote atherosclerotic plaques that can cause heart attacks (Konstantinov et al., 2006). Later work identified the enzymes involved in biosynthesis of cholesterol, the surface proteins that mediate cholesterol uptake and efflux, the particles that carry cholesterol through blood and lymph, and the key regulators that orchestrate these processes (Bloch, 1965; Brown and Goldstein, 1997; Hegele, 2009).

Yet, an enigma in cholesterol metabolism has continued to puzzle biologists: How does cholesterol traffic between cellular membranes? The field of nonvesicular transport has emerged to determine how small molecules are transferred between membranes (Lev, 2010). Nonvesicular transport occurs rapidly and, in contrast to vesicular transport, does not require the fusion of membranes. The clearest example of nonvesicular cholesterol transport has come from the Steroid Acute Regulatory protein (StAR), a protein that harbors cholesterol, shields it from water, and delivers it to the inner mitochondrial membrane to mediate steroidogenesis (Clark, 2012).

How cholesterol is exchanged between the endoplasmic reticulum (ER) and the plasma membrane (PM) has remained an outstanding question. In this dissertation, I address this question by identifying and determining the function of the mammalian Aster (Greek, *aster* for "star") proteins, which I named for their remarkable similarity to StAR. The Aster proteins

(Aster-A, Aster-B, and Aster-C) are integral ER proteins that form a cholesterol-dependent bridge between the ER and the PM. Aster proteins bind cholesterol through a central ASTER domain that we determined to broadly resemble StAR at the atomic structure. Finally, through studies in knockout mice I determined that Aster-B is required for the PM to ER trafficking of HDL-derived cholesterol in the adrenal glands. Along with StAR and the Niemann-Pick Type C proteins, NPC1 and NPC2, Aster-B is one of few intracellular cholesterol transfer proteins demonstrated to be critical for physiologic cholesterol transport (Carstea et al., 1993; Lin et al., 1995a; Sleat et al., 2004). The discovery of the Aster proteins as key mediators of PM to ER cholesterol trafficking establish principles for understanding how cholesterol trafficking operates in many tissues and physiologic contexts.

In Chapter 1, I introduce general aspects of cholesterol biology, and discuss how cholesterol is transcriptionally regulated and transported among specific intracellular compartments and throughout the body.

Chapter 2 is a recently accepted manuscript entitled "Aster proteins facilitate nonvesicular plasma membrane to ER cholesterol transport in mammalian cells," and will be published in Cell. This manuscript summarizes the key results of my thesis work identifying and characterizing the function of the Aster proteins, encoded by *Gramd1a*, *Gramd1b*, and *Gramd1c*.

Finally, Chapter 3 summarizes the key findings of my dissertation and reviews important questions that remain unaddressed with respect to the Aster family and cholesterol homeostasis.

Cholesterol

Cholesterol contains four-fused rings, a hydroxyl group, and a hydrophobic tail (Lippincott-Schwartz and Phair, 2010). The unique structure of cholesterol provides key biophysical properties that allow mammalian cell membranes to control solute movement and remain fluid over a range of temperatures and lipid compositions (Holthuis and Menon, 2014). By interfering with phospholipid acyl-chain packing, cholesterol prevents membrane transition to a solid gel state. On the other hand, cholesterol also restricts flexibility of phospholipid acyl chains to thicken the plasma membrane and decrease fluidity (Drin, 2014). Different organellar membranes vary in cholesterol concentration in a manner that corresponds function (Ikonen, 2008). For example, enrichment of cholesterol at the plasma membrane promotes thickness and solute impermeability to protect cellular contents from the environment. Derivatives of cholesterol, such as steroids, vitamin D, and bile acids have important roles in signaling and solubilizing dietary lipids.

Sources of Whole Body Cholesterol

Total body cholesterol levels originate from *de novo* biosynthesis (~70%) and dietary intake (~30%) (Tontonoz and Mangelsdorf, 2003). Dietary and synthetic contributions likely vary between individuals according to genetic and environmental differences. The cholesterol biosynthetic pathway was elucidated in the 1950s and occurs in all nucleated cells through repeated polymerizations of acetate (Bloch, 1965). Importantly, the conversion of HMG-CoA to mevalonate is rate limiting and catalyzed by the ER-resident enzyme HMG-CoA Reductase (HMGCR) (Goldstein and Brown, 2015b).

Dietary cholesterol is absorbed by the small intestine through enterocytes. NPC1L1 is the best characterized determinant of cholesterol absorption and a target of the cholesterol-lowering drug ezetimibe (Garcia-Calvo et al., 2005). Following absorption, enterocytes package cholesterol along with triglycerides to form chylomicrons (Ikonen, 2008). Through chylomicron production, dietary cholesterol is transported from the small intestine to the liver, from which it is delivered to the whole body.

Enterocytes and hepatocytes package cholesterol and cholesteryl esters into lipoproteins for transfer between cells. Chylomicrons from the intestine lose triglycerides through the actions of lipoprotein lipase, and gain new apoproteins to generate remnants that are taken up by the liver (Hegele, 2009). Consequently, hepatocytes secret cholesterol in very low density lipoprotein (VLDL) particles that are processed into low density lipoprotein (LDL) in the circulation for cholesterol delivery to peripheral cells (Ikonen, 2008). Hepatocytes and enterocytes also produce high density lipoprotein (HDL), which receives excess cholesterol from peripheral tissues for delivery back to the liver in a process known as reverse cholesterol transport (RCT) (Wasan et al., 2008). Excess hepatic cholesterol is secreted along with bile into the small intestine for excretion or reabsorption. Interestingly, the brain is isolated from receiving cholesterol but instead relies on *de novo* synthesis from astrocytes and uses unique lipoproteins to transport lipids between cell types (Zhang and Liu, 2015).

Cholesterol Uptake from Lipoproteins

Cells acquire cholesterol through uptake of LDL by the LDL receptor (LDLR) or uptake of HDL by the HDL receptor, Scavenger Receptor Class B1 (SR-B1) (Hegele, 2009). The LDLR is present on the plasma membrane of most mammalian cells and binds particles that are

rich in ApoB or ApoE (e.g. VLDL and LDL). Since the 1980s the LDLR-mediated uptake pathway has been known to result in clathrin-mediated endocytosis of lipoprotein particles (Goldstein et al., 1985). LDL containing endosomes are eventually transported to acidic endocytic compartments where LDL dissociates from LDLR. Cholesterol esters are then hydrolyzed in the lysosome to provide un-esterified 'free' cholesterol for cellular use and the LDLR is recycled (Brown and Goldstein, 1997).

After the LDLR function in endocytic cholesterol uptake was identified the existence of a non-endocytic (i.e. selective) uptake pathway for HDL-associated lipids was reported (Pittman et al., 1987). SR-B1 acts as the physiologic high-density lipoprotein (HDL) receptor and primarily acts in selective uptake or influx of HDL-derived cholesterol esters into cells but also facilitates cholesterol efflux from peripheral cells such as macrophages (Shen et al., 2018).

Cholesterol in Health and Disease

Cholesterol is an essential component of cell membranes and a precursor to steroid hormones, bile acids, and vitamin D. However excess cholesterol is cytotoxic and serum lipoproteins have emerged as key risk factors in cardiovascular disease. Cholesterol is implicated in atherosclerotic disease, dementias, metabolic syndrome, cancer, and several rare monogenic diseases such as FH and lysosomal cholesterol-sphingolipid diseases (Ikonen, 2008).

Atherosclerotic plaques were first described in the 19th century. Derived from the Greek word 'gruel', atherosclerosis refers to the cheesy substance exuding from plaques upon sectioning (Goldstein and Brown, 2015a). In 1910, human aortic plaques were found to contain a 25-fold enrichment in cholesterol when compared with normal aortic tissue (Couzin, 2008).

Early feeding experiments also demonstrated that a diet high in cholesterol produces profound atherosclerosis in rabbits.

Later genetic studies identified autosomal dominant Familial Hypercholesterolemia (Muller 1938). Familial Hypercholesterolemia is a genetic condition caused by mutations impairing the LDLR pathway, impairing the clearance of LDL cholesterol from the blood, thereby elevating plasma LDL cholesterol (Ajufo and Rader, 2018). FH is characterized by premature atherosclerotic cardiovascular disease due to elevated LDL cholesterol. With this discovery, it was soon recognized that elevated serum cholesterol carries an increase in risk of heart attack in middle age (Mahmood et al., 2014).

The importance of studying cholesterol is highlighted by the success of cholesterol-modifying drugs. Two major drug classes, the statins and more recently proprotein convertase subtilisin kexin 9 (PCSK9) modulators, act to reduce serum LDL cholesterol levels and have a proven benefit in lowering the incidence of heart attacks (Ajufo and Rader, 2018). Despite the availability of cholesterol modifying drugs, one in 4 industrialized deaths still result from coronary artery disease (Heron, 2013), necessitating the continued study of cholesterol metabolism and trafficking. Understanding the fundamental biology of how we handle and transfer cholesterol within the body may pave the way for the development of novel therapeutics to treat costly cholesterol-related conditions.

Transcriptional Control of Cholesterol Homeostasis

Cholesterol is an essential component of cell membranes and a precursor to steroid hormones. However, excess cholesterol is cytotoxic and a major risk factor for cardiovascular disease. Therefore, cholesterol levels in individual cells and whole animals must be tightly regulated to sustain life.

Cholesterol biosynthesis, uptake, efflux and processing are largely regulated by two major pathways, sterol regulatory element binding proteins (SREBPs) and Liver X Receptors (LXRs) (Ikonen, 2008; Wang and Tontonoz, 2018). The SREBP pathway promotes transcription of genes that promote cellular cholesterol levels such as HMGCR and the LDLR. Conversely, LXR activation facilitates reverse cholesterol transport, leading to cholesterol removal from peripheral cells and increased biliary secretion.

Schoenheimer's early bottle experiments provided the first evidence of end-product feedback of cholesterol synthesis (Goldstein and Brown, 2015a). These studies laid the foundation for cloning of the LDL receptor, and subsequently identification of the Sterol Regulatory Element (SRE) in the *LDLR* promoter. SREBP-1 and SREBP-2 were identified through their binding to the SRE and named accordingly (Brown and Goldstein, 1997). SREBP cleavage activating protein (SCAP) was later recognized as the central regulatory of mammalian cholesterol homeostasis as it regulates the activity of the SREBPs (Brown et al., 2002; Brown et al., 2017; Sokolov and Radhakrishnan, 2010).

De novo cholesterol synthesis occurs in the ER and is regulated by the ER-resident transcription factor SREBP-2. When ER cholesterol declines, SREBP2 is processed and released to induce transcription of the cholesterol biosynthetic program. Reciprocally, excess ER sterols inhibit SREBP-2 processing and thereby cholesterol synthesis. This feedback mechanism ensures a constant supply of ER-derived sterols to distal organelles. Sterols act through SCAP's sterol-sensing domain to cause a conformational change that inhibits SREBP-2 processing (Brown et al., 2002; Radhakrishnan et al., 2004). When this inhibition is relieved, processed SREBP-2 is imported into the nucleus where it switches on the transcription of HMGCR, LDLR, and other sterol-regulated genes (Ikonen, 2008).

Liver X Receptors (LXRs) are nuclear receptors that sense cellular cholesterol levels by binding oxysterols (Calkin and Tontonoz, 2010, 2012). Exactly how membrane cholesterol levels control oxysterol generation remains to be determined, but the ER hydroxylases that convert cholesterol to oxysterols are located in the ER. There are two LXR paralogs, LXRα and LXRβ. LXRβ is expressed ubiquitously whereas LXRα primarily acts in metabolically active tissues such as the liver and intestine (Wang and Tontonoz, 2018). In the unliganded state, LXRs act as repressors through interactions with nuclear corepressors. Upon ligand binding, LXR undergoes a conformational shift that results in the exchange of corepressors for coactivators, thereby promoting transcription of nearby genes. LXR target genes lower cellular cholesterol levels by promoting cholesterol efflux and inhibiting cholesterol uptake (Calkin and Tontonoz, 2010).

Given that the SREBP-2 and LXR pathways have opposing effects, it makes intuitive sense that they should participate in crosstalk. Recent studies, including those from our own laboratory, have identified key players mediating crosstalk between the two pathways, including the microRNA miR-33, the ubiquitin ligases IDOL and RNF145, and the long non-coding RNA *LeXis* (Rayner et al., 2010; Sallam et al., 2016; Zelcer et al., 2009; Zhang et al., 2017).

Overview of Cholesterol Trafficking

Cholesterol by nature is hydrophobic. Sophisticated mechanisms are required for cholesterol uptake, trafficking, release and storage. The successful integration of these activities across cell-types and tissues results in organismal cholesterol homeostasis.

At the subcellular level, cholesterol is differentially enriched among membranes to support organelle function (Lippincott-Schwartz and Phair, 2010). For example, a higher plasma membrane cholesterol concentration provides a thicker and more rigid barrier between

intracellular and extracellular environments (Holthuis and Menon, 2014). Conversely, a lower ER cholesterol concentration facilitates protein insertion. Many cholesterol processing steps take place at different subcellular locations, and delivery between sites is a critical means to regulate reactions and maintain cellular function (Ikonen, 2008). Perturbations in membrane cholesterol concentration result in cytotoxicity. For example, depletion of PM cholesterol results in an ineffective barrier to solute exchange and perturbed ER cholesterol content either impairs protein import or results in protein mistargeting (Holthuis and Menon, 2014). Therefore, ensuring the proper transport and enrichment of cholesterol represents a critical goal for the cell.

Cholesterol Efflux

Mammalian cells cannot catabolize cholesterol and therefore must eliminate it through cholesterol efflux (Lippincott-Schwartz and Phair, 2010). Cholesterol efflux represents the first step in reverse cholesterol transport (RCT), a process through which excess cholesterol is transferred through HDL to the liver for bile acid synthesis and excretion (Wang and Tontonoz, 2018).

ATP-binding cassette (ABC) transporters act as key mediators of cellular cholesterol export in mammalian cells. LXRs promote RCT through the coordinated activation of a number of key ABC transporters including ABCA1. Mutations in *ABCA1* cause Tangier disease, a disorder characterized by peripheral cholesterol accumulation and diminished plasma HDL cholesterol (Calkin and Tontonoz, 2012). Mechanistic studies have determined that ABCA1 acts as the rate-limiting step in HDL particle formation (Oram and Vaughan, 2006). Inactivation of ABCA1 in the liver or intestine deletion of *ABCA1* diminishes HDL concentrations suggesting

these tissues are the major determinants of HDL levels (Brunham et al., 2006; Timmins et al., 2005).

In the macrophage, ABCA1 activity is key to preventing cholesterol retention in atherosclerotic lesions (Wang et al., 2007). Binding of free ApoA1 to ABCA1 triggers the net transfer of PM cholesterol and phospholipids, resulting in the formation of discoidal HDL (Ikonen, 2008). Additional ABC transporters, such as ABCG5/G8 and ABCG1 also promote cholesterol efflux in specific tissues such as the liver and intestine (Bonamassa and Moschetta, 2013; Repa et al., 2002; Yu et al., 2002).

Cholesterol Storage by Esterification

Cholesterol ester (CE) is synthesized when an ester bond forms between a fatty acyl-CoA and the hydroxyl group of cholesterol. Cholesterol esterification is catalyzed by acyl-CoA cholesterol acyltransferases (ACAT1 and ACAT2) and acts as a buffering mechanism for reducing free cholesterol in the ER (Farese, 2006). ACAT1 is widely expressed and ACAT2 is restricted to liver and intestine. Both ACATs are activated when excess plasma membrane cholesterol is trafficked to the ER and a critical ER concentration threshold is reached (Lange et al., 1999; Xu and Tabas, 1991). Importantly, cholesterol esters that arrive from lipoproteins must be re-esterified by ACATs before being incorporated into lipid droplets, implying they are hydrolyzed before arrival to the ER.

CEs do not partition effectively into bilayers but instead form lipid droplets, along with triglycerides (Walther and Farese, 2012). Lipid droplets emerge from the ER and function as cellular cholesterol and fatty acid stores (Krahmer et al., 2009). In certain contexts, such as in foam cells, CEs may accumulate to levels exceeding that of free cholesterol (Maxfield and

Tabas, 2005).

Non-Vesicular Cholesterol Transport

Cellular lipids are known to traffic through vesicular (exchange of membranes) and non-vesicular (in the absence of membrane fusion) mechanisms. Work over the past few decades have concluded that bulk cholesterol transport is not dependent on vesicles. Indeed, some compartments such as the mitochondria and lipid droplets are devoid of vesicular transport altogether. How is lipid transport maintained in the absence of vesicular trafficking?

Vesicular traffic involves the export of secretory proteins from the ER through the Golgi apparatus to the PM or the import of macromolecules from the PM through endocytosis (Lippincott-Schwartz and Phair, 2010). By contrast, non-vesicular trafficking (NVT) of lipids is thought to occur through lipid transfer proteins (LTPs). Such proteins act by extracting lipid from a donor membrane into a hydrophobic pocket where it can be shielded from water, and subsequently deposited into another membrane upon a successful encounter (Phillips and Voeltz, 2016). In theory, successful encounters between LTPs and the appropriate membrane are promoted by the formation of membrane contact sites, defined as close (~10nm) appositions between two organelles (Stefan et al., 2013). To facilitate the formation of high proximity membrane contact sites, LTPs may also harbor membrane tethering domains (Chiapparino et al., 2016).

Among the best-characterized mediators of intracellular cholesterol transport are Steroid Acute Regulatory Protein (StAR) and Niemann-Pick Type C proteins, NPC1 and NPC2. The compartmentalization and biochemical mechanisms of StAR-mediated transfer are better understood than most cholesterol transfer proteins (Ikonen, 2008). StAR contains a cholesterol-

binding pocket and facilitates the trafficking of cholesterol to the inner membrane of the mitochondria, a rate limiting step in steroidogenesis (Alpy and Tomasetto, 2005). StAR knockout mice lack adrenal cholesterol esters and human mutations in StAR result in congenital lipoid adrenal hyperplasia (Caron et al., 1997; Lin et al., 1995a). Since the discovery of StAR, primary sequence homology studies have identified StAR-like transfer domains (START) across a superfamily of proteins that span across the animal, plant, and fungal kingdoms (Alpy and Tomasetto, 2005; Phillips and Voeltz, 2016). START proteins in mammals bind and transfer cholesterol or other lipid species such as phosphatidylcholine and ceramide (Alpy and Tomasetto, 2005).

NPC1 and NPC2 also harbor cholesterol-binding pockets and reside within the late endosome/lysosome (Infante et al., 2008a; Infante et al., 2008c). These proteins are sequentially critical for cholesterol movement out of the lysosome. Loss of either protein causes accumulation of LDL-derived cholesterol in lysosomes, characteristic of the Niemann-Pick Type C syndrome. NPC1 appears to operate downstream of NPC2 through a proposed hand-off mechanism, since neither protein can compensate for one another (Kwon et al., 2009). How cholesterol exits the lysosome and which membrane is subsequently targeted for delivery remain outstanding questions. Recent studies have suggested that LDL-derived cholesterol is first delivered to the plasma membrane before transport to the endoplasmic reticulum (Infante and Radhakrishnan, 2017).

Many proteins that preserve cellular cholesterol homeostasis exhibit considerable functional redundancy (Ikonen, 2008). For example, several proteins of the START family, and an analogous family, the oxysterol-binding protein related protein (ORP) family, have affinity for cholesterol or other lipids *in vitro,* but loss-of-function studies *in vivo* have not revealed clear

and compelling phenotypes. Thus, it has heretofore been difficult to determine whether unassigned START or ORP proteins function as direct cholesterol transporters or as lipid sensors that orchestrate other functions in lipid homeostasis, vesicular trafficking and/or signaling.

Forward Trafficking of Cholesterol Does Not Require Vesicles

Current models recognize the ER as the principal supplier of lipids to other organelles (Holthuis and Menon, 2014). Through an extensive network, ER tubules interface at contact sites with most other subcellular membranes to maintain control of lipid transport and respond to cellular demands (Holthuis and Menon, 2014; Wu et al., 2018).

Radiotracer studies in mammalian cells treated with the COPI inhibitor brefeldin A have shown that newly synthesized cholesterol is transported to the plasma membrane in a process that does not depend on vesicular transport (Heino et al., 2000; Kaplan and Simoni, 1985; Lange and Matthies, 1984; Urbani and Simoni, 1990). Thus the consensus view has been that cholesterol transport from the ER to the PM likely relies on NVT by unknown cytosolic transfer proteins, membrane contact sites, or a combination of both (Holthuis and Menon, 2014).

Interestingly, cholesterol enrichment of the Golgi apparatus is somewhat intermediate between ER and PM concentrations and thought to be important to the forward trafficking of integral membrane proteins. A 2013 study proposed that Oxysterol Binding Protein (OSBP) mediates this concentration gradient by forming ER-Golgi contact sites and exchanging cholesterol with PI(4)P, which is subsequently hydrolyzed by Sac1 (Mesmin et al., 2013). This study provided an energetic explanation for how cholesterol could move up a concentration gradient.

An analogous counter-transport mechanism was also proposed in the forward trafficking of phosphatidylserine by OSBP-related protein 5 (ORP5) (Chung et al., 2015). ORP5 resides at, and promotes the formation of, ER-PM contact sites through its integral ER transmembrane domain and an N-terminal Pleckstrin Homology (PH) domain. Interestingly, ORP5 moves phosphatidylserine from the endoplasmic reticulum, where it is synthesized, to the inner leaflet of the plasma membrane where it is enriched (Yeung et al., 2008). De Camilli and colleagues proposed this feat is accomplished through an energetically favorable counter-transport of PI(4)P from the PM to the endoplasmic reticulum where it can be hydrolyzed by Sac1 (Chung et al., 2015).

PM to ER Transport Is Required for Cholesterol Sensing and Esterification

When ER Cholesterol exceed 5 mol % of total lipid, SREBP-2 transport is abruptly blocked through conformational changes in SCAP (Radhakrishnan et al., 2008). Transport resumes again once ER cholesterol falls below the 5% threshold. Yet, the ER resident SREBP-2 program is responsible for sensing total cellular cholesterol, most of which resides in the 40% molar PM. How does SCAP sense plasma membrane concentrations?

Recent cholesterol probes developed from bacterial proteins have provided insight into this problem. Perfringolysin O (PFO) and the D4 domain Anthrolysin O (ALOD4) have been used to probe membrane cholesterol. Both probes operate by binding membranous cholesterol that is not sequestered by sphingomyelin (i.e. cholesterol that is “accessible”). PFO-binding experiments with intact cells have demonstrated that the plasma membrane cholesterol is organized into three distinct pools (Das et al., 2014; Das et al., 2013; Infante and Radhakrishnan, 2017). The “accessible” pool of plasma membrane cholesterol (~5 mol%) is bound by PFO at

steady-state conditions and subject to change with additional or depletion of cholesterol. An additional "inaccessible" pool only binds PFO upon treatment with sphingomyelinase, this pool is thermodynamically trapped by sphingomyelin (Das et al., 2013). Finally, a residual pool does not bind PFO even after sphingomyelinase treatment.

PFO binding experiments in purified ER membranes have found that cholesterol accessibility of ER membranes increases at ~5 mol %, the same concentration at which SREBP-2 is suppressed (Sokolov and Radhakrishnan, 2010). Interestingly, cholesterol loading of the plasma membrane first expands the plasma membrane's PFO-accessible pool, and after a short lag, also increases the ER's PFO-accessible pool. This mechanism allows cells to ensure optimal cholesterol levels in the PM while avoiding cholesterol over accumulation in the endoplasmic reticulum (Das et al., 2014).

Transbilayer distribution of cholesterol is unknown, but it is thought that cholesterol readily exchanges between leaflets (Steck et al., 2002). Taking advantage of this idea, the Radakrishnan group recently used ALOD4 to 'lock' cholesterol to the outer leaflet of the plasma membrane. Under these conditions, the SREBP-2 pathway is stimulated despite steady cellular cholesterol levels, demonstrating that a fraction of plasma membrane cholesterol is continuously transported to the endoplasmic reticulum for sensing (Infante and Radhakrishnan, 2017).

The presumptive cholesterol transfer protein required for the continuous sensing of PM cholesterol by Scap is unknown. Members of the OSBP family have been proposed to traffic cholesterol from the ER to the PM, but have yet to be demonstrated to be required for such trafficking in loss-of-function studies (Holthuis and Menon, 2014).

Clues from Non-Vesicular Ergosterol Trafficking in Yeast

Yeast do not have cholesterol. They instead utilize ergosterol through *de novo* synthesis. Yeast provide an amenable system for generating knockout cells and confirming, for example, that ER-to-PM trafficking of newly synthesized sterol does not require vesicular transport (Baumann et al., 2005). Yeast have also been successfully used for establishing principles of membrane contact sites. Whereas mammalian contact sites may be tissue-specific or rely on dynamic switches, yeast tend to have stable contact sites as evidenced by the ER-Mitochondrial Encounter Structure (ERMES). The ERMES complex promotes ER-mitochondrial contact sites in yeast. To date the analogous complex in mammalian cells remains to be identified.

ER-PM contact sites stably occupy approximately 50% of the PM in yeast, facilitating identification of proteins that reside at these locations. Recently, six novel proteins involved in ergosterol trafficking have been identified in yeast, forming what is now known as the Lam or LCT family (Elbaz-Alon et al., 2015; Gatta et al., 2015; Murley et al., 2015). These proteins contain combinations of GRAM and START-like domains. Two such proteins have been localized to ER-PM contact sites where they facilitate the uptake of exogenously delivered ergosterol. Additional members of this family have been localized to ER-Vacuole and ER-Mitochondrial sites, sparking a search for analogous mammalian proteins. The absence of Lam/LCT family one-to-one orthologs in mammals has sparked interest in identifying mammalian proteins that may serve similar functions.

The Selective Uptake Problem

HDL cholesterol levels are inversely correlated with cardiovascular disease risk (Hoekstra, 2017). However, recent genetic studies and clinical trials suggest that elevating HDL cholesterol levels is not protective per say. For example, a recent report identified a homozygous

SR-B1 missense mutation in a human subject associated with increased coronary heart disease despite an increased plasma HDL cholesterol concentration (Zanoni et al., 2016). Likewise, SR-B1 loss of function mutations in mice result in elevated HDL cholesterol levels and accelerated atherosclerosis (Braun et al., 2002). As a result, the consensus in the field has been that the functional activity of HDL, i.e. the flux of cholesterol to and from HDL, is more protective than merely its concentration.

In physiology, SR-B1 not only mediates reverse cholesterol transport but is also key to steroidogenesis (Shen et al., 2018). Ablation of SR-B1 or ApoA1 in mice results in the near absence of CE containing lipid droplets, suggesting that selective uptake provides most of the cholesterol needed for steroidogenesis. In humans, SR-B1 may also be important in steroidogenesis as individuals with *SR-B1* mutations have diminished adrenal steroid production (Shen et al., 2018; Vergeer et al., 2011).

In contrast to the clathrin-dependent LDL uptake pathway that has been well-elucidated, the selective uptake pathway involved in HDL cholesterol uptake is poorly understood. HDL binding to the cell surface is distinct from that of LDLR-mediated internalization. Instead of being internalized, HDL particles bind to SR-B1 on the cell surface and CEs are selectively transferred with cholesterol to the PM. In support of this model, crystallization of the SR-B1 homolog, LIMP-2 demonstrated the existence of a hydrophobic channel of sufficient size for cholesterol and CE passage (Neculai et al., 2013; Shen et al., 2018). But what happens next? The mechanisms that mobilize cholesterol or CE downstream of SR-B1 mediated uptake have not been identified.

In this dissertation, I identify and characterize three GRAM domain-containing proteins, Aster-A, Aster-B, and Aster-C (encoded by the genes *Gramd1a*, *Gramd1b*, and *Gramd1c*). My

interest in studying this family began with my discovery that *Gramd1b* is an LXR target gene. Through study of the Aster family I provide the first formal proof of the importance of PM to ER cholesterol trafficking to physiology *in vivo.* I determine the structure of the sterol liganded ASTER domain with atomic resolution and demonstrate this domain binds and transfers cholesterol between membranes. I further identify the Aster family as integral ER proteins that are recruited to ER-PM contact sites in response to cellular cholesterol loading. Using antisense oligonucleotides against Aster-A and an Aster-B knockout mouse, I demonstrate that Aster proteins are critical mediators of PM to ER cholesterol trafficking *in vitro* and *in vivo*. Finally, Aster-B is critical to SR-B1-mediated selective uptake in the adrenal glands, providing an explanation for how cholesterol is trafficked downstream of SR-B1 at the PM and upstream of the ER-resident ACAT enzyme.

Chapter 2:

Aster Proteins Facilitate Nonvesicular Plasma Membrane to ER Cholesterol Transport in Mammalian Cells

Aster proteins facilitate nonvesicular plasma membrane to ER cholesterol transport in mammalian cells

Jaspreet Sandhu[1,2], Shiqian Li[7,8#], Louise Fairall[10#], Simon G. Pfisterer[7,8#], Jennifer E. Gurnett[10], Xu Xiao[1], Thomas A. Weston[4], Dipti Vashi[10], Alessandra Ferrari[1], Jose L. Orozco[1], Celine L. Hartman[9], David Strugatsky[5], Stephen D. Lee[1], Cuiwen He[3], Cynthia Hong[1], Haibo Jiang[12], Laurent A. Bentolila[6], Alberto T. Gatta[11], Tim P. Levine[11], Annie Ferng[13], Richard Lee[13], David A. Ford[9], Stephen G. Young[3,4], Elina Ikonen[7,8,14], John W.R. Schwabe[10,14] and Peter Tontonoz[1,2,14*]

[1]Department of Pathology and Laboratory Medicine
[2]Molecular Biology Institute
[3]Department of Medicine, Division of Cardiology
[4]Department of Human Genetics
[5]Department of Chemistry and Biochemistry
[6]California NanoSystems Institute
University of California, Los Angeles, CA 90095 USA

[7]Department of Anatomy and Research Programs Unit, Faculty of Medicine, University of Helsinki, Helsinki 00290, Finland.

[8]Minerva Foundation Institute for Medical Research, Helsinki 00290, Finland.

[9] Edward A. Doisy Department of Biochemistry and Molecular Biology, and Center for Cardiovascular Research, Saint Louis University School of Medicine, St. Louis, MO 63104, USA.

[10]Institute of Structural and Chemical Biology, Department of Molecular and Cell Biology, University of Leicester, Leicester. LE1 7RH

[11]Department of Cell Biology, UCL Institute of Ophthalmology, London, United Kingdom

[12]Centre for Microscopy, Characterisation and Analysis, University of Western Australia, Perth 6009, Australia

[13]Ionis Pharmaceuticals, Carlsbad, California 92008, USA

[14]Senior Author

[#]Equal contributions

*Lead Contact. To whom correspondence should be addressed at ptontonoz@mednet.ucla.edu

SUMMARY

The mechanisms underlying sterol transport in mammalian cells are poorly understood. In particular, how cholesterol internalized from HDL is made available to the cell for storage or modification is unknown. Here we describe three ER-resident proteins (Aster-A, -B, -C) that bind cholesterol and facilitate its removal from the plasma membrane. The crystal structure of the central domain of Aster-A broadly resembles the sterol-binding folds of mammalian StARD and yeast Lam proteins, but sequence differences in the Aster pocket result in a distinct mode of ligand binding. The Aster N-terminal GRAM domain binds phosphatidylserine and mediates the formation of inducible plasma membrane–ER contacts in response to cholesterol accumulation in the plasma membrane. Mice lacking Aster-B are deficient in adrenal cholesterol ester storage and steroidogenesis due to an inability to transport cholesterol from SR-BI to the ER. These findings identify a nonvesicular pathway for plasma membrane to ER sterol trafficking in mammals.

INTRODUCTION

HDL cholesterol levels in the plasma are inversely associated with coronary heart disease (CHD) risk (Emerging Risk Factors et al., 2009), but recent genetic studies have strongly implied that HDL cholesterol levels are not causally related to risk for CHD (Rader and Tall, 2012). For example, the P376L mutation in scavenger receptor class B member 1 (SR-BI) is associated with greater cardiovascular disease risk despite high plasma levels of HDL cholesterol (Zanoni et al., 2016). Mounting evidence suggests that the *function* of HDL, in particular its role in cholesterol movement in cells and tissues, may be key to its role in physiology and disease (Khera et al., 2011; Rader, 2014). HDL appears to be important in the reverse cholesterol transport pathway that brings surplus cholesterol from peripheral tissues to the liver for excretion (Braun et al., 2002). A better understanding of the pathways by which HDL cholesterol moves through cells and tissues may aid in the development of novel diagnostic tools and therapies.

Integral membrane receptors involved in cholesterol uptake at the plasma membrane (PM) have been characterized extensively, but little is known about mechanisms that traffic cholesterol from the plasma membrane to other compartments within the cell (Goldstein and Brown, 1985; Horton et al., 2002; Ikonen, 2008). Scavenger Receptor class B member 1 (SR-BI) is the principal cell-surface receptor for HDL (Acton et al., 1996). SR-BI is abundant in steroidogenic organs and the liver, where it facilitates the selective uptake of cholesterol (both esterified and unesterified) from HDL (Glass et al., 1983; Neculai et al., 2013; Williams et al., 2000). In the liver, HDL-cholesterol uptake facilitates reverse cholesterol transport by delivering surplus peripheral cholesterol to hepatocytes for secretion into bile or for conversion into bile acids (Zhang et al., 2005b). In steroidogenic organs, HDL-derived cholesterol accumulates in the form of cholesterol ester, and these stores are used for the synthesis of steroid hormones (Hoekstra, 2017). The selective HDL-cholesterol uptake pathway mediated by SR-BI is distinct from the LDLR pathway by which LDL particles are taken up and delivered to lysosomes for degradation (Goldstein and Brown, 2015b). HDL-cholesterol uptake does not require clathrin-

dependent receptor-mediated uptake or lysosomal targeting, but at this point our understanding of what happens to HDL cholesterol after SR-BI–mediated uptake is unknown. The pathways downstream of SR-BI that move cholesterol within the cell have never been defined.

Given the remarkable differences in cholesterol abundance between the plasma membrane and different cellular compartments, it seems likely that cholesterol homeostasis in mammalian cells requires the coordinated action of dedicated proteins. Dozens of candidate cholesterol-transfer proteins have been shown to be capable of mediating sterol transfer *in vitro* (Ikonen, 2008; Ikonen, in press); however, assigning physiologic functions to those proteins has proven challenging. To our knowledge, only three intracellular cholesterol-transfer proteins have been shown to have clear physiologic functions *in vivo*. The Niemann Pick type C proteins 1 and 2 (NPC1, NPC2) are critical for the export of LDL-derived cholesterol from the lysosome (Infante et al., 2008a; Infante et al., 2008b; Pfisterer et al., 2016). Mutations in either NPC1 or NPC2 lead to accumulation of lysosomal lipids *in vivo*, explaining the phenotypes associated with Niemann Pick Type C syndrome. Steroid Acute Regulatory Protein (StARD1) is required for the trafficking of cholesterol to the mitochondrial inner membrane (Arakane et al., 1998; Lin et al., 1995a; Stocco and Clark, 1996). Mutations in StARD1 are the major cause of lipoid congenital adrenal hyperplasia (Lin et al., 1995a). Recently, Song and colleagues showed that the lysosome forms contact sites with peroxisomes in the trafficking of LDL-derived cholesterol (Chu et al., 2015). The ER also makes dynamic contact sites with other organelles, and these have been proposed to facilitate the transfer of small molecules including Ca^{++} and lipids between membranes (Chung et al., 2015; Lees et al., 2017; Zhang et al., 2005a). A recent study from the Hotamisligil group has also identified a novel mechanism by which ER cholesterol content is sensed by NRF1 (Widenmaier et al., 2017). However, no mammalian transporter has yet been shown to be required for trafficking of cholesterol from the PM to the ER (Ikonen, 2008; Ikonen, in press).

Here we characterize three previously uncharacterized mammalian proteins (Aster-A, -B, and -C) that bind and transfer cholesterol between membranes. We show that Aster proteins are anchored to the ER by a single transmembrane helix and facilitate the formation of ER–PM contact sites in response to cholesterol loading. We hypothesized that the Aster proteins could be the missing links in the trafficking of HDL-derived cholesterol to the ER. In testing this hypothesis, we focused on the rodent adrenal gland, given the well-defined biological function of the SR-BI pathway in cholesterol ester storage and steroidogenesis (Connelly, 2009; Hoekstra et al., 2013; Rigotti et al., 1997). We found that Aster-B was selectively enriched in steroidogenic organs and that its expression was required for the storage of HDL-derived cholesterol ester and steroidogenesis in the adrenal cortex. Our findings elucidate a nonvesicular pathway for PM–ER sterol trafficking in mammalian cells, and they also suggest new mechanisms by which HDL-derived cholesterol is mobilized in a variety of physiological contexts.

A Family of Mammalian Lipid-Binding Proteins

We discovered that the *Gramd1b* gene was regulated by the sterol-responsive Liver X Receptors (LXRs) in mice, suggesting that it could play a role in sterol homeostasis (Janowski et al., 1996; Mangelsdorf et al., 1995). *Gramd1b* was induced by a synthetic LXR agonist in wild-type (WT) but not LXR-null mouse macrophages (Figure 1A). Moreover, ChIP-seq analyses revealed binding of LXRα and LXRβ to the regulatory regions of *Gramd1b*, identifying it as a direct transcriptional target (Figure 1B). *Gramd1b* belongs to a family of highly-conserved genes, which have been designated *Gramd1a*, *-b*, and *-c* in databases. One-to-one orthologs of *Gramd1b* are present in all vertebrate classes (Supplemental Figure 1A). The predicted amino acid sequence of the human protein is 78% identical to that from *Oreochromis niloticus* (nile tilapia). These genes have not previously been characterized; their structures are incorrectly annotated in databases; and the function of their protein products is unknown. We determined the correct exon–intron structures of *Gramd1a*, *-b*, and *-c* (Supplemental Figure 1B), which are predicted to encode proteins of 723, 699, and 662 amino acids, respectively. We will refer to the protein products as Aster-A, -B, and -C. Real-time PCR analysis of mouse tissues revealed that the three genes are expressed in a tissue-specific manner, with *Gramd1a* being most abundant in the brain; *Gramd1b* prominently expressed in steroidogenic tissues and macrophages; and *Gramd1c* expressed in liver and testes (Supplemental Figure 1C).

The Aster proteins contain an N-terminal GRAM domain, which is structurally similar to a pleckstrin homology domain (Begley et al., 2003), and a single transmembrane domain near the C-terminus (Figure 1C). The large central domain of the Aster proteins shows low sequence similarity to structurally characterized proteins. However, structural modeling programs such as Phyre and I-TASSER predicted that the central ASTER domain of Asters would resemble the sterol-binding domains from the mammalian StarD proteins and the Starkin domains from the

yeast Lam proteins, despite minimal identity at the amino acid level. Given its similarity to the structure of the START domain, we named this domain the ASTER (Greek for “star”) domain.

The ASTER Domain Binds Sterols and Promotes Sterol Transfer Between Membranes

Molecular modeling of the ASTER domain indicated the presence of a hydrophobic pocket capable of accommodating a lipophilic molecule. To test their ability of the ASTER domain to bind lipids, we expressed and purified the ASTER domains from Aster-A, -B, and -C (Supplemental Figure 1D). Using a fluorescent NBD-cholesterol binding assay, we found that all three Aster domains avidly bound sterols (Petrescu et al., 2001). As shown in Figure 1D, increasing the concentration of NBD-cholesterol (over the range 10–3,000 nM) (while maintaining the concentration of the ASTER-domain constant) increased the fluorescence emission of NBD-cholesterol. Fitting the data to a single exponential yielded an average K_d of <100 nM. By contrast, 6-NBD-cholesterol, which would place the NBD inside of the binding pocket, did not bind to the ASTER domains, indicating that only certain sterol species can be accommodated (Figure 1D) (Wei et al., 2016). Using the Aster-B ASTER domain, we further confirmed increased NBD fluorescence in response to increasing protein concentration (Figure 1E). We also confirmed direct binding of [^{3}H]cholesterol to the ASTER domain of Aster-B (Figure 1F).

Competition studies further showed that binding of NBD-cholesterol to the ASTER domain from Aster-B was inhibited by 22-R, 25-, and 20α-hydroxycholesterol in addition to cholesterol itself (Figure 1G and Supplemental Figure 1E). However, alternative sterols such as estradiol and 4β-, 22S-, and 7β-hydroxycholesterols were comparatively poor competitors. The inability of these oxysterols to compete for NBD-cholesterol binding suggests that the different ASTER domain binding affinities are not due to differences in the solubility of the different sterols. Finally, the affinity of the Asters for sterols was comparable to that of the sterol binding domain

from the canonical START domain protein StARD1 (Supplemental Figure 1F).

To test the ability of the ASTER domain to transfer cholesterol between membranes, we optimized an *in vitro* assay with heavy and light liposomes (Baker et al., 2007; Chung et al., 2015). Purified recombinant ASTER domain was incubated with "heavy" PC/dansyl-PE liposomes and "light" PC/cholesterol/dansyl-PE liposomes under agitation for 15 min. The liposomes were separated by centrifugation, and cholesterol levels were determined. Dansyl-PE intensities of heavy liposomes were used to normalize the cholesterol values. The ASTER domain from Aster-A, -B, and –C, but not BSA, efficiently facilitated cholesterol transfer to the heavy liposomes (Figure 1H). Preheating the ASTER domain to 95°C for 10 min substantially reduced its activity. Interestingly, the ASTER domains were more efficient transporters of cholesterol in this assay than the START domain of the canonical StARD1 protein (Supplemental Figure 1G). We conclude the ASTER domain efficiently binds and transfers cholesterol between membranes *in vitro*.

Crystal structure of the Aster sterol-binding domain

To determine the structure and to characterize the mode of sterol binding, we crystalized the ASTER domain from Aster A (aa: 334-562) with 25-hydroxycholesterol. The domain was expressed as a GST fusion protein in *E.coli*, purified and crystalized in the presence of 25-hydroxycholesterol. Despite the predicted similarity to the StARD and Lam proteins, solving the structure by molecular replacement proved to be challenging. A solution was found using a truncated model based on the structure of the first start domain from the yeast protein Lam4 (5YQJ) with 23% sequence identity (Tong et al., 2018). Overall the structure of the ASTER domain consists of a highly curved 7-stranded beta-sheet forming a groove to accommodate the hydroxycholesterol ligand. The cavity is closed by a long carboxy-terminal helix and two shorter helices following the amino-terminal beta-strand (Figure 2A). The electron density for the 25-

hydroxycholesterol unambiguously defined the position and orientation of the sterol, which was identical in all four molecules within the asymmetric unit (Figure 2B and Supplemental Figure 2A). Interestingly, there was additional volume within the cholesterol-binding cavity adjacent to the C3-OH group of the cholesterol. Within this volume we observed electron density for a glycerol molecule adjacent to the hydroxyl group on the cholesterol (Figure 2C and Supplemental Figure 2A). Glycerol was present during purification of ASTER domain and also used as a cryo-protectant. Interestingly the glycerol is ideally sized to fill the remaining volume of the pocket that is not occupied by the hydroxycholesterol.

Despite the relatively low sequence identity, the three-dimensional structure of Aster A broadly resembles the START domain fold, and is even more similar to the START-like domains in the Lam2 and Lam4 proteins (C-alpha RMSD c.2Å; Tong et al., 2018; Horenkamp et al., 2018; (Jentsch et al., 2018) Supplemental Figure 2B). However, sequence differences within the cholesterol binding pocket result in a different binding mode for the ligand, such that in Aster-A the sterol is rotated by approximately 120° about the long axis of ligand compared with the ligands in the START domains. This appears to be a concerted effect of multiple amino acid differences, but in particular F405, Y524 and F525 in mouse Aster-A seem to influence the ligand orientation (Figure 2B and Supplemental Figure 3A, B). Interestingly these residues are conserved in all 3 mammalian Aster proteins but not the yeast Lam proteins (Supplemental Figure 3B).

The sterol-binding pocket within the ASTER domain is largely enclosed with the exception of a relatively small opening adjacent to the loop between beta-strands 3 & 4. In order for the sterol to gain access to the pocket it is very likely that this loop will open (Figure 2D and E). In all four complexes within the asymmetric unit, this loop has relatively high B-factors or could not be modeled, consistent with conformational flexibility. Interestingly, there is an abundance of surface-exposed non-polar residues located at the “tip” of the Aster domain around the presumed opening of the sterol-binding cavity (Figure 2C and D). Alongside these

non-polar residues, are a number of conserved basic residues. These give the tip of the ASTER domain an overall positive charge but with the opportunity to make non-polar interactions. This conserved surface chemistry of Aster proteins may assist exchange of sterol with negatively-charged / non-polar phospholipid membranes through interaction with and/or partial insertion of the domain into the membrane.

Asters Are Integral ER Proteins Recruited to the Plasma Membrane by Cholesterol

The structure of the Aster proteins suggested that they may promote the transfer of cholesterol between biological membranes. A critical question, therefore, was where these proteins are located with cells. To determine the location of Aster-A, -B, and –C, we expressed N-terminally tagged fusion proteins in A431 and HeLa cells. When cultured in standard lipid-poor conditions (1% lipoprotein-deficient serum, LPDS), all three Aster proteins displayed a reticular pattern that largely overlapped with the ER marker Sec61β (Figure 3A-C and Supplemental Figure 4A). An Aster-B fusion protein lacking the GRAM domain was localized to the ER, but one containing the isolated GRAM domain was mainly located within the cytoplasm (Figure 3A). We conclude the Aster proteins tethered to the ER by a single pass transmembrane helix.

We hypothesized that the ER-localized Aster proteins might facilitate lipid transfer by making transient contacts with another cellular membrane, perhaps in response to changes in the abundance of one or more lipids. Prior work has shown that cholesterol loading by methyl-β-cyclodextrin results in rapid delivery of plasma membrane cholesterol to the ER (Das et al., 2014; Infante and Radhakrishnan, 2017). Remarkably, we found that cholesterol loading also resulted in the relocalization of all 3 Aster proteins to the periphery of the cell where they appeared to be in close proximity to the PM (Figure 3B and Supplemental 4A). To explore the association of ER-anchored Aster proteins with the PM in more detail, we generated an A431

cell line expressing both BFP-KDEL and Cherry-CAAX. We visualized the location of GFP-Aster-A, -B and -C in these cells using live cell Airyscan imaging. When cells were cultured in low-cholesterol media (LPDS), all 3 Aster proteins showed a punctate pattern of distribution in ER structures throughout the cell (Figure 3C and Supplemental Figures 4B and C). However, when cholesterol-cyclodextrin was added to the media, the Aster proteins were found almost exclusively in ER tubules that were in close proximity to the PM (yellow arrows, Figure 3E and Supplemental Figures 4B and C).

These findings suggested that Aster proteins were facilitating the formation of cholesterol-dependent PM-ER appositions by bridging the two membranes. To better define the nature of these Aster-dependent PM-ER contacts we assessed their relationship to the previously-described PM-ER contacts associated with the proteins ORP5, E-Syt2 and E-Syt3 (Chung et al., 2015; Ghai et al., 2017; Giordano et al., 2013). We generated A431 cell lines expressing both BFP-KDEL and Cherry-ORP5, Cherry-E-Syt2, or Cherry-E-Syt3. We then analyzed the cellular location of GFP-Aster-B in the presence or absence added cholesterol. In cells cultured in low-cholesterol media, ORP5, E-Syt2 and E-Syt3 were found predominantly in ER tubules located in proximity to the PM (Figure 4A and B and Supplemental Figure 4D). By contrast, Aster-B was located throughout the ER under these conditions and showed minimal colocalization with ORP5, E-Syt2 or E-Syt3. Addition of cholesterol to the cells had little if any effect on the location of ORP5, E-Syt2 or E-Syt3, but caused a dramatic relocalization of Aster-B to ER tubules that were in close proximity to the PM. Moreover, there was substantial, but not complete, overlap of Aster-B signal with signals for ORP5, E-Syt2 and E-Syt3 in cholesterol-loaded cells. Interestingly, while ER-PM contacts containing Aster-B were frequently located in the same ER tubules in which ORP5, E-Syt2 or E-Syt3 resided, domains containing only Aster-B could also be readily be identified in proximity to the plasma membrane. The colocalization of Aster-B with other PM-ER contact proteins is quantified in Figure 4C.

We further analyzed cholesterol-dependent Aster recruitment to the plasma membrane using total internal reflection (TIRF) microscopy, which permits signal detection within 100 nm of the plasma membrane. We analyzed A431 cells expressing GFP-Aster-B and Cherry-ORP5 after loading of the cells with cyclodextrin cholesterol. While ORP5 was detected in the TIRF plane regardless of cellular sterol status, Aster-B was rapidly recruited to the TIRF plane in response to cholesterol (Figure 4D and Supplemental Movie 1). We conclude from these studies that, in contrast to ORP5, E-Syt2 and E-Syt3, which reside in ER-PM contact sites regardless of cellular sterol status, Aster-B is selectively recruited to form distinct ER-PM contacts in response to excess cholesterol in the PM.

We also assessed the influence of cholesterol loading on the size of ER structures in close proximity the PM by TIRF video microscopy. U2OS cells stably expressing Cherry-KDEL were treated with control or Aster-A-specific siRNA. Video imaging was then performed to assess the size of ER foci in the TIRF plane following cholesterol loading. Cholesterol administration resulted in the enlargement of ER-structures in close proximity to the plasma membrane and this effect was dependent on Aster-A expression (Figure 4E).

The Gram Domain Mediates Cholesterol-Dependent Aster Localization at the Plasma Membrane

The Aster proteins contain an N-terminal GRAM domain, a structural motif related to the pleckstrin homology domain that is found in glucosyltransferases, Rab-like GTPase activators, myotubularins, and other membrane-associated proteins (Doerks et al., 2000). Interestingly, the GRAM domains of myotubularins have been shown to interact with phospholipids (Begley et al., 2003). We found that purified Aster-B GRAM domain interacted strongly with both phosphatidylserine (PS) and phosphatidic acid (PA) (Figure 5A). Given that phosphatidylserine is highly enriched in the inner leaflet of the PM, we further determined if the Aster-B GRAM domain was associated with phosphatidylserine-containing liposomes. Co-sedimentation

assays revealed that the GRAM domain pelleted with phosphatidylserine-containing, but not phosphatidylcholine-containing, liposomes (Figure 5B). The inclusion of cholesterol in PS-containing liposomes did not enhance their association with the GRAM domain.

To determine if the Aster GRAM domain is required for the formation of Aster-dependent ER–PM contact sites, we transfected Hela and A431 cells with mutant form of Aster-B in which the GRAM domain had been deleted (Figure 5C and Supplemental Figure 4E). Loss of the GRAM domain abolished recruitment of Asters to the PM in response to cholesterol loading. We also expressed the Aster-B GRAM domain alone in CHO-K1 and A431 cells (Figure 5D and Supplemental Movie 2). Under basal culture conditions, the soluble GRAM domain was cytoplasmic, but it was recruited to the PM upon cholesterol loading. TIRF microscopy confirmed that C-terminal GFP-tagged Aster-B GRAM domain was largely cytoplasmic in cells cultured in medium containing lipoprotein-deficient serum (LPDS) but that it was recruited to the PM in a time- and concentration-dependent manner after cholesterol loading (Figure 5E and Supplemental Movies 3 and 4). We conclude that the phosphatidylserine-binding GRAM domain is both necessary and sufficient for cholesterol-dependent Aster redistribution to the PM.

Aster-B Is Required for Adrenal Sterol Homeostasis

Movement of cholesterol from the PM to the ER is believed to be an important step in the utilization of HDL-derived cholesterol after selective uptake by SR-BI. We hypothesized that Asters may contribute to cholesterol transport from SR-BI at the PM to the ER. To test this idea, we focused on the rodent adrenal gland, which depends on SR-BI–mediated uptake of HDL cholesterol for steroidogenesis (Connelly, 2009; Hoekstra et al., 2008; Rigotti et al., 1997). Among the Aster proteins, Aster-B exhibited the highest expression in the adrenal gland, suggesting that it was likely to be the most physiologically relevant Aster family member in this

tissue (Supplemental Figure 5A) (Consortium, 2012). Using an antibody that we generated against Aster-B, we confirmed that Aster-B is expressed at high levels in the adrenal, similar to SR-BI (Figure 6A).

To assess the physiological relevance of cholesterol transport by Aster-B, we generated knockout mice by CRISPR/Cas9 genome editing. We deleted exon 7, which results in a frameshift mutation (Supplemental Figure 5B). We confirmed the absence of Aster-B in homozygous Aster-B knockout mice (Figure 6B). By visual inspection, the adrenal glands of Aster-B–deficient mice were red (rather than a pinkish white), suggesting an absence of cholesterol ester stores (Figure 6C). Indeed, oil red O staining revealed a complete loss of neutral lipid stores in the adrenal cortex in Aster-B–deficient mice (Figure 6D), and electron microscopy revealed a complete absence of cytosolic lipid droplets (Figure 6E). Analysis of tissue lipids showed that, while levels of free cholesterol in the adrenal gland were not different between genotypes, loss of Aster-B expression led to a dramatic decrease in cholesterol esters (Figure 6F, G). These findings show that loss of Aster-B expression abolishes tissue cholesterol homeostasis *in vivo*.

Aster-B Promotes PM to ER Cholesterol Transport

We also investigated the consequence of loss of Aster function for sterol movement from the PM to the ER in cultured cells. Since Aster-B expression is minimal in most cultured cell lines, we chose to knockdown Aster-A expression, which is abundant 3T3-L1 cells. When ER cholesterol levels rise, cells respond first by suppressing SREBP-2 cleavage (thereby blocking sterol synthesis) and second by activating ACAT-dependent CE synthesis (Brown and Goldstein, 1997; Lange et al., 1999; Radhakrishnan et al., 2008; Xu and Tabas, 1991). We therefore assessed cholesterol movement to the ER following exogenous delivery by measuring two endpoints: 1. the activity of the SREBP-2 pathway and 2. the formation of cholesterol

esters. Treatment of 3T3-L1 cells with an Aster-A-specific ASO (which nearly abolished *Gramd1a* expression; Figure 7) led to induction of SREBP-2 processing, increased LDLR protein levels, and increased expression of SREBP-2 target genes, including *Hmcgr,* and *Hmgcs* (Figure 7A and B). Such a change SREBP-2 processing is demonstrative of a change in ER cholesterol levels (Brown and Goldstein, 1997). Moreover, the ability of exogenously added cyclodextrin-cholesterol to suppress SREBP-2 processing was clearly delayed in Aster-A silenced cells. The fact that some suppression of the SREBP-2 pathway at later time points was still observed even with Aster-A ASO was not unexpected, since vesicular sterol transport pathways were presumably still operative. Interestingly, expression of *Abca1*, which is controlled by the sterol-activated nuclear receptor LXR, was reciprocally reduced in the absence of Aster-A, both at the protein (Figure 7A) and the mRNA level (Figure 7C), consistent with reduced intracellular cholesterol availability.

To assess the effects of Aster deficiency on CE production, cells were incubated in the presence of [^{3}H]oleate, treated with cyclodextrin-cholesterol complexes, and the incorporation of label into CE was quantified. We found that the rate at which cholesterol delivered to the PM was incorporated into CE was markedly slower in cells in which Aster-A was silenced (Figure 7D). Two hours after cholesterol addition the amount of CE formed in Aster-A-silenced cells was less than 25% of controls cells. Again, the fact that some CE could still be formed in the absence of Aster-A was not unexpected given that vesicular transport pathways were intact.

Rodent adrenal glands rely on the selective uptake of HDL-cholesterol by SR-BI to provide free cholesterol for the generation of cholesterol esters by the ER enzyme ACAT1 (Meiner et al., 1996a; Rigotti et al., 1997). Interestingly, the adrenal phenotype of Aster-B knockout mice is virtually identical to that described for mice lacking SR-BI or ACAT1 (Hoekstra et al., 2008; Hoekstra et al., 2013; Meiner et al., 1996a; Rigotti et al., 1997). To further address whether Aster-B plays an important role in facilitating the transport of HDL cholesterol, we asked whether HDL-mediated cholesterol delivery to cells affects Aster-B localization. We expressed both

Aster-B and SR-BI in A431 cells and incubated them with HDL (Supplemental Figure S6A, B). TIRF microscopy showed that incubation of cells with HDL2 stimulated recruitment of Aster-B to the PM (Supplemental Figure 6C-E).

We next assessed whether Aster-B was important for cholesterol delivery to adrenal cortical ER *in vivo*. A failure to transport HDL-cholesterol from SR-BI at the PM to the ER in adrenocortical cells would be expected to reduce levels of cholesterol in the ER and render the cells dependent on endogenous cholesterol synthesis for production of cortisol (Hoekstra et al., 2008; Rigotti et al., 1997; Temel et al., 1997). To test whether the ER in Aster-B adrenal cortex was deficient in cholesterol, we analyzed expression of SREBP-2 target genes, whose expression is tightly linked to the cholesterol content of ER membranes (Brown and Goldstein, 1997). SREBP-2 target gene expressing in the adrenal was far higher in Aster-B-deficient mice than in WT mice (Figure 7E), indicating that the ER is starved for cholesterol in the absence of Aster-B. To confirm that Aster-B deficiency promotes SREBP-2 processing in mice, we prepared nuclear fractions from the adrenal in WT and Aster-B knockout mice. We found that the nuclear fractions from Aster-B–deficient adrenal glands had dramatically increased levels of the mature SREBP-2, despite comparable levels of the membrane-bound SREBP-2 precursor (Figure 7F). We also observed normal to elevated levels of SR-BI in Aster-B–deficient mice, indicating that the phenotype was not an indirect consequence of SR-BI deficiency (Figure 7F).

Cholesterol esters are utilized, particularly during times of stress, for generating corticosteroids. To assess the physiologic consequence of Aster-B deficiency for steroidogenesis, we assessed both serum cholesterol and corticosterone levels. While serum cholesterol levels did not differ significantly between WT and Aster-B knockout mice (Figure 7G), basal serum corticosterone levels were lower in Aster-B knockout mice than in controls (Figure 7H). The induction of stress through an overnight fast exacerbated the deficiency in corticosterone (Hoekstra et al., 2008). By contrast, levels of epinephrine and dopamine (non-

steroid mediators made by the adrenal medulla) were not different between groups (Supplemental Figure 6F).

Collectively, our data demonstrate that Aster-B moves cholesterol from the PM to the ER downstream of the HDL receptor SR-BI (Supplemental Figure 7). To our knowledge, Aster-B is the only mammalian PM–ER cholesterol transporter to show a loss-of-function phenotype *in vivo* and to be implicated in the transport of HDL-derived cholesterol.

DISCUSSION

How cholesterol moves between the PM and the ER in mammalian cells has been a longstanding conundrum. Here we have characterized and determined the atomic structure of three mammalian ER-resident lipid transport proteins. Cell-based studies indicated that Aster proteins bind sterols through their ASTER domain and phosphatidylserine through their N-terminal GRAM domain. Remarkably, Aster proteins are able to sense changes in PM cholesterol and drive the formation of ER–PM contact sites when PM cholesterol levels are elevated. We further showed that one member of this family, Aster-B, is highly expressed in steroidogenic tissues and is required for the ability of HDL-cholesterol to move to the ER in adrenocortical cells and to be stored as cholesterol esters. These studies outline a critical function for Aster-B in nonvesicular transport of cholesterol in mammalian cells, and raises the possibility that other members of the Aster family could play important roles in facilitating ER–PM cholesterol movement in other cell types.

Trafficking of cholesterol between the ER and PM has long been recognized to occur through rapid nonvesicular mechanisms. Studies have emphasized the ability of the ER to sense fluctuations in PM cholesterol and to link these with regulation of the sterol-sensing SREBP-2 pathway, and more recently with NRF1 (Das et al., 2014; Das et al., 2013; Infante and Radhakrishnan, 2017; Widenmaier et al., 2017). Excess free cholesterol in the PM leads to increased cholesterol in the ER, resulting first in the suppression of SREBP-2 cleavage and cholesterol biosynthesis, and at higher concentrations to the generation of cholesterol esters by ACAT enzymes. Many putative sterol-trafficking proteins have been identified by *in vitro* experiments. However, defining the physiologic roles of these proteins has been challenging because of the absence of clear loss-of-function phenotypes. It has been suggested that assigning functions to these proteins may be complicated by redundancy, but an alternative possibility is that the various lipid-binding proteins have not yet been associated with the correct biological function. For example, the Osh family in yeast (OSBP family in mammals) was previously proposed to mediate PM to ER sterol trafficking; however, deletion of all Osh family

members did not block the trafficking, suggesting that they may perform alterative functions (Georgiev et al., 2011).

Defining the physiologic roles of mammalian START family proteins, which lack one-to-one orthologs in invertebrates, have proven particularly difficult. The founding member of the family, StARD1, is the only one that has been shown to mediate cholesterol trafficking *in vivo* in both mice and humans (Caron et al., 1997; Lin et al., 1995b). StARD1 mutations result in defective trafficking of cholesterol to the mitochondrial inner membrane and cause a massive accumulation of cholesterol esters in the adrenal—a phenotype opposite to that elicited by Aster-B deficiency. START-like domains with homology to the ASTER domain have been previously identified through bioinformatics approaches in plants, yeast, and other lower organisms (Elbaz-Alon et al., 2015; Gatta et al., 2015; Khafif et al., 2014; Murley et al., 2015). In yeast, a family of six Ltc proteins was identified that contain combinations of one or more GRAM domains, START-like domains, and transmembrane segments (Elbaz-Alon et al., 2015; Gatta et al., 2015; Horenkamp et al., 2018; Murley et al., 2015; Tong et al., 2018; Wong and Levine, 2016). These proteins have been linked to ergosterol transport at the ER–PM, ER–mitochondria, and ER–vacuole contact sites. However, one-to-one orthologs for the Aster proteins are restricted to vertebrates, where they appear to have evolved alongside SR-BI and other proteins involved in lipoprotein metabolism. In contrast to yeast, higher organisms must move lipids between tissues to maintain systemic homeostasis. It is therefore logical that mammals would have evolved specific transporters to facilitate the movement of lipoprotein-derived cholesterol into cells. Indeed, key residues lining the ASTER domain sterol-binding pocket are not conserved in yeast STAR-like domain proteins, resulting in a distinct mode of ligand binding. Finally, since, our studies indicate that all three Aster proteins are likely to be involved in ER-PM sterol transport, identification of the mammalian proteins that mediate cholesterol trafficking between the ER and other cellular compartments remains an important goal for future studies.

One of the most remarkable features of the Aster proteins is their ability to localize to the PM based on the level of cholesterol in the membrane. Interestingly, NPC1L1, which facilitates intestinal cholesterol absorption, also relies on a cholesterol-mediated switch (Ge et al., 2008). NPC1L1, the target of the cholesterol-lowering drug ezetimibe, is internalized with cholesterol at the PM and then traffics to endosomes. This effect relies on a sterol-sensing domain (SSD) in NPC1L1. The mechanism of Aster recruitment by cholesterol appears to be distinct. The Aster GRAM domain, which binds phosphatidylserine rather than cholesterol, is necessary and sufficient for PM localization in response to cholesterol loading. Phosphatidylserine is enriched on the inner leaflet of PM; hence, phosphatidylserine binding by the GRAM domain could mediate PM localization of Asters (Vance and Steenbergen, 2005; Yeung et al., 2008). An open question is why the Aster GRAM domain is able to recognize phosphatidylserine only in the presence of excess membrane cholesterol. Additional studies will be needed to test whether cholesterol loading changes the biophysical presentation of phosphatidylserine, stimulates the generation of other plasma membrane lipids, or triggers the production of secondary messengers.

While ER–PM junctions are stable and prominent in yeast, they appear to have more dynamic and tissue-adapted roles in mammalian systems (*e.g.,* STIM1, E-Syts) (Zhang et al., 2005a). While this paper was under review, Nunnari and colleagues reported that Gramd2 and Gramd1a (Aster A) were localized in ER-PM contact sites (Besprozvannaya et al., 2018). Gramd2 has an N-terminal GRAM domain and is anchored in the ER like the Aster proteins, but lacks the central sterol-binding fold. Recent work suggests that Gramd2 may participate in cellular calcium homeostasis (Besprozvannaya et al., 2018). Our data have revealed that the Aster proteins are unique among known ER-PM contact proteins in their ability to form membrane bridges in a cholesterol-dependent manner. Interestingly, we observed substantial, but not complete, colocalization of Aster-B with ORP5, E-Syt2 and E-Syt3 in cholesterol-loaded cells. ER-PM contacts containing Aster-B were frequently located in the same ER tubules in

which ORP5, E-Syt2 or E-Syt3 were found, but some contacts appeared to contain only Aster-B, consistent with the idea that they are functionally distinct. The questions of whether other proteins such as E-Syts help to stabilize Aster-dependent contacts and whether lipid transport by ORP5 and Asters is coordinated remain to be addressed.

The striking phenotype of Aster-B-deficient mice suggests principles that are likely to be relevant to understanding the functions of other Aster family members in other contexts. The trafficking of cholesterol from the PM to the ER and *vice versa* is likely to be critical for lipid homeostasis in many if not all cells. Furthermore, the cell type–selective expression of Aster proteins in tissues with active lipid metabolic programs suggests that Asters are likely to play important roles in sterol transport and HDL metabolism in other tissues. For example, while Aster-B is expressed at low levels in the liver, other Asters are abundant. Given that the liver is an important destination for HDL-cholesterol, it will be of interest to determine whether Aster proteins function downstream of SR-BI in that tissue. The high level of Aster-A expression in the brain suggests that this family member could be particularly important for sterol trafficking in neurons (about which very little is known).

We expect that future studies will uncover roles of Asters in disease. In humans, SR-BI mutations have been linked to adrenal disease (Vergeer et al., 2011). Aster-B was recently reported to exist among uncharacterized proteins that are induced during the development of human adrenal glands (Del Valle et al., 2017). Our study will likely prompt geneticists to search for Aster-B mutations in humans with adrenal disease, for example patients with congenital adrenal hyperplasia or hypocortisolism. Furthermore, the numerous links between defective cholesterol metabolism and human pathologies underscore the importance of understanding the mechanism of cellular sterol transport. Uniting the function of individual cholesterol trafficking proteins *in vitro* with their physiologic roles *in vivo* will advance our understanding of physiology and may highlight opportunities to target lipid metabolism in the treatment and diagnosis of human disease.

ACKNOWLEDGMENTS

We thank Jason Kim, Prashant Rajbhadari and Tamer Sallam for technical assistance and experimental guidance. J.S. was supported by the UCLA Medical Scientist Training Program (NIH training grant GM08042) and also supported by NIH T32HL69766 and the Philip Whitcome Fellowship. J.O. was supported by NIH 5T34GM008563. This research was also supported by NIH grants HL066088, DK100627, S10RR019232 and GM115553, Academy of Finland grants 307415, 312491 (to E.I.) and 275964 (to S.P.), and grant from Sigrid Juselius Foundation (E.I.), and the Helsinki Institute of Life Science infrastructures Biomedicum Imaging Unit and Biomedicum Functional Genomics Unit. J.W.R.S. is a Wellcome Trust Senior Investigator (grant WT100237) and Royal Society Wolfson Research Merit Award Holder. Confocal laser scanning microscopy was performed at the California NanoSystems Institute (CNSI) Advanced Light Microscopy/Spectroscopy Shared Resource Facility at UCLA. Electron microscopy was performed at the Electron Imaging Center for Nanomachines (EICN) at CNSI. We thank Diamond Light Source for beamtime (proposal MX14692), and the staff of beamlines I04-1, I03 and I24 for assistance with crystal testing and data collection. We thank Sharon Munday (PROTEX, University of Leicester) for the cloning of the constructs used in the crystallization experiments. We dedicate this manuscript to the memory of Jaspal Singh Sandhu. His courageous battle with coronary artery disease has been a key inspiration to this work.

AUTHOR CONTRIBUTION

Conceptualization, J.S., E.I., S.G.Y., J.W.R.S., P.T.; Methodology, J.S., S.L., S.G.P., J.L.O., A.F., R.L., D.A.F., E.I., S.G.P.; Investigation, J.S., S.L., T.W., S.G.P., J.E.G., D.V., D.A.F., X.X., A.F., L.F., J.L.O., C.L.H., D.S., S.D.L., C.H., L.A.B.; Writing – Original Draft, J.S., J.W.R.S., P.T.; Writing – Review & Editing, J.S., P.T., J.W.R.S., E.I., S.G.Y.; Funding Acquisition, D.A.F.,

J.W.R.S., C.H., S.G.Y., E.I., P.T.; Resources, L.B., D.A.F., A.F., R.L., J.W.R.S., S.G.Y., E.I., P.T.; Supervision, P.T., J.W.R.S., E.I., S.G.Y.

CONFLICTS OF INTEREST

The authors declare no conflicts of interest.

FIGURE LEGENDS

Figure 1. Aster Proteins Contain a Lipid-Binding Fold

(A) Gene expression was quantified by real-time PCR from WT (white) and LXR-null (*LXRα*−/− and *LXRβ*−/−, red) mouse peritoneal macrophage. Cells were kept in 1% lipoprotein deficient serum (LPDS, 1%), 5 μM simvastatin and 100 μM mevalonate overnight, then treated with LXR ligand GW3965 (GW, 1 μM), or LXR ligand plus RXR ligand LG 100754 (LG, 100 nM) for 16 h. Values are means ± SEM. Results are representative of three independent experiments.

(B) ChIP-Seq bedgraph of LXRα and LXRβ binding patterns in mouse immortalized macrophages at the promoter region of the *Gramd1b* locus of chromosome 9 (Sallam et al., 2018; Sallam et al., 2016; Zhang et al., 2017). Input (Ctrl) served as a control for LXR enrichment.

(C) Schematic representation of Aster-A, Aster-B, and Aster-C proteins. The N-terminal GRAM (green), central ASTER (blue) and transmembrane (TM, red) domains are indicated.

(D) Purified Aster domains (Aster-$A_{261-576}$, Aster-$B_{224-560}$, and Aster-$C_{206-528}$) bind to 22-NBD-cholesterol but not 6-NBD-cholesterol (right) with nanomolar affinity. Values are means ± SEM.

(E) Aster-$B_{334-562}$ (1-10 μM) was titrated with 10–3000 nM 22-NBD-cholesterol in PBS and fluorescent ligand-binding assays were performed as described in Methods.

(F) Binding of [^{3}H]cholesterol to purified Aster-$B_{224-560}$ was assessed using a GST-agarose-based assay as described in methods. Protein was incubated with [^{3}H]cholesterol in 1x PBS

binding buffer containing 0.003% Triton X-100 and protein-bound cholesterol separated using GST-agarose columns. Competition assays were performed using increasing concentrations of unlabeled cholesterol as indicated. Results values are means ± SD.

(G) Aster-$B_{334-562}$ was titrated with 22-NBD-cholesterol in the presence of vehicle, estradiol, or various hydroxycholesterol (HC) sterol competitors as indicated (10 μM). Results values are means ± SD.

(H) Sucrose-loaded heavy PC/Dansyl-PE liposomes 85:15 mol/mol, 2 mM lipids, 400 nm diameter) and light PC/Dansyl-PE-Cholesterol liposomes (80:15:5 mol/mol/mol, 2 mM lipids, 100 nm diameter) were incubated with no protein (buffer) or with 5 μM albumin, pre-heated Aster-$B_{224-560}$ (left, 95°C x 10 min), or native Aster-$A_{261-576}$, Aster-$B_{224-560}$, and Aster-$C_{206-528}$ (right) for 20 min at 25°C. After centrifugation, pellet fractions were collected, and the cholesterol recovered in the heavy fraction was assessed using a cholesterol oxidase (Sigma-Aldrich) assay. Pellet fractions were normalized by dansyl-PE recovery and the cholesterol/dansyl-PE ratio was compared with that of the light liposome sample (% transfer). Purified Aster domains from Aster-A, Aster-B, and Aster-C rapidly transferred cholesterol between the artificial phospholipid bilayers. Values are means ± SEM. All results are representative of at least two independent experiments. See also Supplemental Figures 1E-G.

Figure 2. Crystal structure of the sterol-binding domain of Aster-A

(A) The crystal structure of the ASTER domain of the mouse Aster-A. The ribbon representation is colored from blue-red amino-carboxy terminus. The 25-hydroxycholesterol ligand is shown as atomic spheres: grey-carbon, red-oxygen. The right-hand panel is rotated 90°about the indicated axis. The ligand-binding pocket is situated between a concave beta-sheet and a long carboxy-terminal helix.

(B) Details of the 25-hydroxycholesterol ligand-binding pocket. The left-hand panel shows key sidechains within the ligand pocket that mediate interaction with the ligand. In particular,

Phe405, Tyr524 and Phe525 (cyan) seem to determine the orientation of the ligand and are markedly different in character from the equivalent residues in the yeast Lam proteins (see also Supplemental Figure 3).

(C) Cut-away view of the surface of mouse Aster A to show the ligand-binding pocket. It is notable that the ligand is completely enclosed with the exception of an opening towards the left of the pocket. The pocket is significantly larger than the ligand beyond the C3-OH group. This additional space is occupied by a glycerol molecule in all four copies of the complex in the asymmetric unit.

(D-E) Potential mechanism for loading cholesterol into the ASTER domain. Structural rearrangements would be essential for cholesterol to gain access to the binding pocket. This is very likely to involve the loop comprising amino acids 430-439 that wraps around the ligand. Interestingly the surface of this region of the ASTER domain is relatively non-polar in character (see labeled amino acids), but with a number of prominent basic residues. It seems likely that this region of the protein will come into contact with the negatively charged / non-polar lipid bilayer into order to facilitate both loading and unloading of the cholesterol ligand. See also Supplemental Figures 2 and 3.

Figure 3. Asters are Integral ER Proteins that Form PM Contact Sites in Response to Cholesterol.

(A) Comparative analysis of the cellular localization of full-length (1-699), B ΔGRAM (225-669), or B GRAM (1-171) alone (indicated above) Aster-B-GFP constructs with ER marker (Sec61β) in HeLa cells imaged by live-cell confocal microscopy. Scale bar 5 μm.

(B) Analysis of Aster-B-GFP (N-terminal, 1-738) localization and PM (CellMask PM stain) in A431 cells imaged by confocal microscopy. Cells were cultured in lipoprotein-deficient serum (LPDS; 5%) or loaded with cholesterol by the addition of 200 μM cholesterol:cyclodextrin complex for 1 h. Images were taken from live cells. Scale bar 5 μm. See also Supplemental

Movie 1.

(C) Live-cell imaging of GFP-Aster-B localization in A431 cells stably expressing BFP-KDEL (ER marker) and Cherry-CAAX (PM marker). Yellow arrows indicate ER tubules in close proximity to the PM containing foci of Aster-B expression. Results are representative of three independent experiments. Large images, scale bar = 10 μm; insets, scale bar = 2 μm. See also Supplemental Figure 4A-C.

Figure 4. Aster-B forms ER–PM Contacts in Response to Cholesterol Loading.

(A) Live-cell imaging of GFP-Aster-B localization in A431 cells stably expressing BFP-KDEL (ER marker) and Cherry-ORP5 (ER-PM contact protein) cultured in 5% LPDS (left) or following cholesterol loading for 20 min (right). Large images, scale bar = 10 μm; insets, scale bar = 2 μm.

(B) Live-cell imaging of GFP-Aster-B localization in A431 cells stably expressing BFP-KDEL (ER marker) and Cherry-E-Syt2 (ER-PM contact protein) cultured in 5% LPDS (left) or following cholesterol loading for 40 min (right). Large images, scale bar = 10 μm; insets, scale bar = 2 μm.

(C) Quantification of Aster-B colocalization with ER-PM contact proteins. Quantification was done by selecting a square region from the bottom plane (near the PM), thresholding the punctate structures, and calculating their pixel overlap by using a colocalization tool. N = 8-12 cells per construct and treatment from 2 independent experiments.

(D) Time course of Cherry and GFP fluorescence visible in the total internal reflection fluorescence (TIRF) (basal PM-associated fluorescence) field of A431 cells expressing with GFP-Aster-B and Cherry-ORP5 after the addition of cyclodextrin-cholesterol to the media.

(E) Quantification of TIRF video imaging of stable U2OS Cherry-KDEL cells treated with control or Aster-A-specific siRNA following addition of cholesterol. Video imaging was started 40 s to 90 s after addition of 1 mM cholesterol. Images were acquired every minute. Cholesterol administration resulted in the enlargement of ER-structures in close proximity to the

plasma membrane and this effect is dependent on Aster-A expression. See also Supplemental Figure 4D.

Figure 5. The GRAM Domain Mediates Cholesterol-dependent Aster Recruitment

(A) Protein-lipid overlay over purified mouse Aster-B GRAM domain with various phospholipid species. PA and PS correspond to phosphatidic acid and phosphatidylserine, respectively.

(B) Purified Aster-B GRAM domain was incubated with sucrose-loaded heavy liposomes containing Dansyl-PE and 80-85% PC or 80-85% PS +/- 5% Cholesterol. Liposomes were sedimented, washed, and analyzed by immunoblotting for associated Aster-B Gram protein (anti-His antibody).

(C) Localization of full-length and B ΔGRAM Aster-B-GFP (green) constructs with plasma membrane (magenta, CellMask stain) expressed in HeLa cells in the presence or absence of cholesterol loading imaged by live cell confocal microscopy.

(D) Comparative analysis of localization of B GRAM-GFP in CHO-K1 cells (left) and A431 cells (right) culture in LPDS (top) loaded with cholesterol (bottom). The GRAM domain is recruited to the PM in response to cholesterol-loading. PM marker: PM-cherry; ER marker: mCherry-Sec61β. Scale bar: 5 μM. Results are representative of at least five independent experiments. See also Supplemental Movie 2.

(E) Quantification of Aster-B PH-EGFP intensity in the TIRF plane upon cholesterol loading (left panel; n = 2-3 cells, error bars +/- SD). Representative TIRF images (right panel) from GFP and Aster-B PH domain-EGFP expressing cells at the indicated time following cholesterol loading. TIRF videos recorded 5 slices (slices 3-5 were used to calculate F0) before cholesterol addition. See also Supplemental Movie S3 and S4. All results are representative of at least two independent experiments. See also Supplemental Figure 4E.

Figure 6. Aster-B Ablation Disrupts Adrenal Cholesterol Homeostasis

(A) Immunoblot analysis of SR-BI and Aster-B in various tissues from 7-week-old C57BL/6J mice. HMGB1 was used as a loading control.

(B) Representative immunoblot from adrenal lysates of WT and Aster-B KO mice.

(C) Gross appearance of adrenal glands from representative 6-week-old WT and Aster-B knockout mice (1 mm scale). Results are 100% penetrant and representative of at least ten independent mice of both genders.

(D) Histological sections of the adrenal cortex from wild-type and Aster-B KO mice stained with oil red O. Representative of eight images per group; 12 μm sections; cale bar: 50 μm.

(E) Representative electron micrographs of adrenal fasciculata cells from WT and Aster-B KO adrenal sections. Samples were fixed and processed as described in the Methods. Lipid droplets, nuclei and mitochondria are indicated (LD, N, MT; N = 2 mice, 35-52 sections each).

(F) ESI-MS/MS analysis of the abundance of free cholesterol in adrenal glands from WT and Aster-B KO mice (n=7). Statistical analysis was performed using Student's t-test. Values are mean ± SEM.

(G) ESI-MS/MS analysis of the abundance of cholesterol ester species in adrenal glands from WT and Aster-B KO mice (N = 7). Statistical analysis was performed using Student's t-test. Values are means ± SEM. *p < 0.05; **p < 0.01; ***p<0.001; ****p<0.0001. All results are representative of two independent experiments.

Figure 7. Aster-B-Deficient Mice Are Defective in PM to ER Cholesterol Transport

(A) Immunoblot analysis of membrane (top) and nuclear (bottom) protein levels in 3T3-L1 cells treated for 48 h with control or Aster-A-specific ASO and then for the indicated times with cyclodextrin-cholesterol. Calnexin was used as a membrane loading control and Lamin A/C as a nuclear loading control.

(B) Realtime PCR analysis of gene expression in 3T3-L1 cells treated for 48 h with control or Aster-A-specific ASO and then for the indicated times with cyclodextrin-cholesterol. ***p<0.001.

(C) Realtime PCR analysis of Abca1 expression in 3T3-L1 cells treated for 48 h with control or Aster-A-specific ASO and then for the indicated times with cyclodextrin-cholesterol. **p<0.01.; ***p<0.001.

(D) Time course of cholesteryl ester formation in 3T3-L1 fibroblasts treated with control or Aster-A-specific ASO for 48 h. Cells were incubated with [^{3}H]oleate for the indicated time, CE was isolated by TLC, and the incorporation of label into CE quantified by scintillation counting and normalized to protein (mg). *p < 0.05; ***p<0.001.

(E) Expression levels of the indicated genes in adrenal glands from WT and Aster-B KO mice (mean ± SEM; N = 6-8 per group). Statistical analysis was performed using Student's t-test. Values are means ± SEM. *p < 0.05; **p < 0.01; ***p<0.001; ****p<0.0001.

(F) Immunoblot analysis of membrane (top) and nuclear (bottom) protein levels in adrenals from WT and Aster-B KO mice (n=5). Calnexin was used as a membrane loading control and Lamin A/C as a nuclear loading control.

(G) Serum cholesterol levels in WT and Aster-B KO mice that were fasted for five h (mean ± SEM; N = 6 per group).

(H) Serum corticosterone levels measured by ELISA in WT and Aster-B KO mice that were fed ad-lib or fasted overnight (~16 hours). N = 4 per group. Statistical analysis was performed using Student's t-test. Values are mean ± SEM. *p < 0.05; **p < 0.01; ***p<0.001; ****p<0.0001. See also Supplemental Figure 6. All results are representative of at least two independent experiments.

SUPPLEMENTAL FIGURE LEGENDS

Figure S1, related to Figure 1. Evolutionary conservation and tissue distribution of the Aster protein family.

(A) Simplified phylogram of Aster-B one-to-one conservation across vertebrates. The scale represents 10% amino acid divergence. Phylogram was made using ClustalW2 and protein sequences were downloaded from Uniprot.

(B) Depiction of annotated intron-exon structure of *Gramd1a*, *Gramd1b*, and *Gramd1c* loci in *Mus musculus* strain C57BL/6J assembly GRCm38. Coding exons are depicted in black. 5' and 3' UTRs are represented with no fill. Exons which correspond to the Gram domain, Aster domain, and Transmembrane (TM) are depicted in green, blue, and red, respectively. Scale bar represents 1kb.

(C) Aster family expression by qPCR from tissues of C57BL/6 mice (n = 5).

(D) Coomassie blue–stained SDS–PAGE gel of purified FLAG-Aster domains (Aster-$A_{261-576}$, Aster-$B_{224-560}$, Aster-$C_{206-528}$) and control (albumin).

(E) Aster-$B_{334-562}$ was titrated with 22-NBD-cholesterol in the presence of cholesterol competitor as indicated. Results values are means ± SD and representative of at least three independent experiments.

(F) Comparison of NBD-cholesterol binding to Aster-A, Aster-B and StarD1.

(G) Comparison of *in vitro* cholesterol transport by Aster proteins and StarD1.

Figure S2, related to Figure 2. Structural comparison of sterol binding proteins.

(A) Structure of the Aster-A sterol-binding domain showing 25-hydroxycholesterol ligand and a glycerol molecule in the binding cavity.

(B) Comparison of mouse AsterA, yeast Lam4p-SD2 and StARD5. Despite the low sequence identity (18%), the Aster and Lam domains have a very similar architecture creating a largely non-polar binding cavity for the 25-hydroxycholesterol. However, the orientation of the ligands is quite distinct. The beta-sheets are most similar between AsterA and yeast Lam4p-SD2. The

three helices are somewhat different. In particular, the carbxoxy-terminal helix in Aster A is one turn longer at its amino-terminus and shorter at its carboxy-terminus compared with Lam4p-SD2.

Figure S3, related to Figure 2. The mode of sterol binding is not conserved between Asters and yeast Lam proteins.

(A) Orientation of the 25-hydroxycholesterol ligand. A simulated annealing composite omit map unambiguously identifies the ligand orientation in mouse Aster A (left panel - contoured at 1.0 sigma). The orientation of the 25-hydroxycholesterol ligand in mouse Aster A is markedly different from that in the distantly related yeast Lam4p (right panel - pdbcode 6bym) (Jentsch et al., 2018). The ligand is rotated by approximately 120° about it long axis such that the axial methyl groups on the cholesterol are orientated very differently.

(B) Alignment of the mammalian ASTER domains with the yeast Lam2/4 proteins. Although structurally similar, there is only limited sequence homology between the sterol-binding domains of the Aster and Lam proteins (23% identity between Aster A and Lam4p-1). Residues that are identical, have high, or low similarity are colored red, orange or yellow respectively. Residues colored cyan likely determine the different orientation of the sterol and are very different in character between the Aster and Lam proteins. Cyan asterisks indicate residues lining the pocket in contact with the hydroxycholesterol. Purple and green asterisks indicate surface non-polar and basic residues conserved in the Aster proteins that likely mediate interaction with the phospholipid membrane to facilitate sterol exchange.

Figure S4, related to Figure 3. Cholesterol-dependent movement of Aster proteins to the PM.

(A) Aster-A-GFP, Aster-B-GFP and Aster-C GFP localization in A431 cells imaged by live cell confocal microscopy in 1% LPDS (top) or following cholesterol loading for 1 h (bottom).

(B) Live-cell imaging of GFP-Aster-A localization in A431 cells stably expressing BFP-KDEL (ER

marker) and Cherry Lyn (PM marker). Yellow arrows indicate ER tubules in close proximity to the PM containing foci of Aster-A expression.

(C) Live-cell imaging of GFP-Aster-C localization in A431 cells stably expressing BFP-KDEL (ER marker) and Cherry Lyn (PM marker). Yellow arrows indicate ER tubules in close proximity to the PM containing foci of Aster-C expression.

(D) Live-cell imaging of GFP-Aster-B localization in A431 cells stably expressing BFP-KDEL (ER marker) and Cherry-E-Syt3 (ER-PM contact protein) cultured in 5% LPDS (left) or following cholesterol loading for 40 min (right). Large images, scale bar = 10 μm; insets, scale bar = 2 μm.

(E) Localization of full-length Aster-B and B ΔGRAM GFP constructs expressed in A431 cells in the presence or absence of cholesterol loading imaged by live cell confocal microscopy.

Figure S5, related to Figure 6. Development of mice lacking Aster-B.

(A) RNA-seq expression of *Gramd1a, Gramd1b, and Gramd1c* in female adult C57BL/6J mouse adrenal gland tissue (10 weeks or age). Data was collected for the ENCODE consortium by the Snyder Lab at Stanford (GEO GSM2453460).

(B) Strategy for generating Crispr-Cas9 mediated global *Gramd1b* (Aster-B) knockout mice. Coding exons are depicted in black. Exons that correspond to the Gram domain, ASTER domain, and transmembrane (TM) domain are depicted in green, blue, and red respectively. Scale bar represents 1kb.

Figure S6, related to Figure 7. Aster-B facilitates HDL-cholesterol uptake.

(A) Immunoblot validation of GFP-Aster-B and SR-BI expression compared to A431 wild-type cells.

(B) Lipid composition of HDL2 purified from human plasma by ultracentrifugation. HDL2 was used for the experiment because of higher lipid content and better SR-B1 interaction compared to HDL3.

(C) A431-SR-BI/Aster-B-GFP cells were lipid depleted for 24 h (LPDS) and treated with control medium (LPDS), 150-200 μg/mL FC-HDL2, or 200 μM cholesterol-cyclodextrin for 1 h. Cells were then fixed and imaged with TIRF microscopy to visualize Aster-B in close proximity to the PM. Dashed lines indicate individual cells. Scale bar 10 μm.

(D) Cells were automatically identified using DAPI (nuclei) and CellMask (cytoplasm) images and used to quantify single cell TIRF intensities.

(E) Quantification of the mean cellular GFP-Aster-B TIRF intensity from cells treated as in (A). N = 254 cells for control, 307 cells for HDL2 and 187 cells for cholesterol from 4 independent experiments.

(F) Epinephrine and dopamine levels in adrenal glands.

Figure S7, related to Figure 7. Model of Aster function in sterol transport.

(A) Model for the recruitment of Aster-B to the plasma membrane. The GRAM domain binds phosphatidylserine and is recruited to the plasma membrane in response to cholesterol loading. Aster-B forms cholesterol-dependent ER–PM contact sites and facilitates the trafficking of cholesterol to the ER. (B) Model showing PM to ER transport of HDL-derived cholesterol in the presence or absence of Aster-B.

Supplemental Movie 1. Representative video of Aster-B-GFP translocation in response to cholesterol loading. Plasma membrane is indicated by PM-mCherry marker. Time is indicated in minutes after cholesterol loading. Scale bar is 5 μm.

Supplemental Movie 2. Representative video of B GRAM (Aster-B_{1-171}, C-terminal GFP) translocation in response to cholesterol loading (500 μM). Plasma membrane is indicated by PM-mCherry marker. Time is indicated in minutes after cholesterol loading. Scale bar is 5 μm.

Supplemental Movie 3. Representative TIRF video of GFP (negative control) translocation in response to cholesterol loading (500 μM). Time is indicated in minutes after cholesterol loading. Scale bar is 5 μm.

Supplemental Movie 4. Representative TIRF video of B GRAM (Aster-B_{1-171}, C-terminal GFP) translocation in response to cholesterol loading (500 μM). Time is indicated in minutes after cholesterol loading. Scale bar is 5 μm.

EXPERIMENTAL PROCEDURES

CONTACT FOR REAGENT AND RESOURCE SHARING

Further information and requests for resources and reagents should be directed to and will be fulfilled by the Lead Contact, Peter Tontonoz (ptontonoz@mednet.ucla.edu).

EXPERIMENTAL MODEL AND SUBJECT DETAILS

Mice

All mice were housed in a temperature-controlled room under a 12 hr light–dark cycle and under pathogen-free conditions. Mice were placed on a chow diet. Experiments were performed in male and female mice. Investigators were blinded to group allocation for some but not all studies. Aster-B global knockout mice were generated at Mouse Biology Program facility on a C57BL/6N background using the CRISPR/Cas9 strategy outlined in Supplemental Figure S5B. All animal experiments were approved by the UCLA Institutional Animal Care and Research Advisory Committee. Experimental mice were sacrificed at ages 6-12 weeks unless otherwise specified for histological, serum, lipid, and gene expression analyses.

Cell Culture

A431, CHO-K1, 3t3-L1 and HeLa cells were obtained from the American Type Culture Collection. They have been previously verified by STR testing and were confirmed to be mycoplasma-free by regular testing. CHO-K1 and HeLa cells were transfected with Fugene 6 (Promega) following manufacturer's protocol. X-tremeGENE HP DNA or Genecellin transfection reagents were used for transfecting A431 cells. A431, 3T3-L1 and HeLa stable cells were grown in monolayer at 37 C in 5% CO2. The cells were maintained in medium A (DMEM containing 100 units/ml penicillin and 100 mg/ml streptomycin sulfate) supplemented with 10% FBS. CHO-K1 cells were grown in medium B (a 1:1 mixture of F-12K medium and Dulbecco's MEM containing 100 units/ml penicillin and 100 mg/ml streptomycin sulfate) supplemented with 10% FBS. Cholesterol-depleting medium was medium A supplemented with 1-5% lipoprotein-deficient serum (LPDS). Unless otherwise specified, cells were cholesterol loaded using 200 μM cholesterol: methyl-β-cyclodextrin (randomly methylated, Sigma C4555) complexes prepared.

METHOD DETAILS

Contruction of Plasmids and Stable Cell Lines

Mouse Aster-A, -B, and –C and truncations were PCR amplified from *Mus musculus* C57BL/6J cDNA and cloned into pDonr221 by Gateway cloning (BP reaction, ThermoFisher), pEntr4-GFP-C1 or pEntr4-GFP-N2 by Gibson assembly (NEB Gibson Assembly kit) (Gibson et al., 2009). For some studies, human Aster-B (1-738) was used as indicated. For use in transient transfections of GFP-tagged Aster proteins in CHO-K1 cells, pDonr221 plasmids were LR recombined into a pDest53 destination vector containing a CMV promoter and an N-terminal eGFP. For generation of stable C-terminal GFP-tagged Aster protein A431 cells, pEntr-GFP-N2 constructs were LR recombined into a retroviral pBabe DEST vector containing an SV40 promoter. For generation of stable N-terminal GFP-tagged Aster protein A431 cells, pEntr-GFP-C1 constructs were LR recombined into a pLenti Destination vector containing a CMV promoter. After infection, GFP positive cells were selected by flow cytometry based on expression level. PM-mCherry was generated by fusing a plasma membrane targeting sequence of GAP-43 (MLCCMRRTKQVEKNDEDQKI) synthesized as DNA oligo (Biomers, Germany) and inserting into the N-terminus of mCherry (Fig. 5D and Movie S1). SR-BI cDNA (transcript variant 2, NM_001082959.1) was amplified from A431 cDNA with primers SR-BI sense-BglII

(atctAGATCTaccATGGGCTGCTCCGCCAAAG) and SR-BI anti-NotI(atttgcggccgcgtgtgtgcaggtgtgcaa), inserted into mammalian expression vector with a EF1a promoter and puromycin selection marker (Fig. 7A-C and Suppl. Fig. 6B). First A431 cells with a stable expression for SR-BI were selected using 1 µg /µl puromycin. These cells were then transfected with GFP-Aster-B (human) and single cell clones with stable expression of SR-BI and GFP-Aster-B were selected with 500 µg / ml G418. Aster-B PH domain-GFP and control GFP constructs were packed into retrovirus to infect A431 cells in the presence of 6 µg/ml polybrene (Millipore). Cells were selected with 1 µg/ml puromycin for 1 week before using in experiment and used as a pool without further subcloning (Fig. 5D, E and Movie S2, S3, S4).

BFP-KDEL (Friedman et al., 2011) was amplified by PCR, inserted into an AAVS1 safe harbor integration vector (Lombardo et al., 2011) with puromycin selection marker. E-syt2 and E-syt3 (Giordano et al., 2013), and OSBPL5 cDNA (from HeLa cDNA, NM_020896.3) amplified by PCR, and the CAAX box (KLNPPDESGPGCMSCKCVLS) synthesized as DNA oligos (Biomers, Germany), were fused to the C-terminus of mCherry, and inserted into the safe harbor vector with blasticidin selection marker.

A431 cell lines double expressing BFP-KDEL plus the mCherry fusion proteins of interest were generated through CRISPR/Cas9 mediated AAVS1 safe harbor co-integration. Briefly, cells were co-transfected with two constructs (BFP-KDEL with puromycin selection and mCherry fusion protein with blasticidin selection) plus a third Cas9/sgRNA construct (backbones kind gifts from Feng Zhang) (Ran et al., 2013) targeting the AAVS1 locus. Transfected cells were selected with 1 µg/ml puromycin and 5 µg/ml blasticidin for 7 days and used as pools for the experiments. Plasmids and plasmid sequences are available upon request.

Protein Expression and Purification

For crystallization studies, the mouse Aster-A protein (334-562) was cloned into pGEX2T (GE Healthcare) with a TEV protease site. Aster-A was expressed in *E. Coli* Rosetta (DE3) (Novagen) by growing the transformed Rosetta (DE3) at 37◦ C in 2xTY until A600nm = 0.1, then inducing with 40 micromolar Isopropyl-D-1-thiogalactopyranoside (IPTG) and growth overnight at 20◦C. The bacterial cells were lysed by sonication in a buffer containing 1x PBS, 1 mM Dithiothreitol (DTT) and Complete EDTA-free protease inhibitor (Roche). The soluble protein was bound to glutathione sepharose (GE healthcare), and washed with a buffer containing 1x PBS, 0.5% Triton X-100, 0.5mM TCEP. Then the bound protein was washed with TEV cleavage buffer containing 50 mM Tris/Cl pH 7.5, 100 mM NaCl, 5% glycerol and 0.5mM TCEP. The protein was eluted from the resin using TEV protease. After the GST purification excess 25-hydroxy cholesterol was added from a 10 mM stock solution dissolved in ethanol and the complex purified on a Superdex S-200 column in 50 mM Tris/Cl pH 7.5, 100 mM NaCl and 0.5mM TCEP. The peak fractions were concentrated to 11.1 mg/ml and used for the crystallization experiments.

For binding and transfer studies Aster domains (Aster-$A_{261-576}$, Aster-$B_{224-560}$, Aster-$C_{206-528}$) were expressed by baculovirus in *Sf-9* insect cells with an N-terminal FLAG tag and a C-terminal 6x His Tag. Proteins were expressed with P3 baculovirus for 48 hours at 27°C. Cells were recovered by centrifugation, lysed by sonication. Insoluble material was pelleted at 16,000xg for 40 minutes. Soluble protein was first purified using a Ni-NTA column (Qiagen, 30210) and eluted with 250mM imidazole PBS buffer after extensive washing. Following dialysis proteins were purified using FLAG M2 affinity gel (Sigma A2220) columns and eluted with 100 µg/mL 1x FLAG peptide after washing for ten column volumes. Proteins were then either dialyzed to remove the FLAG peptide or purified further by size exclusion chromatography. The B Gram domain was expressed in *Sf9* cells with a 6xHis tag (Aster-$B_{303-533}$) and purified as described above. N-terminal GST Aster-$B_{303-533}$ expression constructs were transformed in Rosetta 2 (DE3) cells (Novagen). LB precultures were diluted into large-scale expression cultures and grown at 37°C to an A_{600} of 0.6-0.8, then induced with 0.5 mM IPTG at 18°C for 16 hours with shaking. Protein was then purified in PBS + 0.5mM DTT using glutathione agarose resin (Pierce PI16100) and eluted with 10mM GSH peptide in 50mM Tris, 150mM NaCl, pH 8.0. Protein was then

dialyzed to remove GSH peptide. HMBP-3C-STAR.66-285 (StAR) was a gift from Nikolai Sluchanko (Addgene plasmid # 100094). Soluble StAR was first purified using a Ni-NTA column (as above) and subsequently purified using amylose resin (NEB E8021S) and eluted with 10 mM maltose in 50mM Tris, 150mM NaCl, pH 8.0. Protein was then dialyzed to remove maltose.

NBD-Cholesterol Binding Experiments
Fluorescent sterol binding assays were carried out as previously described (Petrescu et al., 2001; Wei et al., 2016) in 384-well black flat-bottom plates and equilibrated at room temperature for 1 hour. Measurements were made using a CLARIOstar (BMG LABTECH) microplate reader. The NBD fluorophore was excited with λ(ex) = 470 nm and λ(em) = 525 and plotted using Prism software. Dissociation constants (K_D) were determined by nonlinear regression analysis of dose-response curves.

GST Agarose Assay for [^{3}H]Cholesterol Binding
Reactions were carried out in binding buffer (0.003% Triton X-100 in 1 x PBS) containing 150 nM of Aster-B ASTER protein and [^{3}H]cholesterol. After incubation for 30 min at room temperature, the mixture was incubated with pre-equilibrated of glutathione agarose resin (Pierce PI16100) at 4°C for 2 h, then loaded onto a column and washed. The protein-bound [^{3}H]cholesterol was eluted with 10 mM GSH peptide and quantified by scintillation counting. For competition experiments with unlabeled sterols, the assays were carried out in the presence of ethanol containing the indicated unlabeled sterol (0 –10 μM).

Liposome Preparation
Liposomes were generated by drying lipids in glass tube under liquid nitrogen. Lipid films were then resuspended in 50 mM hepes, 120 mM potassium acetate buffer ± 0.75M sucrose where indicated. Lipid suspensions were then vortexed and incubated for 30 minutes at 37°C (2mM total lipid concentration). Suspensions were then snap frozen in liquid nitrogen and thawed rapidly at 37°C five times. Light liposomes were prepared by extruding through 100 nm polycarbonate filters. Heavy liposomes containing sucrose were prepared by extruding through a 400 nm polycarbonate filter, then washing several times in 50 mM hepes, 120 mM potassium acetate buffer with no sucrose. Liposome sizes were confirmed using an N4 Dynamic Light Scattering instrument.

Crystallization and X-ray Structure Determination
Crystals of the Aster-A (334-562):25-hydroxycholesterol complex were obtained using sitting drop vapor diffusion at room temperature. Crystals were grown using 0.2 M NaCl, 0.1 M sodium cacodylate pH 6.0 and 8% PEG 8000 (condition E3 Proplex, Molecular Dimensions). Data were collected to 2.9 Å on the I03 beamline at Diamond Light Source, UK. Data were processed using XDS (within Xia2) and Pointless/Aimless (within CCP4). The structure was solved using molecular replacement using Phaser (within CCP4) and the first StARkin domain of *S. cerevisiae* Lam4 (pdb code 5YQJ, (Tong et al., 2018) as a model. Model fitting and refinement were performed using Coot, Refmac (within CCP4), PDB-REDO and Phenix.

Live Cell Imaging
For time-lapse fluorescence imaging, cells were plated in poly-d-lysine coated 35 mm glass bottom dishes (Mat-tek) and, when indicated transfected 48hr prior to imaging. Images were acquired using an Inverted Leica TCS-SP8-SMD Confocal Microscope, equipped with CO_2/temperature controlled Tokai Hit system for imaging of live cells at 37°C with 5% CO_2. Images were deconvolved using Huygens Professional software. Brightness and contrast were adjusted with ImageJ software. For some experiments cells were sorted for expression of GFP. TIRF imaging was performed in glass bottom μ-slide 4 well plates (Ibidi) with a Nikon Eclipse Ti-E N-STORM microscope, equipped with Andor iXon+ 897 back-illuminated EMCCD camera and × 100 Apo TIRF oil objective NA 1.49, a 65 mW Argon line combined with Quad filter was used for visualization of TIRF and epifluorescence (Fig. 3E). Live cell TIRF imaging was

performed similarly at 37 ^{o}C, 5% CO_2 with EMBL GP168 incubator controller (Fig. 5E and Movie S3, S4).

For automated quantification of TIRF images, cells were fixed with 4% PFA for 15 min, permeabilized with PBS/0.1% Triton for 5 min and stained with DAPI 5 µg/ml and 0.2 µg/ml CellMask Deep Red (Life Technologies) in PBS for 15 min. TIRF images were acquired for GFP-AsterB together with epifluorescent images for DAPI and CellMask Deep Red. These images were automatically quantified using CellProfiler (Carpenter et al., 2006) and the resulting data analyzed with Python/Pandas. For Airyscan superresolution microscopy, cells in 8 well Lab-Tek™ II Chambered coverglass (Thermofisher) were imaged with a Zeiss LSM 880 confocal microscope equipped with an Airyscan detector using a 63 × Plan-apochromat oil objective, NA 1.4. Live cell imaging was performed at 37 ^{o}C, 5% CO_2 with incubator insert PM S1 and definite focus hardware autofocus system. Images were Airyscan processed automatically using the Zeiss Zen2 software package (Fig. 3D, Movie S1).

For dual color live cell TIRF imaging, A431 cells stably expressing GFP-Aster-B and Cherry-ORP5 were seeded in 4-well LabTek II live cell chamber slides. After two days cells were incubated with DMEM containing 5% LPDS for 8 h. Live cell TIRF imaging was performed in FluoroBrite DMEM containing 5% LPDS: TIRF video microscopy with a frame rate of one image per minute was initiated 50 s after addition of 1 mM cholesterol/cyclodextrin. Images were acquired with a GE Deltavision OMX SR instrument equipped with a 60x Apo-N oil immersion objective. Images were deconvolved using the softWoRx 7.00 software (GE Healthcare).

For imaging Aster-B with PM and other contact site marker proteins, A431 cells stably expressing BFP-KDEL and mCherry fusion proteins of ER/PM contact site markers were seeded in 8-well LabTeK II live cell chamber slides. After 24 h cells were washed with PBS and transiently transfected with GFP-Aster-B expression constructs using X-tremeGENE HP DNA or Genecellin transfection reagents in DMEM containing 5% lipoprotein deficient serum (LPDS). After 24 h cells were switched to FluoroBrite DMEM containing 5% LPDS, with or without 100 - 200 µM cholesterol/cyclodextrin. Cells were imaged 15 to 65 min after cholesterol administration using a Zeiss LSM 880 Airyscan microscope equipped with a 63x Plan-Apochromat oil immersion objective. Images were Airyscan processed and brightness and contrast adjusted with ImageJ. Images from the bottom section of a cell were used for the quantification of the overlap of GFP-Aster-B with contact-site marker proteins. The images were thresholded to select GFP-Aster-B and contact site marker structures and the pixel overlap of the segmented structures was calculated with the JaCOP plugin for ImageJ. For each condition, 9-13 cells from 2 independent experiments were quantified.

For Aster-A siRNA studies, U2OS cells were transfected with mCherry-KDEL and single cell clones were selected with 500 µg/ml G418. U2OS Cherry-KDEL cells were seeded into 8-well LabTeK II live cell chamber slides and reverse transfected with 50 nM control siRNA (Elbashir et al., 2001) or Aster-A siRNA (target sequence: '5-CACGATCTCCATCCAGCTGAA-3') using HiPerfect. After 48 h cells were washed with PBS and incubated with DMEM containing 5 % LPDS for 24 h. For live cell TIRF imaging, medium was changed to FluoroBrite DMEM containing 5% LPDS. TIRF video microscopy with a frame rate of one image per minute was started at 40 – 90 s after addition of 1 mM cholesterol/cyclodextrin. Images were acquired with a GE Deltavision OMX SR instrument equipped with a 60x Apo-N oil immersion objective. Images were deconvolved using the softWoRx 7.00 software (GE Healthcare). ER structures were segmented and the average ER structure size per cell was quantified with ImageJ.

Phospholipid Binding Assays

Lipid binding analysis of 6xHis-tagged B GRAM (Aster-B_{1-337}) was conducted using PIP Strips (Echelon Biosciences), with each spot containing 100 pmol of active lipids. Membranes were blocked with PBS Tween (PBST) solution (supplemented with 3% fatty acid free BSA) for 1 hr at room temperature, and

incubated with B GRAM fusion protein in blocking buffer for 1 hr. After three washes, the membranes were blotted with anti-His antibody (Biorad, MCA1396GA). The strip contained 15 different types of lipids. LPA, lysophosphatidic acid; LPC, lysophosphatidylcholine; PI, phosphatidylinositol; PI(3)P, phosphatidylinositol 3-phosphate; PI(4)P, phosphatidylinositol 4-phosphate; PI(5)P, phosphatidylinositol 5-phosphate; PE, phosphatidylethanolamine; PC, phosphatidylcholine; S1P, sphingosine- 1-phosphate; PI(3,4)P2, phosphatidylinositol 3,4 -phosphate; PI(3,5)P2, phosphatidylinositol 3,5-phosphate; PI(4,5)P2, phosphatidy- linositol 4,5-phosphate; PI(3,4,5)P3, phosphatidylinositol 3,4,5-phosphate; PA, phosphatidic acid; PS, phosphatidylserine. Results were confirmed with a FLAG tagged B GRAM Fusion construct.

Gene Expression Analysis

Total RNA was isolated using TRIzol reagent (Invitrogen) and reverse transcribed with the iScript cDNA synthesis kit (Biorad). cDNA was quantified by real-time PCR using SYBR Green Master Mix (Diagenode) on an ABI 7900 instrument. Gene expression levels were determined by using a standard curve. Each gene was normalized to the housekeeping gene 36B4 and was analyzed in duplicate. Primers used for real-time PCR are available upon request.

Protein Analysis

Whole cell lysate or tissue lysate was extracted using RIPA lysis buffer (Boston Bioproducts) supplemented with complete protease inhibitor cocktail (Roche). Proteins were diluted in Nupage loading dye (Invitrogen), heated at 95°C for 5 min, and run on 4–12% NuPAGE Bis-Tris Gel (Invitrogen). Proteins were transferred to hybond ECL membrane (GE Healthcare), blocked with 5% milk (or 5% BSA for anti-SREBP-2) to quench nonspecific protein binding and blotted with the indicated primary antibody. Horseradish peroxidase-conjugated anti-mouse, anti-goat and anti-rabbit IgG (Jackson) were used as secondary antibodies. The immune signal was visualized using the ECL kit (Amersham Biosciences). Nuclei from mouse adrenal glands were prepared by douncing tissue with a motorized overhead stirrer (Caframo Model BDC2002) in 10mM Hepes-KOH, pH 7.4, 10 mM KCl, 1.5 mM $MgCl_2$, 0.5 mM EDTA sodium, 0.5 mM EGTA sodium, 1 mM DTT, and protease inhibitors. Samples were centrifuged at 1,000xg at 4°C for 5 minutes to isolate nuclei. Nuclei were washed and resuspended in 10mM Hepes-KOH, pH 7.4, 0.42 M NaCl, 2.5% glycerol (w/v), 1.5 mM $MgCl_2$, 0.5 mM EDTA sodium, 0.5 mM EGTA sodium, 1 mM DTT, and protease inhibitors. Nuclei were then incubated on ice for 40 minutes with intermittent pipetting, then centrifuged at 10,000xg at 4°C for 10 minutes. The supernatant was then used as nuclear protein extract. The 1,000xg supernatant was used to prepare a membrane lysate by centrifugation at 100,000xg at 4°C for 30 minutes, followed by resuspension in RIPA buffer.

Oil Red O Staining

Oil Red O staining was performed as described (Mehlem et al., 2013). Adrenal glands were dissected carefully and the surrounding fat tissue was removed. After collected the glands were embedded into Tissue-Tek O.C.T. compound (cat No. 4583), placed on dry ice for twenty minutes, then moved to -80°C. Tissue was sectioned (12 μm thick) using a Microm HM 505 E cryostat and sectioned were placed on glass microscope slides (Superfrost plus). Before staining, sections were allowed to equilibrate to room temperature for 10 minutes. Oil Red O solution working solution (Sigma, cat. No. 00625, ~0.4%) was freshly prepared and filtered before covering the sections. Sections were incubated for 10 minutes, then washed under running tap water for 30 minutes. Sections were then mounted on slides with water-soluble mounting medium (Sigma cat. No. GG1) and images were captured on a Zeiss Axioskop 2 plus bright-field light microscope at a x40 magnification. Background was corrected by white balance, selected as a blank area outside the section.

Electron Microscopy

A431 cell monolayers were treated as indicated, then fixed for 1h in fixative solution containing 4% paraformaldehyde (EMS; Hatfield, PA) 2.5% glutaraldehyde (EMS; Hatfield, PA) buffered with 0.1M

sodium cacodylate (Sigma; Burlington, MA). Next, the cells were gently scraped from the dishes using a cell scraper (Corning; Corning, NY). The suspension was then centrifuged at 350xg for 15min to generate a pellet. The pellets were then allowed to fix for another 45min.Next, pellets were rinsed 3 times with 0.1M sodium cacodylate before being post-fixed with 1% osmium tetroxide (EMS; Hatfield, PA), 1.2% potassium ferricyanide (EMD; Darmstadt, Germany) buffered with 0.1M sodium cacodylate for 1h at room temperature. Next, samples were rinsed 3 times with distilled H2O and stained overnight with 2% uranyl acetate at 4C. Next day, samples were rinsed three times with distilled H2O and dehydrated through a series of increasing acetone concentrations (30,50,70,85,95,100%X3, 10 min each) before being infiltrated with increasing concentrations of EMBed812 epoxy resin (EMS; Hatfield, PA) in acetone (33% 2h, 66% overnight, 100% 4h). Next, samples were embedded in fresh resin and polymerized in a vacuum oven for 24h at 65C. The polymerized blocks were removed from the tubes, trimmed and 65nm sections were made with a Leica UC6 ultramicrotome and picked up on freshly glow-discharged copper grids (Ted Pella; Redding, CA) that were coated with formvar and carbon. Sections on grids were then stained with Reynold's lead citrate solution for 10min. Images were acquired with an FEI T12 transmission electron microscope set to 120kV accelerating voltage using a Gatan 2kX2k digital camera.
Mice were perfused with 0.1 M Sodium Cacodylate buffer (pH 7.4) and fixed with cold 1.5% Glutaraldehyde, 4% PVP, 0.05% $CaCl_2$ in 0.1 M Sodium Cacodylate buffer (pH 7.4) (Angermuller and Fahimi, 1982). Standard transmission EM ultrastructural analysis was performed on adrenal glands with imidazole staining and visualized with a JEOL JEM-123 40-120kV transmission electron microscope at the Gladstone Electron Microscopy Core.

Lipid Analysis
Adrenal glands were weighed and snap-frozen in liquid nitrogen. Blood was centrifuged and serum was snap frozen. 10µl serum was used for analysis. Adrenal glands were pulverized using a hand-held pestle grinder. A modified Bligh-Dyer lipid extraction (Bligh and Dyer, 1959), in the presence of lipid class internal standards including [25,26,26,26-d_4]-cholesterol and cholesteryl heptadecanoate, was performed on 5-10 mg of pulverized tissue. Lipid extracts were dried under nitrogen and diluted in chloroform/methanol (2/1, v/v). Molecular species were quantified using ESI/MS on a triple-quadrupole instrument (Thermo Fisher Quantum Ultra) utilizing shotgun lipidomics methodologies (Bowden et al., 2011; Han and Gross, 2005). Free cholesterol was first derivatized with acetyl chloride (Brown et al., 2013) and then quantified in positive ion mode using product ion scanning for 83.03 amu (collision energy = 18 eV). CE molecular species were quantified using neutral loss scanning for 368.5 amu (collision energy = 25 eV). Individual molecular species were calculated by comparing the ion intensities of the molecular species to the ion intensity of the lipid class internal standard as previously described (Bowden et al., 2011; Han and Gross, 2005). Serum corticosterone was measured by ELISA kit following cardiac puncture per manufacturer's instructions (Cayman Chemical, cat No. 501320).

***In vitro* antisense oligonucleotide (ASO) studies**
Generation 2.5 constrained ethyl ASOs were synthesized as described previously (Seth et al., 2009). For *in vitro* knockdown studies, control or Aster-A ASO (GTGGAATTTATTCAGG) was used. Undifferentiated murine 3T3-L1 cells were plated in 10% FBS DMEM on Day 0. On Day 1 cells were washed and supplemented with 1% LPDS. Cells were then transfected with ASOs using Dharmafect 1 reagent per the manufacturer's recommendations for knockdown studies (Dharmacon, 50nM final concentration). On Day 2, the medium was changed to fresh DMEM with 1%LPDS, simvastatin (5 µM) and mevalonate (50 µM). On Day 3 cells were treated as described in the figure legends and samples were collected. The rate of incorporation of [^{3}H]oleate into cholesteryl [^{3}H]oleate was performed on Day 3 as previously described (Goldstein et al., 1983).

Lipoprotein fractionation
Purification of HDL2 particles was performed using potassium bromide density centrifugation from pooled samples of human plasma obtained from the Finnish Red Cross as described previously (Nguyen

et al., 2012). Lipid content of HDL2 and LDL fractions was quantified using lipid extraction and thin layer chromatography as described before (Bautista et al., 2014).

QUANTIFICATION AND STATISTICAL ANALYSES

Experimental Replicates and Quantification

Replicates are described in the figure legends. For cellular assays, n corresponds to the number of experimental replicates. For animal experiment, n corresponds to the number of mice used per genotype or condition. Each experiment was repeated using at least two cohorts of mice. All data were represented as mean SEM (standard error) as described in the figure legends.

Statistical Analysis

All data are presented as mean ± SEM and analyzed using Microsoft Excel and Prism (Graphpad). Student's t test was used for single variable comparison between two groups. Two-way ANOVA followed by Bonferroni posttests was used to examine interactions between multiple variables. Data are presented as $\pm$ S.E.M. $p < 0.05$ was considered to be statistically significant and is presented as * $p < 0.05$, ** $p < 0.01$, *** $p < 0.001$, or **** $p < 0.0001$.

DATA AND SOFTWARE AVAILABILITY

PDB Code for the crystallography data is 6GQF.

KEY RESOURCES TABLE

REAGENT or RESOURCE	SOURCE	IDENTIFIER
Antibodies		
FLAG M2	Sigma	Cat# F3165
His	Biorad	MCA1396GA
Scarb1 (SR-BI)	Abcam	Cat# ab217318
HMGB1	Abcam	Cat# ab18256
Lamin A/C	Santa Cruz	Cat# sc-6215
Calnexin	Abcam	Cat# ab10286
Tubulin	Millipore	Cat# CP06 RRID:AB_2617116
GFP	Abcam	Cat# ab6556 RRID:AB_
SREBP-2	Millipore	Cat# MABS1988 RRID:AB_
Actin	Sigma	Cat# A2066 RRID:AB_476693
Cell Culture Reagents		
Dharmafect 1	Dharmacon	T-2001-02
Gramd1a generation 2.5 antisense oligonucleotide (ASO)	Ionis Pharma	N/A
DMEM	Corning	MT-10-013-CM
FluoroBrite DMEM	Thermofisher	A1896701
Live Cell Imaging Solution	Thermofisher	A14291DJ
FBS	Omega Scientific	FB11
Lipoprotein Deficient Serum, Bovine	Fisher	AAJ65182AMG
Ham's F-12K (Haighn's) Medium	Thermo Fisher	21127022
Trypsin	Corning	MT-25-053-CI
Penicillin/Streptomycin	Corning	MT-30-002-CI

Promega FuGENE 6 T	Thermo Fisher	E2691
Bacterial and Virus Strains		
Lentivirus: Aster-A, B, C and mutants.	This paper	N/A
Chemicals, Peptides, and Recombinant Proteins		
Bovine Serum Albumin	Sigma	A9418
[1,2-3H(N)]-Cholesterol	PerkinElmer	NET139250UC
Oleic acid [9,10-3H(N)]	ARC	ART 0198
Simvastatin Sodium Salt	Fisher Sci.	56-702-15MG
Mevalonolactone	Sigma	M4667
NBD-22 Cholesterol	Thermo Fisher	N1148
NBD-6 Cholesterol	Avanti Polar Lipids	810251
Cholesterol	Sigma	C8667
β-Estradiol	Sigma	E8875
22(R)-hydroxycholesterol	Avanti Polar Lipids	700058P
27-hydroxycholesterol	Avanti Polar Lipids	700021P
Brain PS L-α-phosphatidylserine (Brain, Porcine)	Avanti Polar Lipids	840032C
16:0-18:1 PC	Avanti Polar Lipids	850457C
Egg PA | 840101 – Chloroform	Avanti Polar Lipids	840101C
18:1 Dansyl PE in chloroform	Avanti Polar Lipids	810330C
Extruder Set	Avanti Polar Lipids	610000
Cholesterol	Sigma	C8667
methyl-β-cyclodextrin (randomly methylated)	Sigma	C4555
Cholesterol/methyl-β-cyclodextrin complexes (2.5 mM)	This paper	Synthesized as described (Brown et al., 2002)
(3H)oleate-albumin complex	This paper	Synthesized as described (Goldstein et al., 1983)
GW3965	This paper	Synthesized as described (Collins et al., 2002)
LG100268	Sigma	SML0279

Puromycin	Sigma	P9620
Blasticidin	Thermofisher	A1113902
Polybrene		
RIPA buffer	Boston BioProducts Inc.	BP-115-500ml
IsoFlo (Isoflurane)	Zoetis	N/A
Formaldehyde	Thermo Scientific	PI-28908
Glutaraldehyde	LADD Research	20210
CellMask Deep Red PM stain	Thermo Fisher	C10046
NEB Gibson Assembly Kit (E5510S)	Thermo Fisher	NC0414992
BP Clonase II Enzyme Mix	Life Technologies	11789020
LR Clonase II	Life Technologies	11791020
Isopropyl-β-D-thiogalactoside	Sigma	10724815001
Complete EDTA-Free Protease Inhibitor Cocktail	Sigma	4693132001
Critical Commercial Assays		
3-CAT Research ELISA	Rocky MTN Diagnostics	BA E-5600
Corticosterone ELISA kit	Cayman Chemical	501320
Amplex Red Cholesterol Assay Kit	Life Technologies	A12216
BCA protein assay kit	Pierce	23225
Prolong Diamond Antifade Mountant	Thermo Fisher	P36965
Deposited Data		
PDB Code for the crystallography data is 6GQF.		
Experimental Models: Cell Lines		
A431	ATCC	CRL-1555
CHO-K1	ATCC	CCL-61
HeLa	ATCC	CCL-2
3T3-L1	ATCC	CL-173

Lenti-X 293T Cell Line	Clontech	632180
Phoenix-A cells (Retrovirus packaging)	ATCC	
Experimental Models: Organisms/Strains		
Mouse: *Gramd1b*$^{-/-}$; C57BL/6N	MBP/KOMP	Produced as described in methods.
Mouse: WT: C57BL/6N	MBP/KOMP	
Oligonucleotides		
GTGGAATTTATTCAGG -*Gramd1a* Generation 2.5 ASO	Ionis Pharma	N/A
Recombinant DNA		
Retroviral pBABE-puro Aster-B	This paper	N/A
Retroviral pBABE-puro Gram (Aster-B)	This paper	N/A
Retroviral pBabe-puro ΔGRAM (Aster-B)	This paper	N/A
Retroviral pBABE-puro GFP	This paper	N/A
pGEX2T-Aster-A ASTER	This paper	N/A
GFP-Aster-A/B/C and mutants	This paper	N/A
PM-mCherry	This paper	
BFP-KDEL	Addgene	#49150, Gift from Gia Voeltz
E-syt2	Addgene	#66831, Gift from Pietro De Camilli
E-syt3	Addgene	#66832, Gift from Pietro De Camilli
OSBPL5-mCherry	This paper	N/A
pEntr4-GFP-C1	Addgene	#17396, Gift from Eric Campeau
pEntr4-GFP-N2	Addgene	#19364, Gift from Eric Campeau and Paul Kaufman
mCherry-Sec61β	Addgene	#49155 Gift from Gia Voeltz
mCherry-Rtn4α	Addgene	#86683, Gift from Tom Rapoport
Bac-to-bac Baculovirus Expression System	Thermofisher	#10360014
pDonr221	Thermofisher	12536017
pDest53	Thermofisher	12288015
pLenti CMV Puro Dest	Addgene	#17452, Gift from Eric Campeau and Paul Kaufman

Software and Algorithms		
Prism6	GraphPad	N/A
Image J	https://imagej.nih.gov/ij/	N/A
MS Excel 2016	Microsoft	N/A
Xia2 (XDS)	https://xia2.github.io/	N/A
CCP4 (Pointless/Aimless, Phaser, Refmac)	http://www.ccp4.ac.uk/	N/A
PDB-REDO	https://pdb-redo.eu/	N/A
Coot, Phenix	https://www.phenix-online.org/download/other.html	N/A
CellProfiler	cellprofiler.org/	N/A
Python/Pandas	https://pandas.pydata.org/	N/A
Zen2	Zeiss	N/A
LASX	Leica	N/A
Huygens Professional	https://svi.nl/Huygens-Professional	N/A
Other		
TissueLyzer	Qiagen	N/A
BD FACSAriaIII cell sorter	BD Bioscience	N/A
Applied Biosystem (ABI) qPCR machine	Thermo Fisher	QuantStudio 6 Flex System
100 μm cell strainer	Falcon	352360
70 μm cell strainer	Falcon	352350
35 mm Dish | No. 1.5 Coverslip | 14 mm Glass Diameter | Poly-D-Lysine Coated	MatTek	P35GC-1.5-14-C
Lab-Tek II Chambered Coverglass	Thermofisher	155360
Neuvitro COVERSLIP PDL – GG-12-1.5PDL	Fisher	NC0672873
Syber Green Master Mix	Diagenode	DMMLD2D600
PIP Strips Membranes	Life Technologies	P23751

E. Coli Rosetta (DE3)	Millipore-Sigma	71400-3
Sf9 cells	Thermo Fisher	11496015
sf900 II insect media	Life Technologies	10902-104
Anti-Flag M2 Affinity Gel	Sigma	A2220
FLAG Peptide	Sigma	F3290
Glutathione Agarose Resin	Pierce	PI16100
HisPur Ni-NTA resin	Fisher	PI88222
Amylose Resin	NEB	E8021S
Sodium Cacodylate	LADD Research Industries	20305
PEG 8000	Molecular Dimensions	condition E3 proplex
Trizol Reagent	Life Technologies	15596018
iScript cDNA Synthesis Kit	Biorad	1708891
Real Time PCR Mastermix SYBR Green	Diagenode	DMSG-2X-A300
X-tremeGENE HP	Sigma	**6366244001**
Genecellin	Fisher	50-999-478

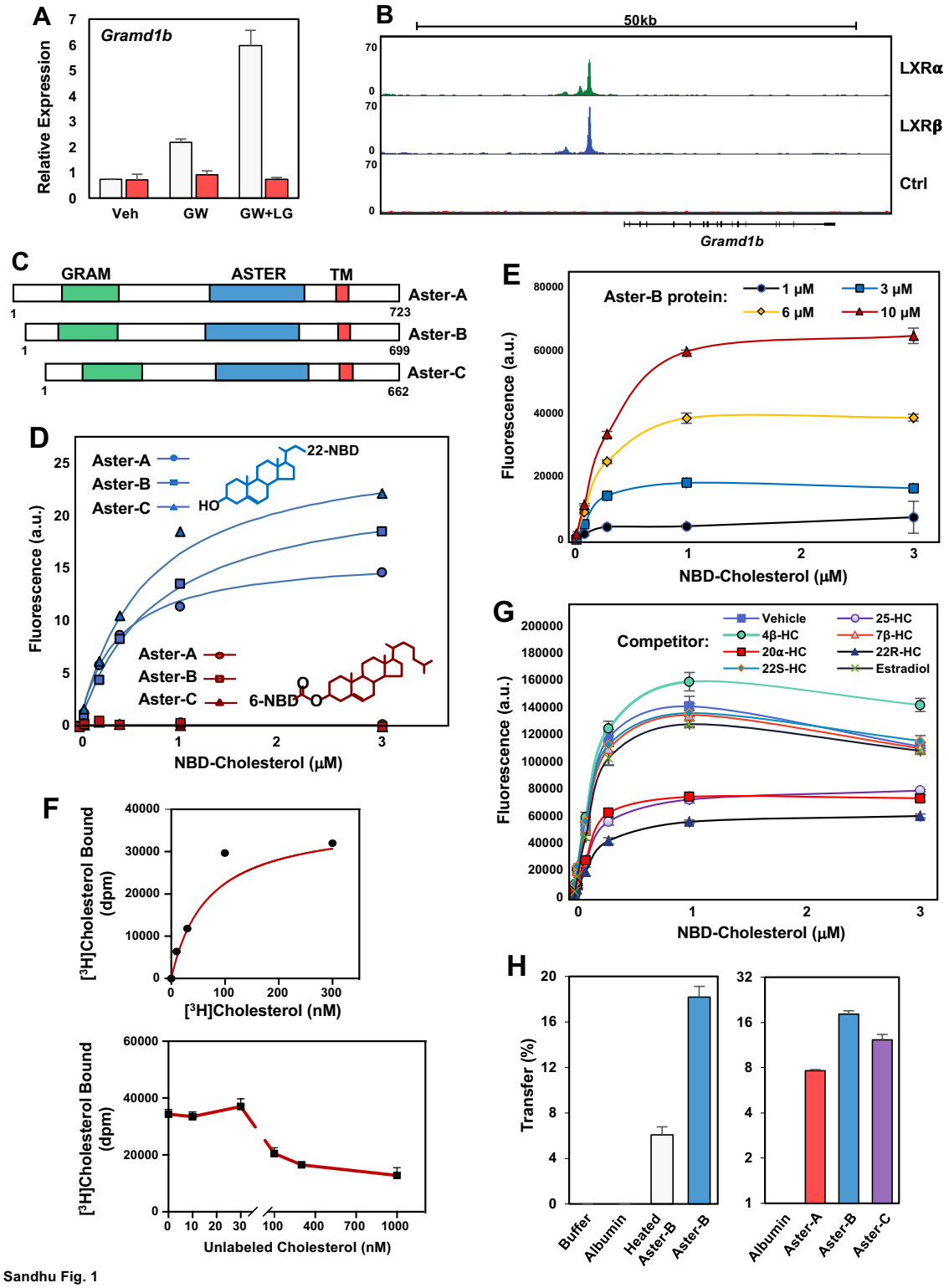

Sandhu Fig. 1

Figure 1

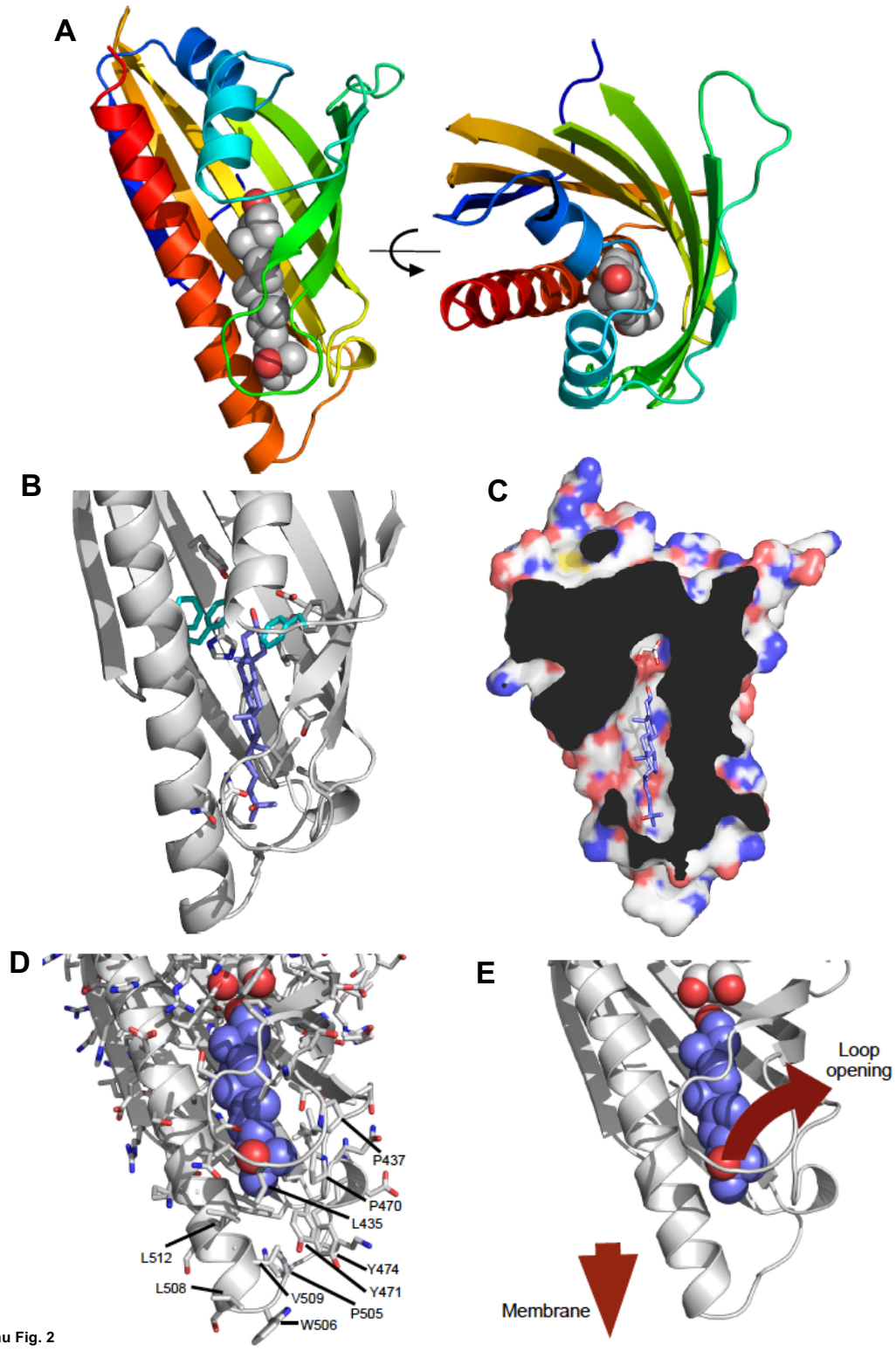
A
B
C
D
E
P437
P470
L435
L512
Y474
L508
Y471
V509
P505
W506
Loop
opening
Membrane
Sandhu Fig. 2

Figure 2

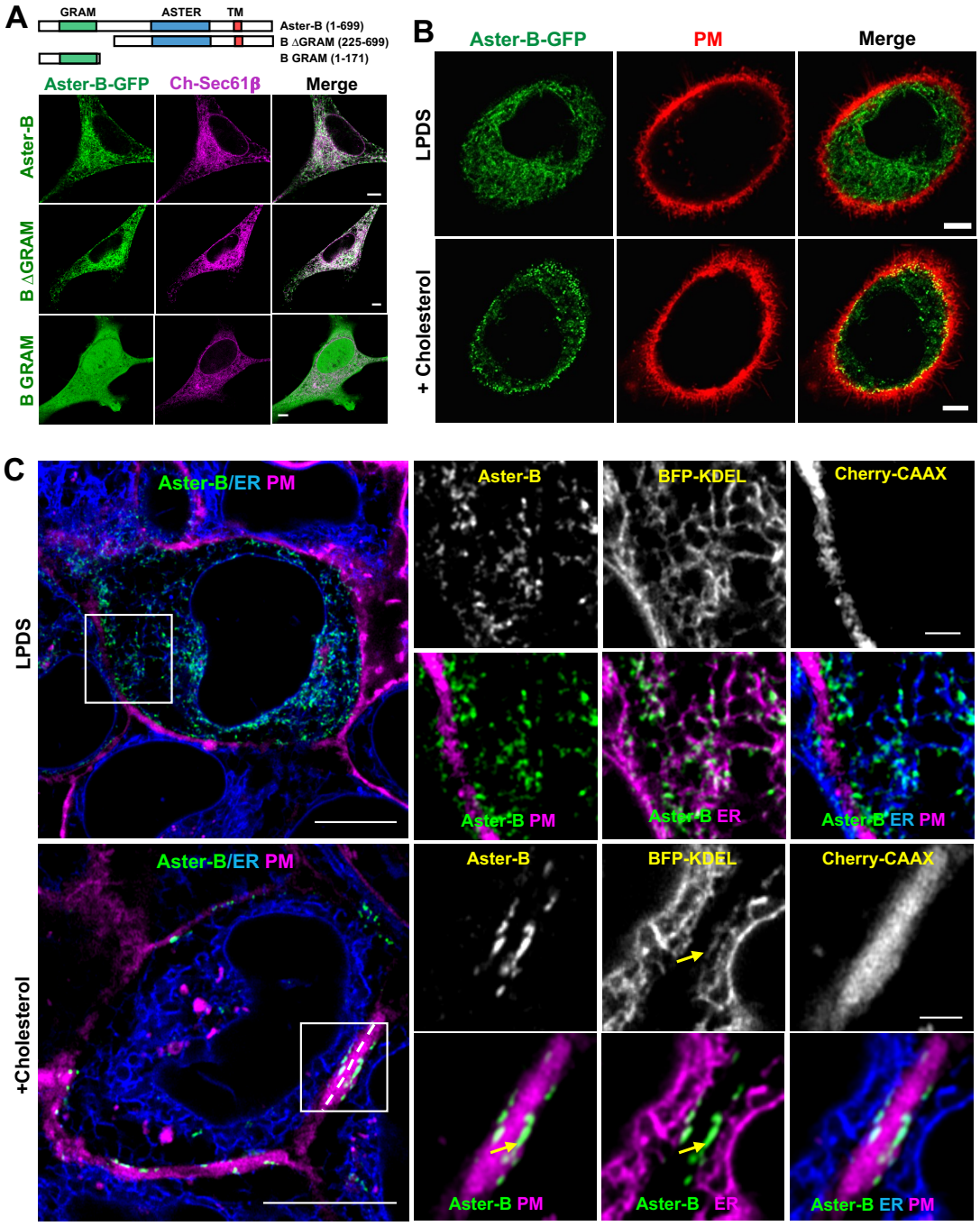

Fig. 3

Figure 3

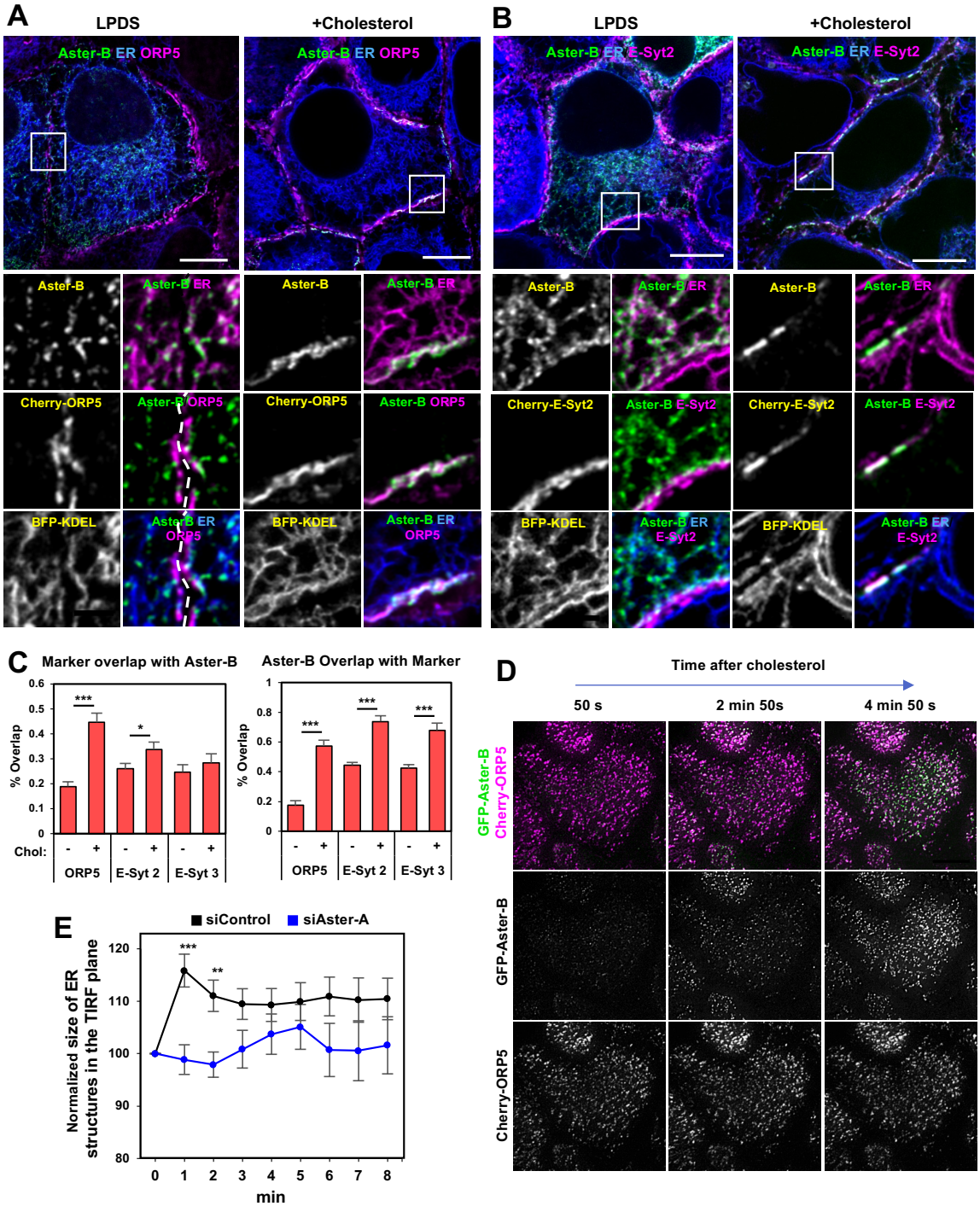

Sandhu Fig. 4

Figure 4

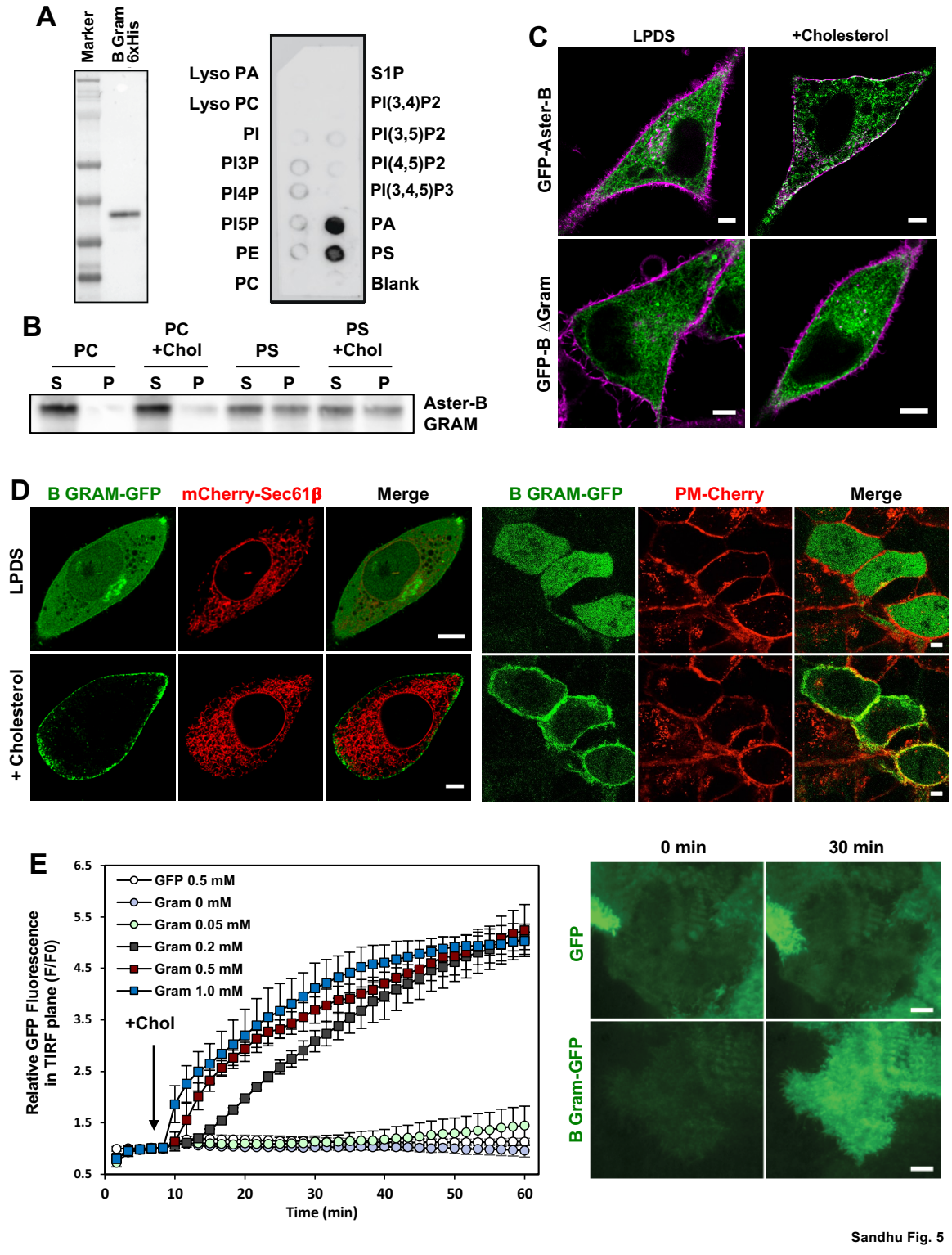
A
Marker
B Gram 6xHis
Lyso PA
Lyso PC
PI
PI3P
PI4P
PI5P
PE
PC
S1P
PI(3,4)P2
PI(3,5)P2
PI(4,5)P2
PI(3,4,5)P3
PA
PS
Blank
B
PC
PC +Chol
PS
PS +Chol
S P S P S P S P
Aster-B GRAM
C
LPDS
+Cholesterol
GFP-Aster-B
GFP-B ΔGram
D
B GRAM-GFP
mCherry-Sec61β
Merge
B GRAM-GFP
PM-Cherry
Merge
LPDS
+ Cholesterol
E
Relative GFP Fluorescence in TIRF plane (F/F0)
GFP 0.5 mM
Gram 0 mM
Gram 0.05 mM
Gram 0.2 mM
Gram 0.5 mM
Gram 1.0 mM
+Chol
Time (min)
0 min
30 min
GFP
B Gram-GFP
Sandhu Fig. 5

Figure 5

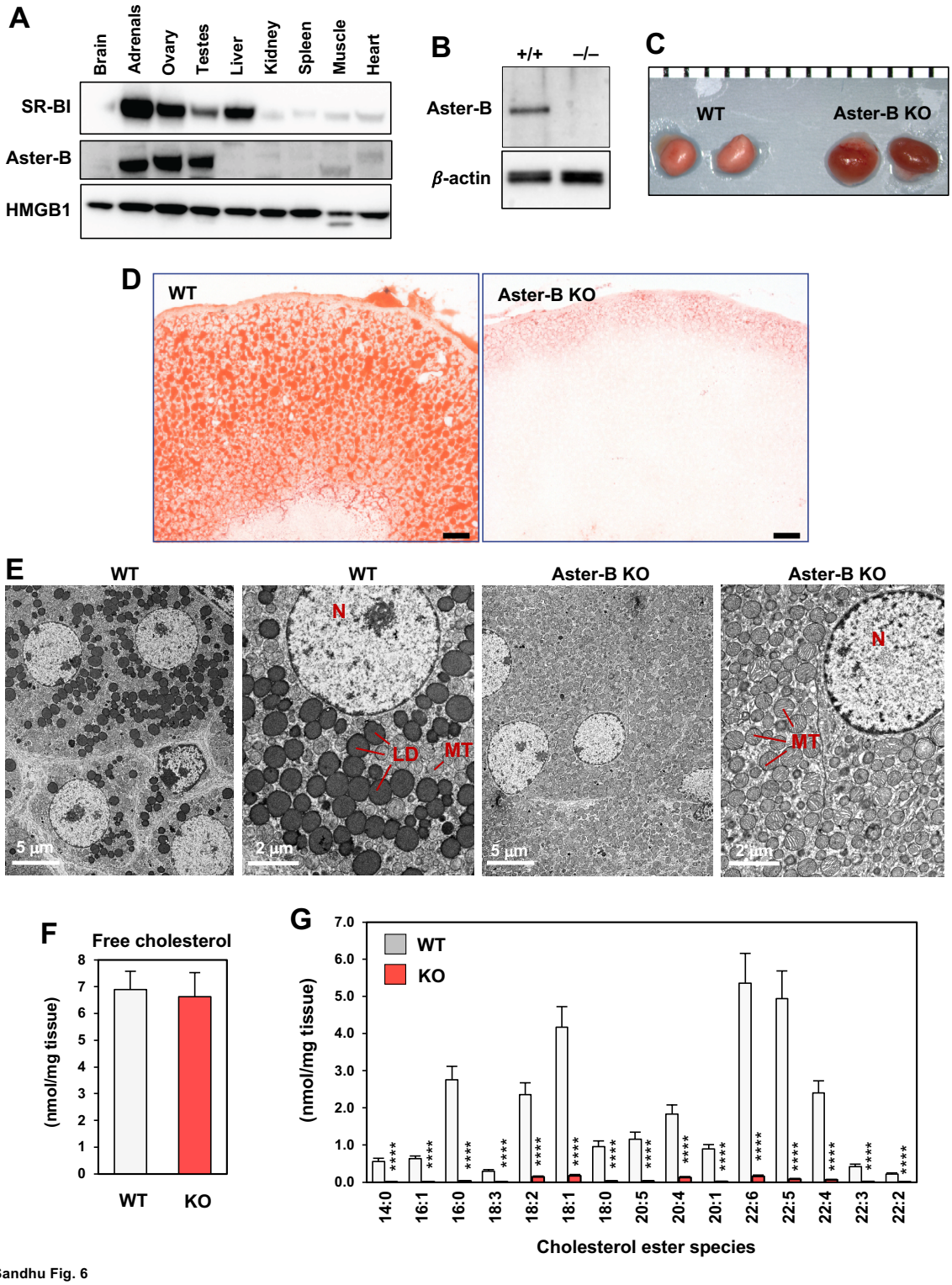

Sandhu Fig. 6

Figure 6

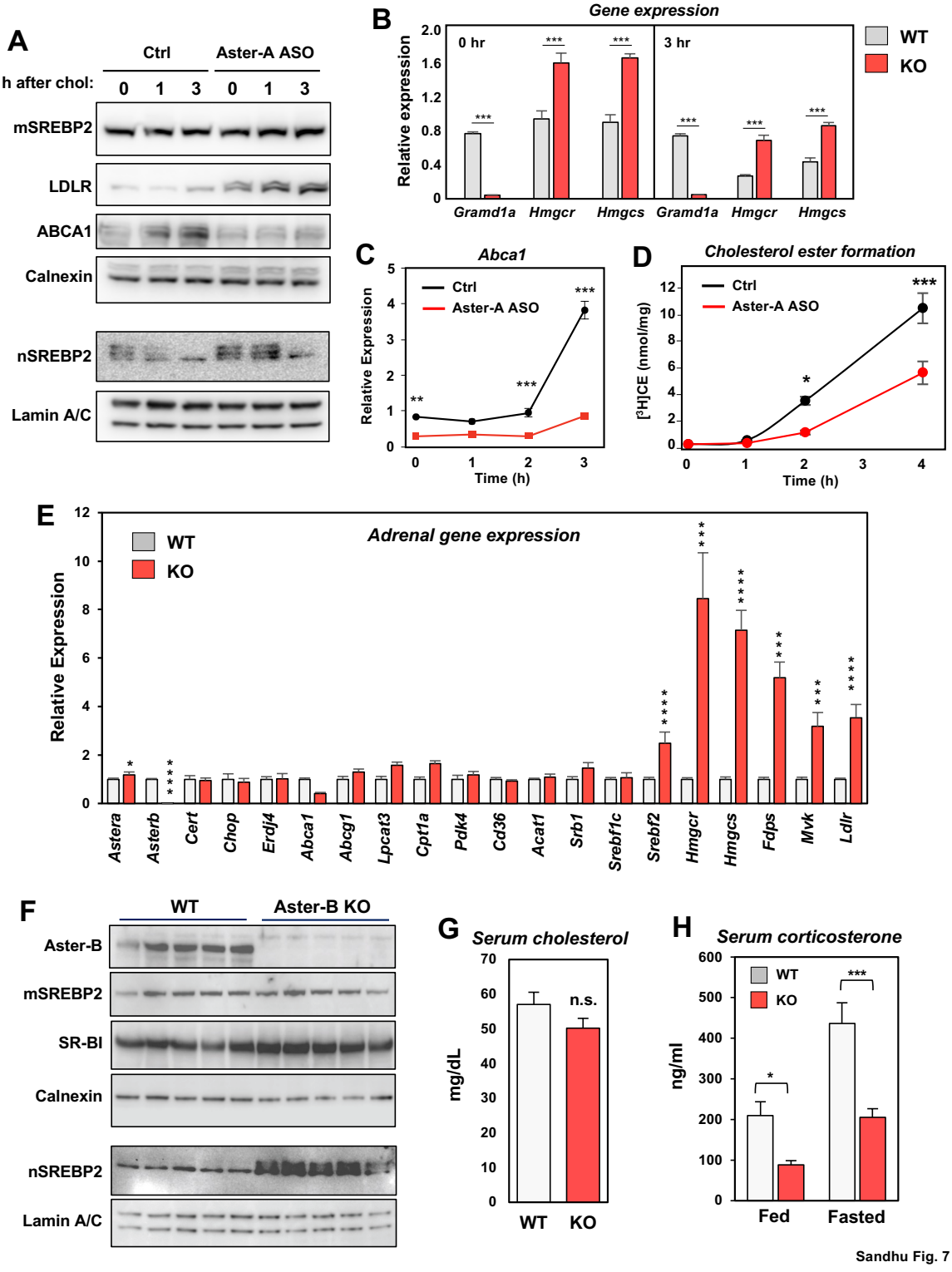

Sandhu Fig. 7

Figure 7

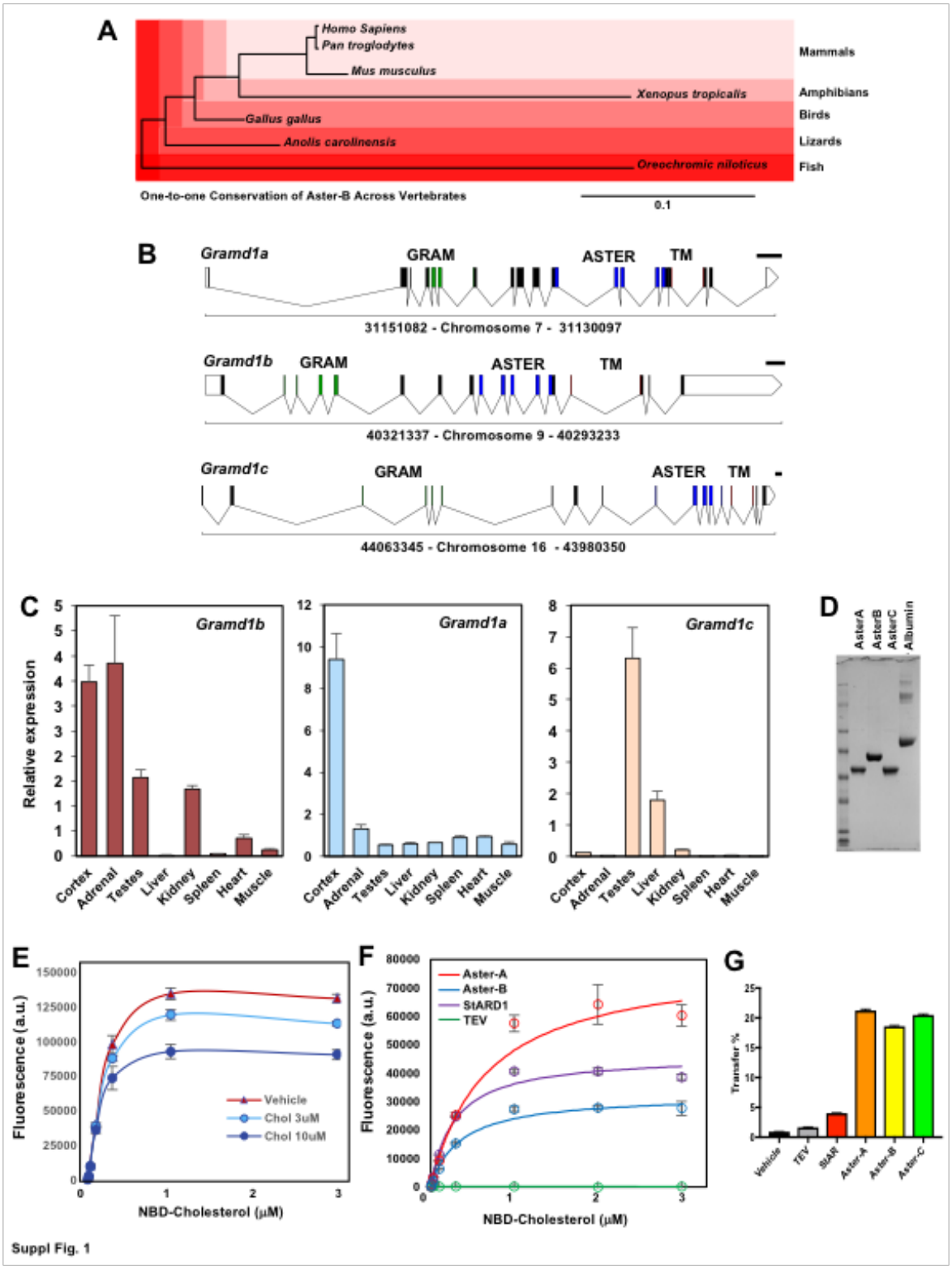
A
Homo Sapiens
Pan troglodytes
Mus musculus
Xenopus tropicalis
Gallus gallus
Anolis carolinensis
Oreochromic niloticus
Mammals
Amphibians
Birds
Lizards
Fish
One-to-one Conservation of Aster-B Across Vertebrates
0.1
B
Gramd1a
GRAM
ASTER
TM
31151082 - Chromosome 7 - 31130097
Gramd1b
GRAM
ASTER
TM
40321337 - Chromosome 9 - 40293233
Gramd1c
GRAM
ASTER
TM
44063345 - Chromosome 16 - 43980350
C
Gramd1b
Gramd1a
Gramd1c
Relative expression
Cortex
Adrenal
Testes
Liver
Kidney
Spleen
Heart
Muscle
D
AsterA
AsterB
AsterC
Albumin
E
Fluorescence (a.u.)
Vehicle
Chol 3uM
Chol 10uM
NBD-Cholesterol (μM)
F
Aster-A
Aster-B
StARD1
TEV
Fluorescence (a.u.)
NBD-Cholesterol (μM)
G
Transfer %
Vehicle
TEV
StAR
Aster-A
Aster-B
Aster-C
Suppl Fig. 1

Figure S1

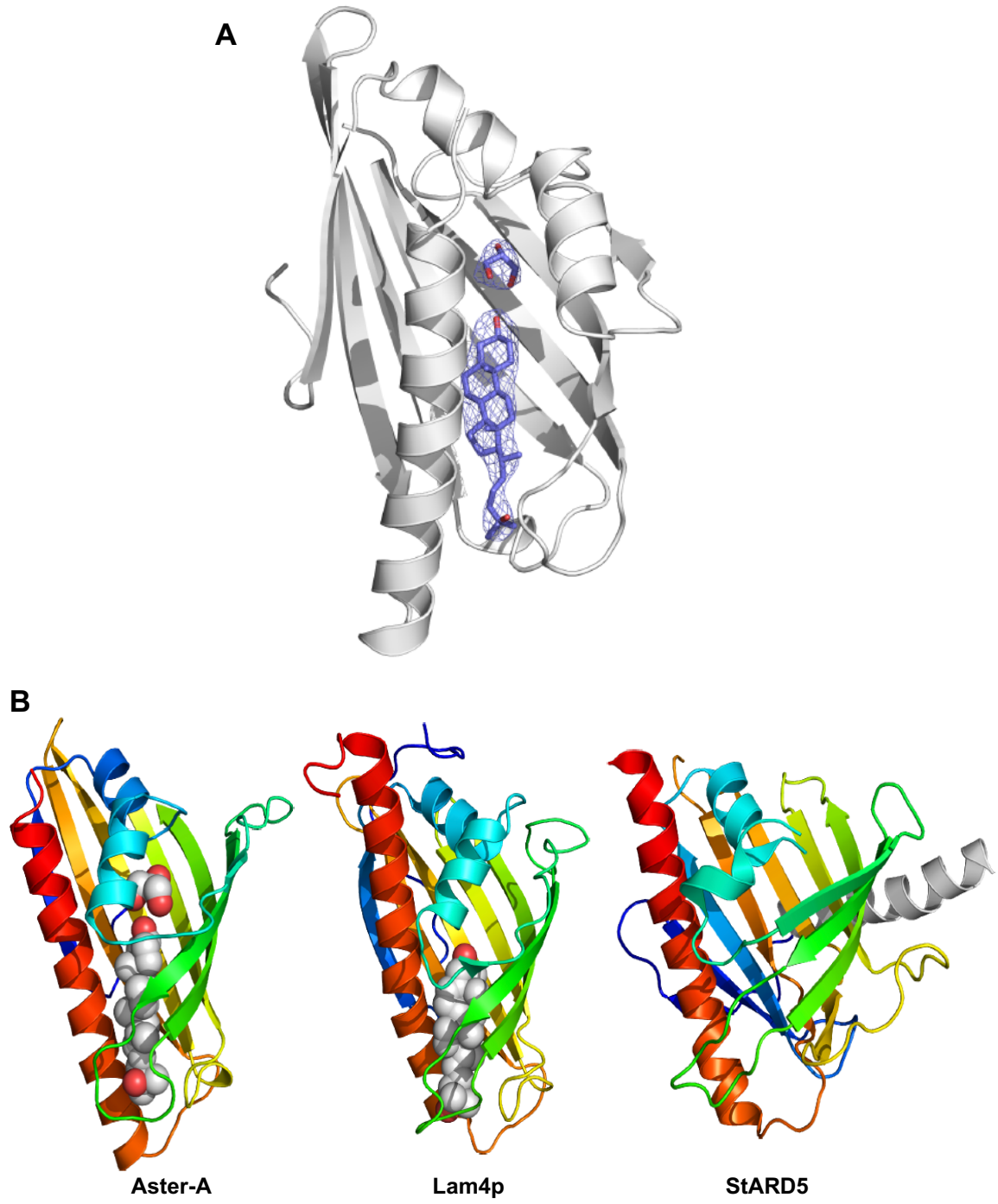

Suppl Fig. 2

Figure S2

A

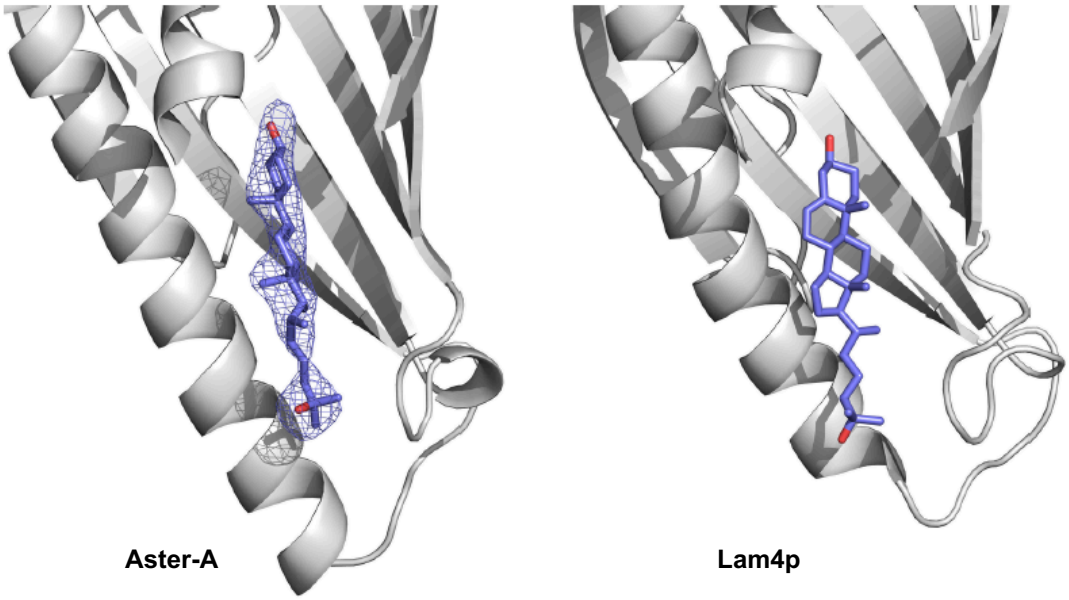

B

```
mmAster-A      LPDLSGRLLINSVFHMGAERLQQMLFSD-SPFLQGFLQ-QRKFTDVTLSPWSSDS---KC     419
mmAster-B      YEDLSGRQYVNEVFNFSVDKLYDLLFTN-SPFLRDFME-QRRFSDIIFHPWKKEE---NG     386
mmAster-C      EKDLQGRLYINRVFHISAERMFELLFTS-SHFMQRFAN-SRNIIDVVSTPWTVES---GG     376
Lam2p-1        KPSNNDHLVIEANINAPLGKVVNLLYGEDVSYYERILK-AQKNFEISPIPNNF-----LT     900
Lam4p-1        KPAPNEKLVNESTIHASLGRVVNILFGKDVSYIMAILK-AQKNSDISPIPVLVDSPTVSE     812
Lam2p-2        KGKDDTVIDEKINIPVPLGTVFSLLYGDDTSYIKKIIE-NQNNFNVCDIPKFV--N----     1108
Lam4p-2        KDKDDSIIRENENIPAPLGTVVQLLFGSNTEYMQKVITRDKNNVNVETIPKFT--PSLVE     1021

mmAster-A      HQRRVLTYTIPISNQLGPKSASVVETQTLFRRGPQAGGCVVDSEVLTQGIPYQDYFYTAH     479
mmAster-B      NQSRVILYTITLTNPLAPKTATVRETQTMYKASQESECYVIDAEVLTHDVPYHDYFYTIN     446
mmAster-C      NQLRTMTYTIVLSNPLTGKYTAATEKQTLYKESREAQFYLVDSEVLTHDVPYHDYFYTLN     436
Lam2p-1        KKIRDYAYTKPLSGSIGPSKTKCLITDTLEHYDL-EDYVKVLSITKNPDVPSGNIFSVKT     959
Lam4p-1        GKKRDYSYVKTTPGAIGPGKTKCMITETIQHFNL-EEYVQVLQTTKTPDVPSGNSFYVRT     871
Lam2p-2        -NAREITYTKKLNNSFGPKQTKCIVTETIEHMDL-NSFFMVKQIVRSPDVPYGSSFSVHT     1166
Lam4p-2        GGSRHYEYTKKLNNSIGPKQTKCLLTESIEHMDI-NNYVLVTQTTKTPDVPSGSNFAVES     1080

mmAster-A      RYCILGLARNKARLRVSSEIRYRKQPWSLVKSLIEKNSWSGIEDYFHHLDRELAKAEKLS     539
mmAster-B      RYTLTRVARNKSRLRVSTELRYRKQPWGFVKTFIEKNFWSGLEDYFRHLETELTKTESTY     506
mmAster-C      RYCIVRSAKQRCRLRVSTDLKYRKQPWGLIKSLIEKNSWSSLESYFKKLESDLLMEESVL     496
Lam2p-1        VFLFSWDKNNSTKLTVYNSVDWTGK--SWIKSMIEKGTFDGVADTTKIMISEIKKILS--     1015
Lam4p-1        VYLLSWANNNETKLKLYVSVEWTGK--SLIKSPIEKGTFDGVTDATKILVEELG------     923
Lam2p-2        RFFYSWGDHNTTNMKVVTNVVWTGK--SMLKGTIEKGSIDGQRSSTKQLVDDLKKIISNA     1224
Lam4p-2        KIFLFWGQHDTTNMTVITKINWTSK--SFLKGAIEKGSVEGQKVSVDYMLSELRDIISRA     1138
```

Suppl Fig.3

Figure S3

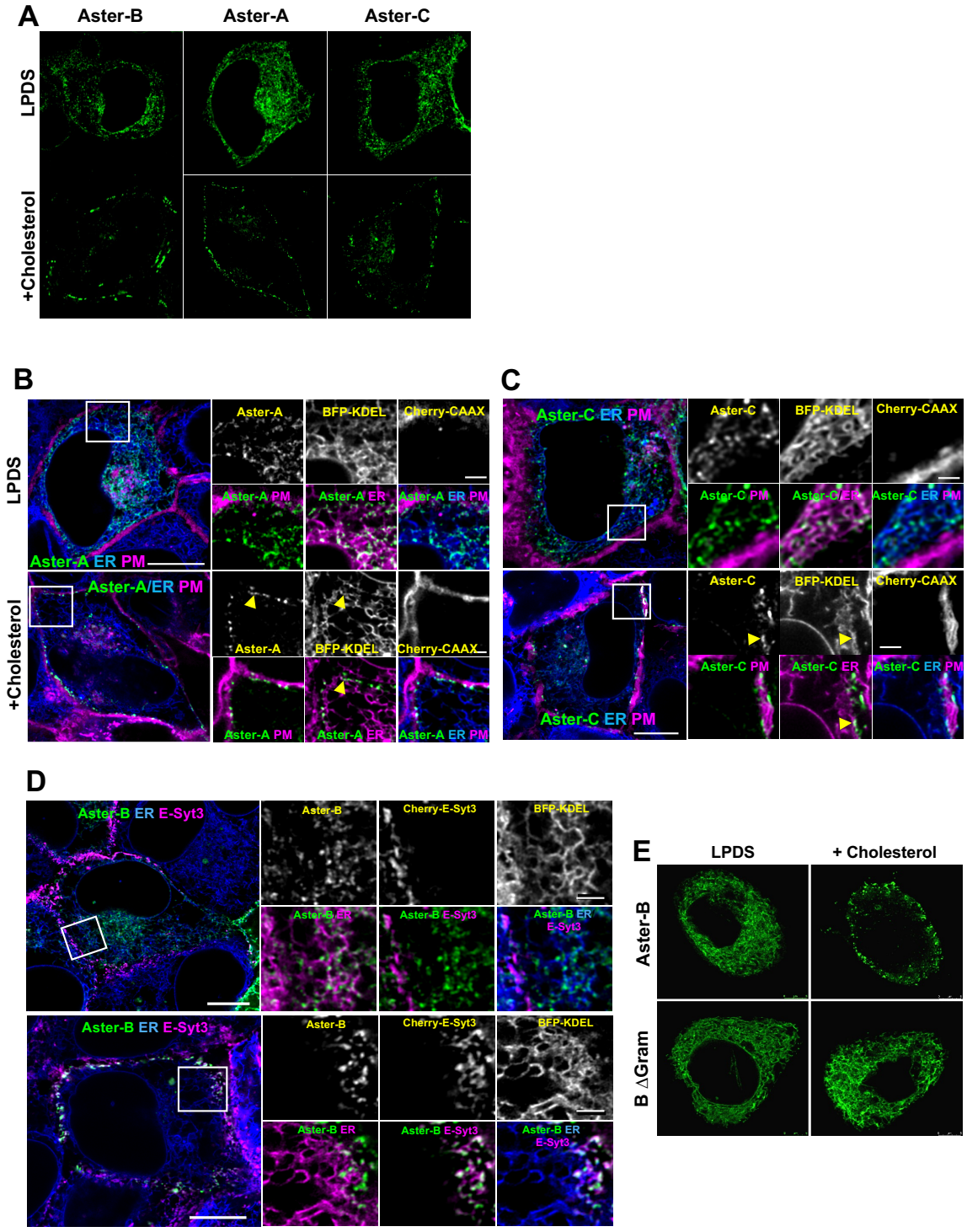

Suppl Fig. 4

Figure S4

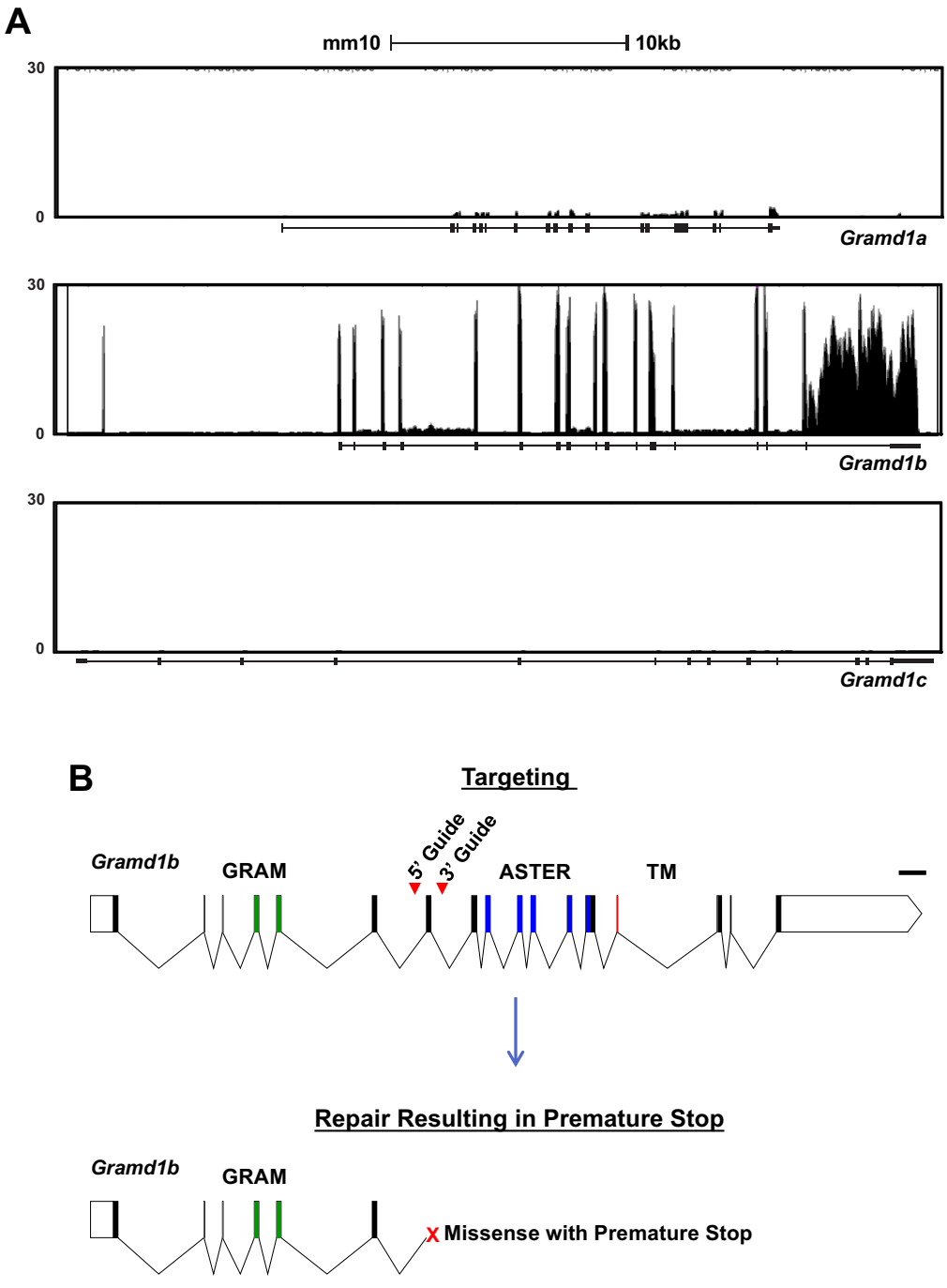

Suppl Fig. 5

Figure S5

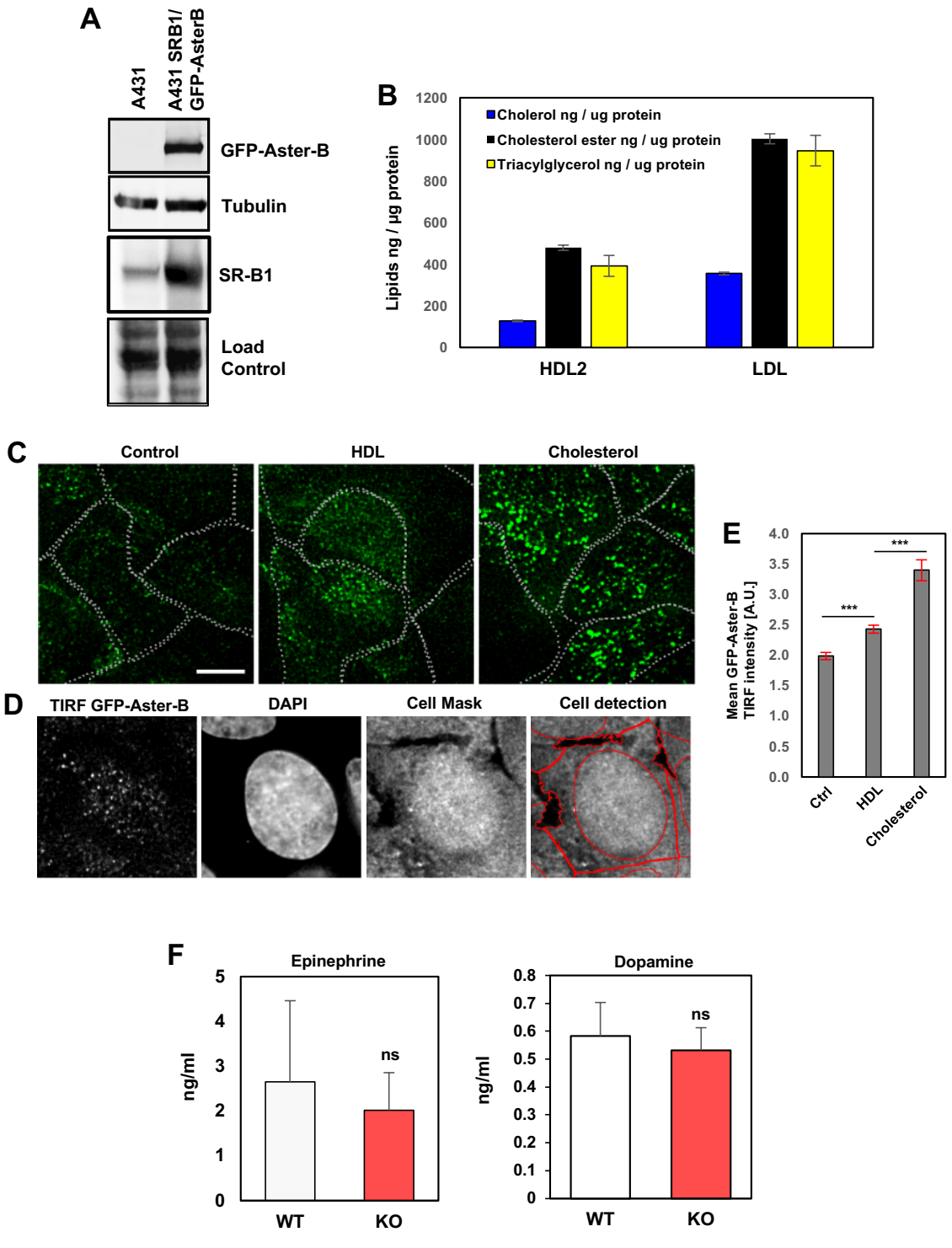

Suppl Fig. 6

Figure S6

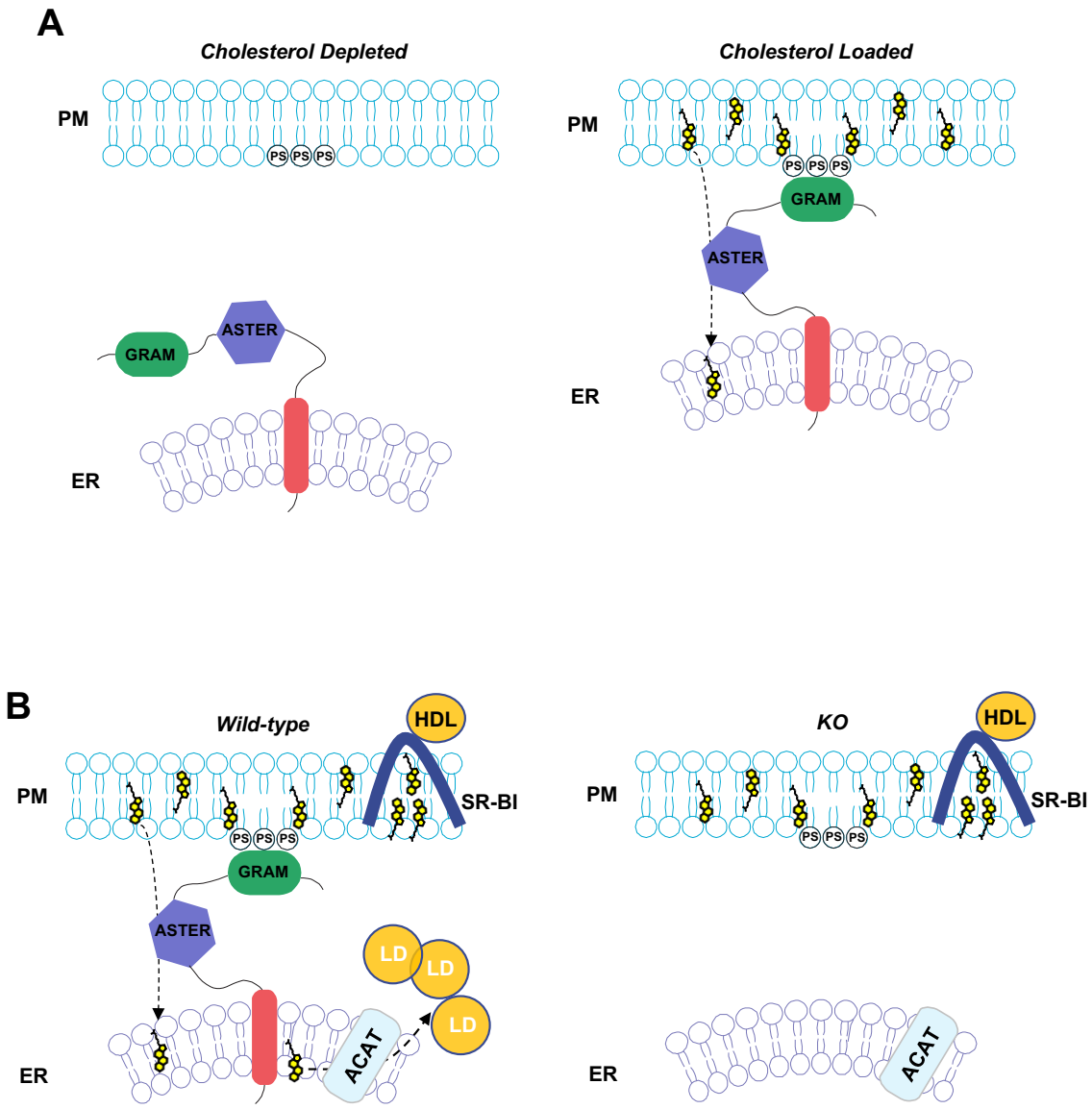

Suppl Fig. 7

Figure S7

Chapter 3:

Conclusion and Future Directions

Discussion

In this dissertation, I identify the function of the Aster family of proteins in mammalian cells. Given LXRs role in mediating efflux, we hypothesized that LXR was also likely to promote cholesterol movement between intracellular organelles and the plasma membrane (Wang and Tontonoz, 2018). This action would enable a rapid response to toxic accumulation of sterols. Through analysis of RNA-seq and ChIP-seq data I initially identified *Gramd1b* as a novel LXR-target gene. Primary sequence alignment readily identified two paralogs (*Gramd1a* and *Gramd1c*) and I decided to name the gene products Aster-A, –B, and –C (Greek *aster* for "star) after their similarity to the cholesterol trafficking protein StAR (Romanowski et al., 2002). The Aster family genes are encoded on separate chromosomes, have different tissue enrichments, and have evolved in vertebrates alongside key proteins in lipoprotein metabolism such as LDLR and SR-B1.

Using primary sequence homology, I determined that Aster proteins have an N-terminal GRAM domain and a C-terminal transmembrane domain (Doerks et al., 2000). Interestingly, bioinformatic analyses using tools such as I-Tasser readily identified secondary structural elements with resemblance to START domains in the central region of the protein (Zhang, 2008). Using this information, I purified all three domains, and demonstrated they are readily capable of binding and transferring cholesterol. Given their similarity to START domains I named the central region of Aster proteins the ASTER domain. Crystallization of the Aster-A ASTER domain demonstrated it broadly resembles START domains but has a clearly distinct mode of ligand binding.

Using live cell microscopy, I determined the Aster proteins are integral to the ER through a single transmembrane domain. Upon cellular cholesterol loading, Aster proteins are recruited to the cell periphery and co-localize with well-established ER-PM contact site markers such as

ORP5 and Syt-2 (Chung et al., 2015; Giordano et al., 2013). I further demonstrate that the PM recruitment requires an intact N-terminal GRAM domain which is sufficient for PM recruitment in response to cholesterol loading. The GRAM domain binds with high affinity to anionic phospholipids phosphatidylserine which is highly enriched at the inner leaflet of the PM (Yeung et al., 2008).

Elucidating the function of cholesterol trafficking proteins can be complicated by redundant pathways. To overcome this issue, I determined the function of Aster-A in 3T3-L1 pre-adipocytes and Aster-B in the adrenal cortex, contexts in which each protein is specifically enriched. Using antisense oligonucleotides (ASOs) that I validated in collaboration with Ionis pharmaceuticals, I knocked down Aster-A with high efficiency in 3T3-L1 cells and demonstrated its importance in the delivery of cholesterol to the endoplasmic reticulum (Seth et al., 2009).

I further demonstrated that Aster-B is critical to SR-B1-mediated selective uptake in the adrenal glands. Deletion of *Gramd1b* with Crispr-Cas9-mediated genome engineering results in Aster-B KO mice that showed absent adrenal cholesteryl esters, elevated SREBP-2 signaling, and impaired corticosteroid production. Interestingly, Aster-B deletion phenocopies Apo-A1, SR-B1, and ACAT1 deletion mice, placing this trafficking protein downstream of ApoA1/SR-B1 at the plasma membrane and upstream of ACAT1 at the endoplasmic reticulum (Meiner et al., 1996b; Rigotti et al., 1997; Williams et al., 2000).

All in all, we provide the first formal proof of the importance of PM to ER cholesterol trafficking to physiology *in vivo*. We determine the structure of the sterol liganded ASTER domain with atomic resolution and demonstrate this domain binds and transfers cholesterol between membranes. We further identify the Aster family as integral ER proteins that are

recruited to ER-PM contact sites in response to cellular cholesterol loading where they facilitate cholesterol trafficking to the ER.

Future Directions

Our understanding of the principles underling cellular cholesterol trafficking and compartmentalization are largely based on amenable cell-culture models. Much remains to be learned from physiologically relevant tissues (Ikonen, 2008). The lack of lipoprotein metabolism and one-to-one orthologs in yeast, for example, make some principles difficult to extrapolate to mammalian physiology. As a case-in-point, the HDL receptor SR-B1 is functionally dependent on inducible PM to ER cholesterol trafficking by the Aster family, all of which emerged early in vertebrate evolutionary history (Shen et al., 2018). Identification of genetic Aster-B mutations in humans represents an important future step in determining the clinical relevance of this protein in adrenal cholesterol uptake and steroidogenesis.

The discovery of the Aster proteins presented here also raises key mechanistic questions. For example, do Aster proteins operate in the anterograde direction, i.e. are they capable of trafficking newly synthesized cholesterol from the ER to the plasma membrane? This question should be addressed with biosynthetic tracers comparing wild-type and Aster-null systems (Urbani and Simoni, 1990). Recent work suggests that the ER cholesterol and the 'accessible' pool of PM cholesterol are in equilibrium at 5 mol% (Das et al., 2014). It is plausible that Aster proteins may simply promote the equilibration of these two pools in either direction without requiring a counter-exchange mechanism. But how would such a mechanism operate in the absence of the tethering activity of the GRAM domain we show to be dependent on excess PM cholesterol?

To address this question, it will be important to investigate the mechanisms underlying the recruitment of the GRAM domain to the PM. There are at least two possibilities that may explain how the GRAM domain is recruited to cholesterol-loaded plasma membranes. The first

possibility is that cholesterol loading modifies the biophysical properties of the PM such that phosphatidylserine is more accessible to binding by the GRAM domain. Another possibility is that cholesterol loading of the PM results in the production of a secondary messenger, or a conformational change in a PM-resident sterol sensing protein, that promotes GRAM binding.

Another provocative possibility is that the GRAM domain may also recruit to different cellular membranes to promote tethering in different contexts. For example, a major question in cholesterol trafficking has been how LDL-derived cholesterol exits the lysosome downstream of NPC1 (Ikonen, 2018). In the current model, soluble NPC2 within the lysosome transfers cholesterol to the membrane-bound NPC1 through a hand-off mechanism (Kwon et al., 2009). NPC1 subsequently is thought to insert cholesterol into the lysosomal membrane for subsequent trafficking steps. The fact that Aster proteins promote PM to ER cholesterol trafficking does not preclude their possible involvement in the trafficking of LDL-derived cholesterol. One possibility is that a switch, such as one activated by cholesterol loading of the lysosomal membrane, may recruit Asters to lysosomes and promote trafficking to the ER. In an alternative scenario, LDL-derived lysosomal cholesterol may be trafficked to the PM, in which case Aster proteins may operate downstream of the vesicular transport pathway (Infante and Radhakrishnan, 2017).

Although Aster-B clearly functions downstream of SR-B1, our data do not definitively address where HDL-derived CEs are first hydrolyzed. Based on the activity of Aster-B and the fact that cholesterol re-esterification by ACAT is required for lipid droplet CEs, I believe that CEs are likely hydrolyzed at the plasma membrane prior to import into the ER (Meiner et al., 1996a). Future studies will need to demonstrate whether or not this is true.

Our study also does not address whether the ASTER domain may participate in the trafficking of other lipids or sterols. While the ASTER domain broadly resembles the START domain, we show that Asters bind sterol with a unique mode of binding and orientation. It is certainly possible that the ASTER domain may have also evolved to accommodate other sterols such as bile acids and oxysterols to facilitate their trafficking in other physiologic contexts that extend beyond HDL cholesterol trafficking.

Indeed, several proteins of the ORP and START family have an affinity for cholesterol but many also bind other physiologically relevant lipids (Ikonen, 2008). Determining the applicability of *in vitro* binding experiments to physiology will necessitates loss of function studies in animal models. Our study of the Aster family has established principles that may be used for understanding physiological cholesterol trafficking in future studies. For example, what are the roles of the many unassigned proteins of the ORP and START family? These proteins are evolutionarily conserved and surely have functions that remain to be uncovered.

Moving beyond the adrenal gland, what is the physiologic role of Asters in other tissues? SR-B1-dependent selective uptake also operates in the liver (Shen et al., 2018). Unlike Aster-B, Aster-A and Aster-C are well expressed in hepatocytes raising the possibility that they may promote RCT downstream of SR-B1 in this tissue. Enhancing our understanding of the RCT pathway will be highly relevant to new diagnostic modalities and therapies to treat atherosclerosis.

Other notable tissues of interest are the intestine and the brain. Our understanding of cholesterol trafficking events downstream of absorption by NPC1L1 in the intestine is limited (Jia et al., 2011). The possibility that one or more of the Aster proteins operates downstream of NPC1L1 would make these proteins compelling drug targets for blocking cholesterol absorption.

Further, a recent report demonstrated that ER-PM contact sites are abundant throughout the brain (Wu et al., 2017). Whether or not these sites operate in cholesterol homeostasis will be a key direction moving forward.

Chapter 4:

References

References

Acton, S., Rigotti, A., Landschulz, K.T., Xu, S., Hobbs, H.H., and Krieger, M. (1996). Identification of scavenger receptor SR-BI as a high density lipoprotein receptor. Science *271*, 518-520.

Ajufo, E., and Rader, D.J. (2018). New Therapeutic Approaches for Familial Hypercholesterolemia. Annu Rev Med *69*, 113-131.

Alpy, F., and Tomasetto, C. (2005). Give lipids a START: the StAR-related lipid transfer (START) domain in mammals. J Cell Sci *118*, 2791-2801.

Angermuller, S., and Fahimi, H.D. (1982). Imidazole-buffered osmium tetroxide: an excellent stain for visualization of lipids in transmission electron microscopy. Histochem J *14*, 823-835.

Arakane, F., Kallen, C.B., Watari, H., Foster, J.A., Sepuri, N.B., Pain, D., Stayrook, S.E., Lewis, M., Gerton, G.L., and Strauss, J.F., 3rd (1998). The mechanism of action of steroidogenic acute regulatory protein (StAR). StAR acts on the outside of mitochondria to stimulate steroidogenesis. J Biol Chem *273*, 16339-16345.

Baker, B.Y., Epand, R.F., Epand, R.M., and Miller, W.L. (2007). Cholesterol binding does not predict activity of the steroidogenic acute regulatory protein, StAR. J Biol Chem *282*, 10223-10232.

Bautista, G., Pfisterer, S.G., Huttunen, M.J., Ranjan, S., Kanerva, K., Ikonen, E., and Kauranen, M. (2014). Polarized THG microscopy identifies compositionally different lipid droplets in mammalian cells. Biophys J *107*, 2230-2236.

Begley, M.J., Taylor, G.S., Kim, S.A., Veine, D.M., Dixon, J.E., and Stuckey, J.A. (2003). Crystal structure of a phosphoinositide phosphatase, MTMR2: insights into myotubular myopathy and Charcot-Marie-Tooth syndrome. Mol Cell *12*, 1391-1402.

Besprozvannaya, M., Dickson, E., Li, H., Ginburg, K.S., Bers, D.M., Auwerx, J., and Nunnari, J. (2018). GRAM domain proteins specialize functionally distinct ER-PM contact sites in human cells. Elife *7*.

Bligh, E.G., and Dyer, W.J. (1959). A rapid method of total lipid extraction and purification. Can J Biochem Physiol *37*, 911-917.

Bloch, K. (1965). The biological synthesis of cholesterol. Science *150*, 19-28.
Bonamassa, B., and Moschetta, A. (2013). Atherosclerosis: lessons from LXR and the intestine. Trends Endocrinol Metab *24*, 120-128.

Bowden, J.A., Shao, F., Albert, C.J., Lally, J.W., Brown, R.J., Procknow, J.D., Stephenson, A.H., and Ford, D.A. (2011). Electrospray ionization tandem mass spectrometry of sodiated adducts of cholesteryl esters. Lipids *46*, 1169-1179.

Braun, A., Trigatti, B.L., Post, M.J., Sato, K., Simons, M., Edelberg, J.M., Rosenberg, R.D., Schrenzel, M., and Krieger, M. (2002). Loss of SR-BI expression leads to the early onset of occlusive atherosclerotic coronary artery disease, spontaneous myocardial infarctions, severe

cardiac dysfunction, and premature death in apolipoprotein E-deficient mice. Circ Res *90*, 270-276.

Brown, A.J., Sun, L., Feramisco, J.D., Brown, M.S., and Goldstein, J.L. (2002). Cholesterol addition to ER membranes alters conformation of SCAP, the SREBP escort protein that regulates cholesterol metabolism. Mol Cell *10*, 237-245.

Brown, M.S., and Goldstein, J.L. (1997). The SREBP pathway: regulation of cholesterol metabolism by proteolysis of a membrane-bound transcription factor. Cell *89*, 331-340.

Brown, M.S., Radhakrishnan, A., and Goldstein, J.L. (2017). Retrospective on Cholesterol Homeostasis: The Central Role of Scap. Annu Rev Biochem.

Brown, R.J., Shao, F., Baldan, A., Albert, C.J., and Ford, D.A. (2013). Cholesterol efflux analyses using stable isotopes and mass spectrometry. Anal Biochem *433*, 56-64.

Brunham, L.R., Kruit, J.K., Iqbal, J., Fievet, C., Timmins, J.M., Pape, T.D., Coburn, B.A., Bissada, N., Staels, B., Groen, A.K*., et al.* (2006). Intestinal ABCA1 directly contributes to HDL biogenesis in vivo. J Clin Invest *116*, 1052-1062.

Calkin, A.C., and Tontonoz, P. (2010). Liver x receptor signaling pathways and atherosclerosis. Arterioscler Thromb Vasc Biol *30*, 1513-1518.

Calkin, A.C., and Tontonoz, P. (2012). Transcriptional integration of metabolism by the nuclear sterol-activated receptors LXR and FXR. Nat Rev Mol Cell Biol *13*, 213-224.

Caron, K.M., Soo, S.C., Wetsel, W.C., Stocco, D.M., Clark, B.J., and Parker, K.L. (1997). Targeted disruption of the mouse gene encoding steroidogenic acute regulatory protein provides insights into congenital lipoid adrenal hyperplasia. Proc Natl Acad Sci U S A *94*, 11540-11545.

Carpenter, A.E., Jones, T.R., Lamprecht, M.R., Clarke, C., Kang, I.H., Friman, O., Guertin, D.A., Chang, J.H., Lindquist, R.A., Moffat, J*., et al.* (2006). CellProfiler: image analysis software for identifying and quantifying cell phenotypes. Genome Biol *7*, R100.

Carstea, E.D., Polymeropoulos, M.H., Parker, C.C., Detera-Wadleigh, S.D., O'Neill, R.R., Patterson, M.C., Goldin, E., Xiao, H., Straub, R.E., Vanier, M.T*., et al.* (1993). Linkage of Niemann-Pick disease type C to human chromosome 18. Proc Natl Acad Sci U S A *90*, 2002-2004.

Chiapparino, A., Maeda, K., Turei, D., Saez-Rodriguez, J., and Gavin, A.C. (2016). The orchestra of lipid-transfer proteins at the crossroads between metabolism and signaling. Prog Lipid Res *61*, 30-39.

Chu, B.B., Liao, Y.C., Qi, W., Xie, C., Du, X., Wang, J., Yang, H., Miao, H.H., Li, B.L., and Song, B.L. (2015). Cholesterol transport through lysosome-peroxisome membrane contacts. Cell *161*, 291-306.

Chung, J., Torta, F., Masai, K., Lucast, L., Czapla, H., Tanner, L.B., Narayanaswamy, P., Wenk, M.R., Nakatsu, F., and De Camilli, P. (2015). INTRACELLULAR TRANSPORT.

PI4P/phosphatidylserine countertransport at ORP5- and ORP8-mediated ER-plasma membrane contacts. Science (New York, NY) *349*, 428-432.

Clark, B.J. (2012). The mammalian START domain protein family in lipid transport in health and disease. J Endocrinol *212*, 257-275.

Collins, J.L., Fivush, A.M., Watson, M.A., Galardi, C.M., Lewis, M.C., Moore, L.B., Parks, D.J., Wilson, J.G., Tippin, T.K., Binz, J.G.*, et al.* (2002). Identification of a nonsteroidal liver X receptor agonist through parallel array synthesis of tertiary amines. J Med Chem *45*, 1963-1966.

Connelly, M.A. (2009). SR-BI-mediated HDL cholesteryl ester delivery in the adrenal gland. Mol Cell Endocrinol *300*, 83-88.

Consortium, E.P. (2012). An integrated encyclopedia of DNA elements in the human genome. Nature *489*, 57-74.

Couzin, J. (2008). Clinical trials and tribulations. Cholesterol veers off script. Science *322*, 220-223.

Das, A., Brown, M.S., Anderson, D.D., Goldstein, J.L., and Radhakrishnan, A. (2014). Three pools of plasma membrane cholesterol and their relation to cholesterol homeostasis. eLife *3*, 19316.

Das, A., Goldstein, J.L., Anderson, D.D., Brown, M.S., and Radhakrishnan, A. (2013). Use of mutant 125I-perfringolysin O to probe transport and organization of cholesterol in membranes of animal cells. Proc Natl Acad Sci U S A *110*, 10580-10585.

Del Valle, I., Buonocore, F., Duncan, A.J., Lin, L., Barenco, M., Parnaik, R., Shah, S., Hubank, M., Gerrelli, D., and Achermann, J.C. (2017). A genomic atlas of human adrenal and gonad development. Wellcome Open Res *2*, 25.

Doerks, T., Strauss, M., Brendel, M., and Bork, P. (2000). GRAM, a novel domain in glucosyltransferases, myotubularins and other putative membrane-associated proteins. Trends Biochem Sci *25*, 483-485.

Drin, G. (2014). Topological regulation of lipid balance in cells. Annu Rev Biochem *83*, 51-77.
Elbashir, S.M., Harborth, J., Lendeckel, W., Yalcin, A., Weber, K., and Tuschl, T. (2001). Duplexes of 21-nucleotide RNAs mediate RNA interference in cultured mammalian cells. Nature *411*, 494-498.

Elbaz-Alon, Y., Eisenberg-Bord, M., Shinder, V., Stiller, S.B., Shimoni, E., Wiedemann, N., Geiger, T., and Schuldiner, M. (2015). Lam6 Regulates the Extent of Contacts between Organelles. Cell Rep *12*, 7-14.

Emerging Risk Factors, C., Di Angelantonio, E., Sarwar, N., Perry, P., Kaptoge, S., Ray, K.K., Thompson, A., Wood, A.M., Lewington, S., Sattar, N.*, et al.* (2009). Major lipids, apolipoproteins, and risk of vascular disease. JAMA *302*, 1993-2000.

Farese, R.V. (2006). The nine lives of ACAT inhibitors. Arteriosclerosis, thrombosis, and vascular biology *26*, 1684-1686.

Friedman, J.R., Lackner, L.L., West, M., Dibenedetto, J.R., Nunnari, J., and Voeltz, G.K. (2011). ER tubules mark sites of mitochondrial division. Science (New York, NY) *334*, 358-362.

Garcia-Calvo, M., Lisnock, J., Bull, H.G., Hawes, B.E., Burnett, D.A., Braun, M.P., Crona, J.H., Davis, H.R., Jr., Dean, D.C., Detmers, P.A.*, et al.* (2005). The target of ezetimibe is Niemann-Pick C1-Like 1 (NPC1L1). Proc Natl Acad Sci U S A *102*, 8132-8137.

Gatta, A.T., Wong, L.H., Sere, Y.Y., Calderon-Norena, D.M., Cockcroft, S., Menon, A.K., and Levine, T.P. (2015). A new family of StART domain proteins at membrane contact sites has a role in ER-PM sterol transport. Elife *4*.

Ge, L., Wang, J., Qi, W., Miao, H.H., Cao, J., Qu, Y.X., Li, B.L., and Song, B.L. (2008). The cholesterol absorption inhibitor ezetimibe acts by blocking the sterol-induced internalization of NPC1L1. Cell Metab *7*, 508-519.

Georgiev, A.G., Sullivan, D.P., Kersting, M.C., Dittman, J.S., Beh, C.T., and Menon, A.K. (2011). Osh proteins regulate membrane sterol organization but are not required for sterol movement between the ER and PM. Traffic *12*, 1341-1355.

Ghai, R., Du, X., Wang, H., Dong, J., Ferguson, C., Brown, A.J., Parton, R.G., Wu, J.W., and Yang, H. (2017). ORP5 and ORP8 bind phosphatidylinositol-4, 5-biphosphate (PtdIns(4,5)P 2) and regulate its level at the plasma membrane. Nat Commun *8*, 757.

Gibson, D.G., Young, L., Chuang, R.Y., Venter, J.C., Hutchison, C.A., 3rd, and Smith, H.O. (2009). Enzymatic assembly of DNA molecules up to several hundred kilobases. Nat Methods *6*, 343-345.

Giordano, F., Saheki, Y., Idevall-Hagren, O., Colombo, S.F., Pirruccello, M., Milosevic, I., Gracheva, E.O., Bagriantsev, S.N., Borgese, N., and De Camilli, P. (2013). PI(4,5)P(2)-dependent and Ca(2+)-regulated ER-PM interactions mediated by the extended synaptotagmins. Cell *153*, 1494-1509.

Glass, C., Pittman, R.C., Weinstein, D.B., and Steinberg, D. (1983). Dissociation of tissue uptake of cholesterol ester from that of apoprotein A-I of rat plasma high density lipoprotein: selective delivery of cholesterol ester to liver, adrenal, and gonad. Proc Natl Acad Sci U S A *80*, 5435-5439.

Goldstein, J.L., Basu, S.K., and Brown, M.S. (1983). Receptor-mediated endocytosis of low-density lipoprotein in cultured cells. Methods Enzymol *98*, 241-260.

Goldstein, J.L., and Brown, M.S. (1985). The LDL receptor and the regulation of cellular cholesterol metabolism. J Cell Sci Suppl *3*, 131-137.

Goldstein, J.L., and Brown, M.S. (2015a). A century of cholesterol and coronaries: from plaques to genes to statins. Cell *161*, 161-172.

Goldstein, J.L., and Brown, M.S. (2015b). A century of cholesterol and coronaries: from plaques to genes to statins. Cell *161*, 161-172.

Goldstein, J.L., Brown, M.S., Anderson, R.G., Russell, D.W., and Schneider, W.J. (1985). Receptor-mediated endocytosis: concepts emerging from the LDL receptor system. Annu Rev Cell Biol *1*, 1-39.

Han, X., and Gross, R.W. (2005). Shotgun lipidomics: electrospray ionization mass spectrometric analysis and quantitation of cellular lipidomes directly from crude extracts of biological samples. Mass Spectrom Rev *24*, 367-412.

Hegele, R.A. (2009). Plasma lipoproteins: genetic influences and clinical implications. Nat Rev Genet *10*, 109-121.

Heino, S., Lusa, S., Somerharju, P., Ehnholm, C., Olkkonen, V.M., and Ikonen, E. (2000). Dissecting the role of the golgi complex and lipid rafts in biosynthetic transport of cholesterol to the cell surface. Proc Natl Acad Sci U S A *97*, 8375-8380.

Hoekstra, M. (2017). SR-BI as target in atherosclerosis and cardiovascular disease - A comprehensive appraisal of the cellular functions of SR-BI in physiology and disease. Atherosclerosis *258*, 153-161.

Hoekstra, M., Meurs, I., Koenders, M., Out, R., Hildebrand, R.B., Kruijt, J.K., Van Eck, M., and Van Berkel, T.J. (2008). Absence of HDL cholesteryl ester uptake in mice via SR-BI impairs an adequate adrenal glucocorticoid-mediated stress response to fasting. J Lipid Res *49*, 738-745.

Hoekstra, M., van der Sluis, R.J., Van Eck, M., and Van Berkel, T.J. (2013). Adrenal-specific scavenger receptor BI deficiency induces glucocorticoid insufficiency and lowers plasma very-low-density and low-density lipoprotein levels in mice. Arterioscler Thromb Vasc Biol *33*, e39-46.

Holthuis, J.C., and Menon, A.K. (2014). Lipid landscapes and pipelines in membrane homeostasis. Nature *510*, 48-57.

Horenkamp, F.A., Valverde, D.P., Nunnari, J., and Reinisch, K.M. (2018). Molecular basis for sterol transport by StART-like lipid transfer domains. EMBO J *37*.

Horton, J.D., Goldstein, J.L., and Brown, M.S. (2002). SREBPs: transcriptional mediators of lipid homeostasis. Cold Spring Harb Symp Quant Biol *67*, 491-498.

Ikonen, E. (2008). Cellular cholesterol trafficking and compartmentalization. Nat Rev Mol Cell Biol *9*, 125-138.

Ikonen, E. (2018). Mechanisms of cellular cholesterol compartmentalization: recent insights. Curr Opin Cell Biol *53*, 77-83.

Ikonen, E. (in press). Mechanisms of cellular cholesterol compartmentalization: recent insights. . Current opinion in cell biology.

Infante, R.E., Abi-Mosleh, L., Radhakrishnan, A., Dale, J.D., Brown, M.S., and Goldstein, J.L. (2008a). Purified NPC1 protein. I. Binding of cholesterol and oxysterols to a 1278-amino acid membrane protein. J Biol Chem *283*, 1052-1063.

Infante, R.E., and Radhakrishnan, A. (2017). Continuous transport of a small fraction of plasma membrane cholesterol to endoplasmic reticulum regulates total cellular cholesterol. Elife *6*.

Infante, R.E., Radhakrishnan, A., Abi-Mosleh, L., Kinch, L.N., Wang, M.L., Grishin, N.V., Goldstein, J.L., and Brown, M.S. (2008b). Purified NPC1 protein: II. Localization of sterol binding to a 240-amino acid soluble luminal loop. J Biol Chem *283*, 1064-1075.

Infante, R.E., Wang, M.L., Radhakrishnan, A., Kwon, H.J., Brown, M.S., and Goldstein, J.L. (2008c). NPC2 facilitates bidirectional transfer of cholesterol between NPC1 and lipid bilayers, a step in cholesterol egress from lysosomes. Proceedings of the National Academy of Sciences of the United States of America *105*, 15287-15292.

Janowski, B.A., Willy, P.J., Devi, T.R., Falck, J.R., and Mangelsdorf, D.J. (1996). An oxysterol signalling pathway mediated by the nuclear receptor LXR alpha. Nature *383*, 728-731.

Jentsch, J.A., Kiburu, I., Pandey, K., Timme, M., Ramlall, T., Levkau, B., Wu, J., Eliezer, D., Boudker, O., and Menon, A.K. (2018). Structural basis of sterol binding and transport by a yeast StARkin domain. J Biol Chem *293*, 5522-5531.

Jia, L., Betters, J.L., and Yu, L. (2011). Niemann-pick C1-like 1 (NPC1L1) protein in intestinal and hepatic cholesterol transport. Annu Rev Physiol *73*, 239-259.

Kaplan, M.R., and Simoni, R.D. (1985). Transport of cholesterol from the endoplasmic reticulum to the plasma membrane. J Cell Biol *101*, 446-453.

Khafif, M., Cottret, L., Balague, C., and Raffaele, S. (2014). Identification and phylogenetic analyses of VASt, an uncharacterized protein domain associated with lipid-binding domains in Eukaryotes. BMC Bioinformatics *15*, 222.

Khera, A.V., Cuchel, M., de la Llera-Moya, M., Rodrigues, A., Burke, M.F., Jafri, K., French, B.C., Phillips, J.A., Mucksavage, M.L., Wilensky, R.L.*, et al.* (2011). Cholesterol efflux capacity, high-density lipoprotein function, and atherosclerosis. N Engl J Med *364*, 127-135.

Konstantinov, I.E., Mejevoi, N., and Anichkov, N.M. (2006). Nikolai N. Anichkov and his theory of atherosclerosis. Tex Heart Inst J *33*, 417-423.

Krahmer, N., Guo, Y., Farese, R.V., and Walther, T.C. (2009). SnapShot: Lipid Droplets. Cell *139*, 1024-1024.e1021.

Kwon, H.J., Abi-Mosleh, L., Wang, M.L., Deisenhofer, J., Goldstein, J.L., Brown, M.S., and Infante, R.E. (2009). Structure of N-terminal domain of NPC1 reveals distinct subdomains for binding and transfer of cholesterol. Cell *137*, 1213-1224.

Lange, Y., and Matthies, H.J. (1984). Transfer of cholesterol from its site of synthesis to the plasma membrane. J Biol Chem *259*, 14624-14630.

Lange, Y., Ye, J., Rigney, M., and Steck, T.L. (1999). Regulation of endoplasmic reticulum cholesterol by plasma membrane cholesterol. J Lipid Res *40*, 2264-2270.

Lees, J.A., Messa, M., Sun, E.W., Wheeler, H., Torta, F., Wenk, M.R., De Camilli, P., and Reinisch, K.M. (2017). Lipid transport by TMEM24 at ER-plasma membrane contacts regulates pulsatile insulin secretion. Science (New York, NY) *355*, eaah6171.

Lev, S. (2010). Non-vesicular lipid transport by lipid-transfer proteins and beyond. Nat Rev Mol Cell Biol *11*, 739-750.

Lin, D., Sugawara, T., Strauss, J.F., 3rd, Clark, B.J., Stocco, D.M., Saenger, P., Rogol, A., and Miller, W.L. (1995a). Role of steroidogenic acute regulatory protein in adrenal and gonadal steroidogenesis. Science *267*, 1828-1831.

Lin, D., Sugawara, T., Strauss, J.F., Clark, B.J., Stocco, D.M., Saenger, P., Rogol, A., and Miller, W.L. (1995b). Role of steroidogenic acute regulatory protein in adrenal and gonadal steroidogenesis. Science (New York, NY) *267*, 1828-1831.

Lippincott-Schwartz, J., and Phair, R.D. (2010). Lipids and cholesterol as regulators of traffic in the endomembrane system. Annu Rev Biophys *39*, 559-578.

Lombardo, A., Cesana, D., Genovese, P., Di Stefano, B., Provasi, E., Colombo, D.F., Neri, M., Magnani, Z., Cantore, A., Lo Riso, P.*, et al.* (2011). Site-specific integration and tailoring of cassette design for sustainable gene transfer. Nat Methods *8*, 861-869.

Mahmood, S.S., Levy, D., Vasan, R.S., and Wang, T.J. (2014). The Framingham Heart Study and the epidemiology of cardiovascular disease: a historical perspective. Lancet *383*, 999-1008.

Mangelsdorf, D.J., Thummel, C., Beato, M., Herrlich, P., Schutz, G., Umesono, K., Blumberg, B., Kastner, P., Mark, M., Chambon, P.*, et al.* (1995). The nuclear receptor superfamily: the second decade. Cell *83*, 835-839.

Maxfield, F.R., and Tabas, I. (2005). Role of cholesterol and lipid organization in disease. Nature *438*, 612-621.

Mehlem, A., Hagberg, C.E., Muhl, L., Eriksson, U., and Falkevall, A. (2013). Imaging of neutral lipids by oil red O for analyzing the metabolic status in health and disease. Nat Protoc *8*, 1149-1154.

Meiner, V.L., Cases, S., Myers, H.M., Sande, E.R., Bellosta, S., Schambelan, M., Pitas, R.E., McGuire, J., Herz, J., and Farese, R.V. (1996a). Disruption of the acyl-CoA:cholesterol acyltransferase gene in mice: Evidence suggesting multiple cholesterol esterification enzymes in mammals. Proceedings of the National Academy of Sciences of the United States of America *93*, 14041-14046.

Meiner, V.L., Cases, S., Myers, H.M., Sande, E.R., Bellosta, S., Schambelan, M., Pitas, R.E., McGuire, J., Herz, J., and Farese, R.V., Jr. (1996b). Disruption of the acyl-CoA:cholesterol acyltransferase gene in mice: evidence suggesting multiple cholesterol esterification enzymes in mammals. Proc Natl Acad Sci U S A *93*, 14041-14046.

Mesmin, B., Bigay, J., Moser von Filseck, J., Lacas-Gervais, S., Drin, G., and Antonny, B. (2013). A four-step cycle driven by PI(4)P hydrolysis directs sterol/PI(4)P exchange by the ER-Golgi tether OSBP. Cell *155*, 830-843.

Murley, A., Sarsam, R.D., Toulmay, A., Yamada, J., Prinz, W.A., and Nunnari, J. (2015). Ltc1 is an ER-localized sterol transporter and a component of ER-mitochondria and ER-vacuole contacts. J Cell Biol *209*, 539-548.

Neculai, D., Schwake, M., Ravichandran, M., Zunke, F., Collins, R.F., Peters, J., Neculai, M., Plumb, J., Loppnau, P., Pizarro, J.C.*, et al.* (2013). Structure of LIMP-2 provides functional insights with implications for SR-BI and CD36. Nature *504*, 172-176.

Nguyen, S.D., Oorni, K., Lee-Rueckert, M., Pihlajamaa, T., Metso, J., Jauhiainen, M., and Kovanen, P.T. (2012). Spontaneous remodeling of HDL particles at acidic pH enhances their capacity to induce cholesterol efflux from human macrophage foam cells. J Lipid Res *53*, 2115-2125.

Oram, J.F., and Vaughan, A.M. (2006). ATP-Binding cassette cholesterol transporters and cardiovascular disease. Circ Res *99*, 1031-1043.

Petrescu, A.D., Gallegos, A.M., Okamura, Y., Strauss, J.F., 3rd, and Schroeder, F. (2001). Steroidogenic acute regulatory protein binds cholesterol and modulates mitochondrial membrane sterol domain dynamics. J Biol Chem *276*, 36970-36982.

Pfisterer, S.G., Peranen, J., and Ikonen, E. (2016). LDL-cholesterol transport to the endoplasmic reticulum: current concepts. Curr Opin Lipidol *27*, 282-287.

Phillips, M.J., and Voeltz, G.K. (2016). Structure and function of ER membrane contact sites with other organelles. Nat Rev Mol Cell Biol *17*, 69-82.

Pittman, R.C., Knecht, T.P., Rosenbaum, M.S., and Taylor, C.A., Jr. (1987). A nonendocytotic mechanism for the selective uptake of high density lipoprotein-associated cholesterol esters. J Biol Chem *262*, 2443-2450.

Rader, D.J. (2014). Spotlight on HDL biology: new insights in metabolism, function, and translation. Cardiovascular Research *103*, 337-340.

Rader, D.J., and Tall, A.R. (2012). The not-so-simple HDL story: Is it time to revise the HDL cholesterol hypothesis? Nat Med *18*, 1344-1346.

Radhakrishnan, A., Goldstein, J.L., McDonald, J.G., and Brown, M.S. (2008). Switch-like control of SREBP-2 transport triggered by small changes in ER cholesterol: a delicate balance. Cell metabolism *8*, 512-521.

Radhakrishnan, A., Sun, L.P., Kwon, H.J., Brown, M.S., and Goldstein, J.L. (2004). Direct binding of cholesterol to the purified membrane region of SCAP: mechanism for a sterol-sensing domain. Mol Cell *15*, 259-268.

Ran, F.A., Hsu, P.D., Wright, J., Agarwala, V., Scott, D.A., and Zhang, F. (2013). Genome engineering using the CRISPR-Cas9 system. Nat Protoc *8*, 2281-2308.

Rayner, K.J., Suarez, Y., Davalos, A., Parathath, S., Fitzgerald, M.L., Tamehiro, N., Fisher, E.A., Moore, K.J., and Fernandez-Hernando, C. (2010). MiR-33 contributes to the regulation of cholesterol homeostasis. Science *328*, 1570-1573.

Repa, J.J., Berge, K.E., Pomajzl, C., Richardson, J.A., Hobbs, H., and Mangelsdorf, D.J. (2002). Regulation of ATP-binding cassette sterol transporters ABCG5 and ABCG8 by the liver X receptors alpha and beta. J Biol Chem *277*, 18793-18800.

Rigotti, A., Trigatti, B.L., Penman, M., Rayburn, H., Herz, J., and Krieger, M. (1997). A targeted mutation in the murine gene encoding the high density lipoprotein (HDL) receptor scavenger receptor class B type I reveals its key role in HDL metabolism. Proc Natl Acad Sci U S A *94*, 12610-12615.

Romanowski, M.J., Soccio, R.E., Breslow, J.L., and Burley, S.K. (2002). Crystal structure of the Mus musculus cholesterol-regulated START protein 4 (StarD4) containing a StAR-related lipid transfer domain. Proc Natl Acad Sci U S A *99*, 6949-6954.

Sallam, T., Jones, M., Thomas, B.J., Wu, X., Gilliland, T., Qian, K., Eskin, A., Casero, D., Zhang, Z., Sandhu, J.*, et al.* (2018). Transcriptional regulation of macrophage cholesterol efflux and atherogenesis by a long noncoding RNA. Nat Med *24*, 304-312.

Sallam, T., Jones, M.C., Gilliland, T., Zhang, L., Wu, X., Eskin, A., Sandhu, J., Casero, D., Vallim, T.Q., Hong, C.*, et al.* (2016). Feedback modulation of cholesterol metabolism by the lipid-responsive non-coding RNA LeXis. Nature *534*, 124-128.

Seth, P.P., Siwkowski, A., Allerson, C.R., Vasquez, G., Lee, S., Prakash, T.P., Wancewicz, E.V., Witchell, D., and Swayze, E.E. (2009). Short antisense oligonucleotides with novel 2'-4' conformationaly restricted nucleoside analogues show improved potency without increased toxicity in animals. J Med Chem *52*, 10-13.

Shen, W.J., Azhar, S., and Kraemer, F.B. (2018). SR-B1: A Unique Multifunctional Receptor for Cholesterol Influx and Efflux. Annu Rev Physiol *80*, 95-116.

Sleat, D.E., Wiseman, J.A., El-Banna, M., Price, S.M., Verot, L., Shen, M.M., Tint, G.S., Vanier, M.T., Walkley, S.U., and Lobel, P. (2004). Genetic evidence for nonredundant functional cooperativity between NPC1 and NPC2 in lipid transport. Proceedings of the National Academy of Sciences of the United States of America *101*, 5886-5891.

Sokolov, A., and Radhakrishnan, A. (2010). Accessibility of cholesterol in endoplasmic reticulum membranes and activation of SREBP-2 switch abruptly at a common cholesterol threshold. Journal of Biological Chemistry *285*, 29480-29490.

Steck, T.L., Ye, J., and Lange, Y. (2002). Probing red cell membrane cholesterol movement with cyclodextrin. Biophys J *83*, 2118-2125.

Stefan, C.J., Manford, A.G., and Emr, S.D. (2013). ER-PM connections: sites of information transfer and inter-organelle communication. Curr Opin Cell Biol *25*, 434-442.

Stocco, D.M., and Clark, B.J. (1996). Role of the steroidogenic acute regulatory protein (StAR) in steroidogenesis. Biochem Pharmacol *51*, 197-205.

Temel, R.E., Trigatti, B., DeMattos, R.B., Azhar, S., Krieger, M., and Williams, D.L. (1997). Scavenger receptor class B, type I (SR-BI) is the major route for the delivery of high density lipoprotein cholesterol to the steroidogenic pathway in cultured mouse adrenocortical cells. Proc Natl Acad Sci U S A *94*, 13600-13605.

Timmins, J.M., Lee, J.Y., Boudyguina, E., Kluckman, K.D., Brunham, L.R., Mulya, A., Gebre, A.K., Coutinho, J.M., Colvin, P.L., Smith, T.L.*, et al.* (2005). Targeted inactivation of hepatic

Abca1 causes profound hypoalphalipoproteinemia and kidney hypercatabolism of apoA-I. J Clin Invest *115*, 1333-1342.

Tong, J., Manik, M.K., and Im, Y.J. (2018). Structural basis of sterol recognition and nonvesicular transport by lipid transfer proteins anchored at membrane contact sites. Proc Natl Acad Sci U S A *115*, E856-E865.

Tontonoz, P., and Mangelsdorf, D.J. (2003). Liver X receptor signaling pathways in cardiovascular disease. Mol Endocrinol *17*, 985-993.

Urbani, L., and Simoni, R.D. (1990). Cholesterol and vesicular stomatitis virus G protein take separate routes from the endoplasmic reticulum to the plasma membrane. J Biol Chem *265*, 1919-1923.

Vance, J.E., and Steenbergen, R. (2005). Metabolism and functions of phosphatidylserine. Prog Lipid Res *44*, 207-234.

Vergeer, M., Korporaal, S.J., Franssen, R., Meurs, I., Out, R., Hovingh, G.K., Hoekstra, M., Sierts, J.A., Dallinga-Thie, G.M., Motazacker, M.M.*, et al.* (2011). Genetic variant of the scavenger receptor BI in humans. N Engl J Med *364*, 136-145.

Walther, T.C., and Farese, R.V. (2012). Lipid droplets and cellular lipid metabolism. Annual review of biochemistry *81*, 687-714.

Wang, B., and Tontonoz, P. (2018). Liver X receptors in lipid signalling and membrane homeostasis. Nat Rev Endocrinol.

Wang, X., Collins, H.L., Ranalletta, M., Fuki, I.V., Billheimer, J.T., Rothblat, G.H., Tall, A.R., and Rader, D.J. (2007). Macrophage ABCA1 and ABCG1, but not SR-BI, promote macrophage reverse cholesterol transport in vivo. J Clin Invest *117*, 2216-2224.

Wasan, K.M., Brocks, D.R., Lee, S.D., Sachs-Barrable, K., and Thornton, S.J. (2008). Impact of lipoproteins on the biological activity and disposition of hydrophobic drugs: implications for drug discovery. Nat Rev Drug Discov *7*, 84-99.

Wei, W., Schwaid, A.G., Wang, X., Wang, X., Chen, S., Chu, Q., Saghatelian, A., and Wan, Y. (2016). Ligand Activation of ERRalpha by Cholesterol Mediates Statin and Bisphosphonate Effects. Cell Metab *23*, 479-491.

Widenmaier, S.B., Snyder, N.A., Nguyen, T.B., Arduini, A., Lee, G.Y., Arruda, A.P., Saksi, J., Bartelt, A., and Hotamisligil, G.S. (2017). NRF1 Is an ER Membrane Sensor that Is Central to Cholesterol Homeostasis. Cell *171*, 1094-1109.e1015.

Williams, D.L., Temel, R.E., and Connelly, M.A. (2000). Roles of scavenger receptor BI and APO A-I in selective uptake of HDL cholesterol by adrenal cells. Endocr Res *26*, 639-651.

Wong, L.H., and Levine, T.P. (2016). Lipid transfer proteins do their thing anchored at membrane contact sites... but what is their thing? Biochem Soc Trans *44*, 517-527.

Wu, H., Carvalho, P., and Voeltz, G.K. (2018). Here, there, and everywhere: The importance of ER membrane contact sites. Science *361*.

Wu, Y., Whiteus, C., Xu, C.S., Hayworth, K.J., Weinberg, R.J., Hess, H.F., and De Camilli, P. (2017). Contacts between the endoplasmic reticulum and other membranes in neurons. Proc Natl Acad Sci U S A *114*, E4859-E4867.

Xu, X.X., and Tabas, I. (1991). Lipoproteins activate acyl-coenzyme A:cholesterol acyltransferase in macrophages only after cellular cholesterol pools are expanded to a critical threshold level. J Biol Chem *266*, 17040-17048.

Yeung, T., Gilbert, G.E., Shi, J., Silvius, J., Kapus, A., and Grinstein, S. (2008). Membrane phosphatidylserine regulates surface charge and protein localization. Science *319*, 210-213.

Yu, L., Li-Hawkins, J., Hammer, R.E., Berge, K.E., Horton, J.D., Cohen, J.C., and Hobbs, H.H. (2002). Overexpression of ABCG5 and ABCG8 promotes biliary cholesterol secretion and reduces fractional absorption of dietary cholesterol. J Clin Invest *110*, 671-680.

Zanoni, P., Khetarpal, S.A., Larach, D.B., Hancock-Cerutti, W.F., Millar, J.S., Cuchel, M., DerOhannessian, S., Kontush, A., Surendran, P., Saleheen, D.*, et al.* (2016). Rare variant in scavenger receptor BI raises HDL cholesterol and increases risk of coronary heart disease. Science *351*, 1166-1171.

Zelcer, N., Hong, C., Boyadjian, R., and Tontonoz, P. (2009). LXR regulates cholesterol uptake through Idol-dependent ubiquitination of the LDL receptor. Science *325*, 100-104.

Zhang, J., and Liu, Q. (2015). Cholesterol metabolism and homeostasis in the brain. Protein Cell *6*, 254-264.

Zhang, L., Rajbhandari, P., Priest, C., Sandhu, J., Wu, X., Temel, R., Castrillo, A., de Aguiar Vallim, T.Q., Sallam, T., and Tontonoz, P. (2017). Inhibition of cholesterol biosynthesis through RNF145-dependent ubiquitination of SCAP. Elife *6*.

Zhang, S.L., Yu, Y., Roos, J., Kozak, J.A., Deerinck, T.J., Ellisman, M.H., Stauderman, K.A., and Cahalan, M.D. (2005a). STIM1 is a Ca2+ sensor that activates CRAC channels and migrates from the Ca2+ store to the plasma membrane. Nature *437*, 902-905.

Zhang, Y. (2008). I-TASSER server for protein 3D structure prediction. BMC Bioinformatics *9*, 40.

Zhang, Y., Da Silva, J.R., Reilly, M., Billheimer, J.T., Rothblat, G.H., and Rader, D.J. (2005b). Hepatic expression of scavenger receptor class B type I (SR-BI) is a positive regulator of macrophage reverse cholesterol transport in vivo. J Clin Invest *115*, 2870-2874.